

12. GEOCHEMISTRY OF BASIC IGNEOUS ROCKS, GULF OF CALIFORNIA, DEEP SEA DRILLING PROJECT LEG 64¹

Andrew D. Saunders, Department of Geology, Bedford College, Regent's Park, London, NW1 4NS, United Kingdom,
Daniel J. Fornari, Department of Geological Sciences, State University of New York at Albany, Albany, New York,
Jean-Louis Joron, Laboratoire Pierre Sue, Groupe des Sciences de la Terre,
Centre d'Etudes Nucléaires de Saclay, Gif/Yvette, France,
John Tarney, Department of Geology, University of Leicester, Leicester, LE1 7RH, United Kingdom,
and
Michel Treuil, Laboratoire Pierre Sue, Groupe des Sciences de la Terre,
Centre d'Etudes Nucléaires de Saclay, Gif/Yvette, France

ABSTRACT

Mafic igneous rocks (basalt, dolerite, gabbro) were recovered from 6 of the 13 holes drilled in the Gulf of California during Leg 64. Sites 474 and 475 are on oceanic and continental crust, respectively, at the southern tip of Baja California; they effectively form secular end-points of a transect from the East Pacific Rise (EPR) completed during Leg 65. Hole 474A penetrated a sequence of olivine-rich dolerite sills before encountering pillow basalts and massive flows typical of Oceanic Layer 2. Although the basement age at this site is estimated to be 3.2 m.y., the sills clearly represent off-axis activity postdating the axis lavas by approximately 1.4 m.y. Detailed X-ray fluorescence (XRF) and instrumental neutron activation analysis (INAA) of samples from Hole 474A demonstrate that the least-altered axis lavas are depleted in the more-hygro-magmatophile (HYG) elements (Cs, Rb, K, Ba, Th, Ta, Nb, La, Ce) relative to the HYG elements (middle to heavy rare earth elements [REE], Y, Zr, Hf, Sr, P, and Ti; e.g., $Ti/Zr = 85-100$, $Zr/Nb \sim 30$, $La_N/Yb_N \sim 0.9$, $Th/Hf \sim 0.12$, $La/Ta \sim 20$). These ratios are similar to those found in basalts recovered during Leg 65 ($Ti/Zr = 100-130$, $La_N/Yb_N \sim 0.5$; $Th/Hf = 0.03-0.08$) but do not indicate such strong more-HYG element depletion. The off-axis sills, however, have high MgO, Ni, and Cr contents; very low more-HYG/HYG element ratios (e.g., $La_N/Yb_N = 0.2$), and high La/Ta ratios (generally in excess of 40). It is difficult to relate the composition of at least one of the sills to that of the basement lavas by fractional crystallization or even by partial melting of chemically similar sources; and it is more likely that the sills were derived from a mantle source that was originally compositionally heterogeneous and that had undergone a previous episode of basalt extraction (possibly during the production of the axis lavas).

Hole 475B is in a continental slope basin, 21 kilometers southeast of the tip of Baja California. Drilling resulted, unexpectedly, in recovering fresh, sparsely olivine-phyric basaltic cobbles. The basalts are nepheline normative, with high MgO, Ni, and Cr contents, and probably represent liquid compositions. They exhibit relative depletion of several of the more-HYG elements (particularly Ta, Nb, and Th); La_N/Yb_N ratios exceed 1, but La_N/Sm_N ratios are less than 1, and Sr/Zr ratios are high. The petrogenesis of these basalts is obscure, but it is likely that they were derived either from a depleted mantle source that contained residual components and a calc-alkaline chemistry or from a depleted, EPR-type source followed by minor sialic contamination prior to eruption.

Sites 477, 478, and 481 are in the Guaymas Basin, a youthful basin containing two small spreading axes beneath a blanket of sediments. Drilling at all three sites failed to recover unequivocal basalt flows; the main igneous bodies were massive basaltic, doleritic, or gabbroic sills. Detailed XRF and INAA analysis show that the units from all three sites are chemically similar and characterized by depletion of more-HYG elements relative to HYG elements—although this depletion is not so marked as in the basalts from the mouth of the Gulf. Thus, $La_N/Yb_N \sim 1.2$; $La_N/Sm_N < 1$; $Th/Hf = 0.1-0.2$; $Ti/Zr \sim 70$; and $La/Ta \sim 18$. Most significantly, the Guaymas Basin samples have high Sr/Zr ratios, a feature also reported in lavas from the adjacent seamount, Tortuga Island.

It is suggested that the differences in chemistry between the basalts recovered from the mouth of the Gulf and the samples from the Guaymas Basin can be explained by differences in the composition of the mantle source. This, in turn, may be explained by the presence of a minor component of subcontinental mantle beneath the northern Gulf region. Nevertheless, this chapter reveals that the Gulf is floored by mafic rocks derived from a source with a chemical signature not very dissimilar to that feeding most of the EPR. This concurs with recent tectonic models proposing that the Gulf of California is underlain by Pacific-type mantle.

INTRODUCTION

Leg 64 of the Deep Sea Drilling Project drilled eight sites in the Gulf of California (Fig. 1), an area that may hold answers to fundamental questions about the early stages of formation of ocean basins and marginal basins

and the nature of the ocean/continent transition zone. The broad objectives of this leg and of Leg 65 included investigating a transect from the East Pacific Rise (EPR) to continental crust at the tip of Baja California; investigating the nature of the ocean crust generated in the central part of the Gulf, where sedimentation rates are very high; and studying the hydrothermal processes associated with such spreading activity. During Leg 64, basaltic rocks were recovered at five of the eight sites: Sites 474 and 475 at the mouth of the Gulf and Sites 477,

¹ Curray, J. R., Moore, D. G., et al., *Init. Repts. DSDP, 64*: Washington (U.S. Govt. Printing Office).

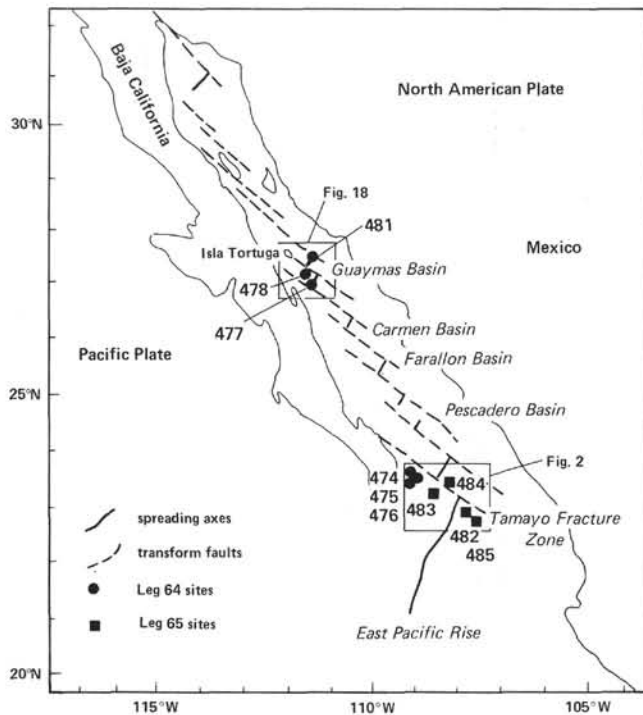


Figure 1. Generalized map of the Gulf of California showing the location of sites occupied during Legs 64 and 65 and the location of major physiographic and tectonic features. (Outlined areas are illustrated in more detail in Figs. 2, 18).

478, and 481 in the Guaymas Basin. The purpose of this chapter is to present a detailed factual account of whole-rock major- and trace-element data from representative suites of basaltic samples. The results will be used to elucidate intra- and intersite chemical variations and to evaluate various causative petrogenetic mechanisms. Particular emphasis will be placed on any compositional differences between basalts at the mouth of the Gulf and those in the Guaymas Basin. Such spatial comparisons are valid, however, only if sufficient control over secular variations is available. Accordingly, brief reference will be made to basalts recovered during Leg 65 (Saunders, in press).

Sites 474, 475, and 476 form part of the passive margin transect at the tip of Baja California Sur; the transect was continued to the EPR during Leg 65. Hole 474A, on positive magnetic anomaly 2" (3.2 m.y.; Larson et al., 1968) and adjacent to the continental margin, penetrated a sequence of turbidites and dolerite sills before encountering basaltic pillows and flows characteristic of Ocean Layer 2. Drilling in Hole 475B, on continental crust some 12 km to the northwest of Hole 474A, penetrated a few meters of olivine basalt cobbles. It is unlikely that the basalts recovered at Site 475 represent part of a typical oceanic sequence. Hole 476 bottomed in granite.

Five of the eight sites occupied during Leg 64 are in the Guaymas Basin, a region containing two active spreading centers separated by a 20-km-long transform fault. Sites 477 and 481 are in the southern and northern rifts, respectively, whereas Site 478 is on the basin floor,

outside the southern rift. Drilling at all three sites recovered a sequence of Quaternary diatomaceous oozes and turbidites intruded by dolerite and gabbro sills, and it is arguable that these igneous rocks are the youngest ever recovered by deep-sea drilling (<400,000 y.).

The Gulf of California has an unusual tectonic setting: it is neither a true back-arc basin, such as those in the Scotia Arc and western Pacific (e.g., Karig, 1974), nor is it merely an extension of the Pacific Ocean Basin. Nevertheless, the samples recovered during Legs 64 and 65 may provide information on several aspects of marginal basin and ocean basin formation—in particular, the nature of the ocean crust formed at the inception of basin opening. For example, Hole 474A, lying only a few kilometers from the ocean crust/continental crust transition, contains oceanic crust formed very early during the history of the Gulf. In the major ocean basins, it is not usually possible to sample such crust, because the ocean/continent transition is invariably buried beneath several kilometers of sediment. In addition, the spread of sites *along* the Gulf can potentially enable an assessment of any mantle heterogeneity in the area. Recent work has shown that basalts erupted along the Mid-Atlantic Ridge (MAR) are chemically and isotopically heterogeneous, reflecting the variable compositions of their sources (see, for example, Hart et al., 1973; White et al., 1976; O'Nions et al., 1977; Tarney, Saunders et al., 1979; Tarney et al., 1980; Wood et al., 1979b; Bougault and Treuil, 1980; Dupré and Allegre, 1980). It is unclear whether similar inhomogeneities exist in the mantle sources feeding the EPR. Because of the possible involvement of subcontinental mantle, the unusual tectonic setting of the Gulf of California may produce chemical variations along the Gulf. By the same line of reasoning, the earliest-formed ocean crust may also possess some continental mantle characteristics. There is, however, a complication. It is now well established that many back-arc basins, particularly those in an ensialic setting, are floored by basalts possessing transitional island arc or even calc-alkaline characteristics (Gill, 1976; Saunders and Tarney, 1979; Weaver et al., 1979; Saunders, Tarney, Marsh, et al., 1980). This feature may occur in the Gulf magmas, because prior to the opening of the Gulf, Baja California and the adjacent mainland formed part of an active orogenic magmatic arc. It will therefore be necessary to carefully investigate the Leg 64 basaltic rocks to trace any vestiges of calc-alkaline chemistry.

GEOLOGICAL SETTING

Prior to the present phase of extension, which began approximately 5 m.y. ago (Larson, 1972), Baja California formed part of the North American Plate and was separated from the Pacific Plate by a destructive plate margin. The latter is indicated by the presence of calc-alkaline plutonic complexes and associated volcanic rocks, ranging in age from late Mesozoic to late Tertiary (e.g., Gastil et al., 1975, 1979), throughout Baja California and parts of the western Mexican mainland. Approximately 15 to 20 m.y. ago, a structural trough, or proto-Gulf, with structural characteristics and a tecton-

ic pattern similar to those in active continental margin arc-trench/marginal basin systems, developed behind the andesitic arc (Karig and Jensky, 1972). The main extensional phase of the proto-Gulf occurred some 10 to 15 m.y. ago and resulted in considerable thinning of the continental crust. It is unlikely that oceanic crust developed at this stage—at least not in any significant quantity (Karig and Jensky, 1972). By this time, the EPR had impinged against the North American Plate, and active subduction of Pacific Ocean crust beneath western Baja California stopped between 15 and 7 m.y. ago. Subsequently, a transform fault system developed along the seaward side of Baja California, with a 'no-slab' window beneath California (Dickinson and Snyder, 1979). Additionally, there appears to have been little or no extension of the proto-Gulf region between 7 and 5 m.y. ago.

The present-day configuration of the Gulf began to develop 5 m.y. ago: The transform fault system, lying to the west of California, jumped northeastward to the east of Baja California (Larson, 1972; Karig and Jensky, 1972; Dickinson and Snyder, 1979). The modern vectors of the North American and Pacific Plates necessitated extension along the transform, resulting in short, spreading centers separated by long transform faults ('leaky transforms'; Moore and Buffington, 1968; Larson, 1972; Larson et al., 1972). Within the Gulf, these spreading centers are poorly defined but probably exist in the Mazatlán, Pescadero, Farallon, Carmen, Guaymas, and Colorado Basins (Fig. 1). Magnetic anomalies are present but difficult to identify, which may be a function of the way oceanic crust is emplaced (Larson et al., 1972); all of these basins are characterized by high sedimentation rates (see discussions by Lawver and Hawkins, 1978). Major geothermal anomalies occur in the Guaymas Basin (Lawver et al., 1975), again indicating active emplacement of magma—a feature confirmed during Leg 64.

The Gulf of California is therefore associated with predominant strike-slip tectonics, with minor crustal extension, and it has no active subduction-related tectonics. The region appears to be underlain by a slab-free window (Dickinson and Snyder, 1979), which in turn implies that it is underlain by Pacific Ocean-type mantle. This suggestion may be confirmed by considering the basalt chemistry.

ANALYTICAL TECHNIQUES

Sample Preparation. Minicores or quarter core sections were washed in distilled water to remove surface contamination, dried at 100°C, and then ground to a fine powder (<240 mesh) in an agate Tema swing mill. For XRF analysis, approximately 15 g of rock powder were mixed with 30 drops of a 7% aqueous solution of polyvinyl alcohol and formed into briquettes with diameters of 46 mm.

Representative samples from all of the igneous units were made into fusion beads for major-element analysis. This technique eliminates mineralogical effects and reduces matrix absorption. The rock powders were dried overnight at 110°C prior to mixing with a lithium metaborate/lithium tetraborate flux (Johnson Matthey Spectroflux 100B; Bennett and Oliver, 1976) in the proportion of 1 rock to 5 flux. Fusion was carried out at 1200°C in a vertical-tube furnace; ignition losses were determined on all of the samples fused. Using equipment similar to that described by Harvey et al. (1973), each glass melt was pressed into a 46-mm disc, annealed for 30 min. at 200°C, and, when cool, stored in a polythene bag.

Aliquots (0.4 g) of powder were sealed in plastic capsules prior to irradiation for instrumental neutron activation analysis at Saclay, Paris and at Bedford College, London.

X-Ray Fluorescence Analysis. We analyzed 135 whole-rock samples with a Philips PW1450 automatic spectrometer at the University of Birmingham; the count data were processed with Digital PDP 11-03 and ICL 1906A computers. Major- and minor-element analyses were determined on 46-mm powder briquettes and representative fusion beads using a rhodium-anode X-ray tube. To obtain maximum sensitivity, trace elements were determined on powder briquettes, using molybdenum (Y, Sr, Rb, Th, Pb, Ga, Zn, Ba) and tungsten (Ni, Cr, La, Ce, Nd, Zr, Nb) anode X-ray tubes. Instrumental replication was ensured by ratioing counts to a reference sample, reanalyzing every fourth sample (Rh tube), or reanalyzing a sample at the beginning of every loading of 60 samples (Mo and W tubes).

Details of the instrumental conditions for the analysis of trace elements are given in Tarney et al. (1979a); for the analysis of major and minor elements using the Rh tube, see Marsh et al. (1980). Calibration methods were similar to those of Leake et al. (1968) and are outlined in Marsh et al. (1980).

The precision of XRF analytical techniques at Birmingham is generally high, particularly for the trace elements. This has been demonstrated by the data in Marsh et al. (1980). Unfortunately, several of the trace elements analyzed have very low abundances in the Leg 64 basalts. Those elements approaching the lower level of determination include Nb (2 ppm), Th (3 ppm), Pb (3 ppm), and, in some samples, La (~5 ppm) and Ce (~8 ppm). Analytical values approaching these levels should be treated with due caution. The Leg 64 basalts were analyzed with basalts from several other DSDP legs to minimize long-term machine drift and to ensure compatibility among results from different legs.

Accuracy of analysis must be judged against international reference samples which, for trace elements, do not cover the range of concentrations encountered in most DSDP basalts. Data for trace elements in basalt BCR-1 are given in Tarney, Saunders et al. (1979) and, for a wider range of materials, in Hendry (1975). Data for the standard basalt BOB-1 are given in Table 1 and cross referenced to Marsh et al. (1980).

In addition to the X-ray fluorescence analyses, 47 samples have been analyzed for the elements Ni, Cr, Co, Sc, Ba, Sr, Cs, Rb, U, Th, Zr, Hf, Ta, Sb, La, Ce, Eu, and Tb at Saclay using INA techniques (Treuil et al., 1972 and Chayla et al., 1973). The elements La, Ce, Nd, Sm, Eu, Tb, Tm, Yb, Lu, Hf, Ta, and Th have been determined on 16 additional samples, using INAA at Bedford College, London. Details of analytical technique are given in Saunders (in press), and values for International Standard W-1 are given in Table 1.

All of the XRF and INAA data are presented in this chapter. This has resulted in duplication of some elements, and to avoid inter-laboratory error, all the diagrams use analytical data from only one laboratory for each element unless otherwise stated. Preference will be given to the more complete Birmingham data for those elements which can be sufficiently and precisely analyzed by XRF (major and minor elements, Ni, Cr, Zr, Nb, Y, Sr, Ga, Ba). For the chondrite-normalized, rare-earth element diagrams, the Bedford data (La, Ce, Nd, Sm, Eu, Gd, Tb, Tm, Yb, Lu) will be used, and the Saclay data (Cs, Rb, La, Ce, Tb, U, Th, Hf, Ta) will be used on the remaining diagrams.

Mineral Analysis. Occasional reference to mineral analyses has been made in the text. Full data and methods of analysis are given in Fornari et al. (this volume), from whom the data were obtained.

TRACE-ELEMENT NOMENCLATURE

Recent comprehensive studies of trace- and minor elements with bulk solid/liquid distribution coefficients (D) of less than one have shown that they may be conveniently grouped, according to their relative incompatibility, into hygromagmatophile (HYG) or more-hygromagmatophile types (see, for example, Wood et al., 1979a). As an approximate guideline, HYG elements are those with D values of approximately 0.1, and more-HYG elements are those with D values significantly less than 0.01. In oceanic basalt systems where the predominant crystal phases are olivine, clinopy-

Table 1. Analyses of standard reference samples.

	BOB-1 ^a	BOB-1 ^b	W-1 ^c		
SiO ₂	51.2	51.0	La	10.1	
TiO ₂	1.29	1.28	Ce	22.6	
Al ₂ O ₃	16.75	16.55	Nd	13.2	
tFe ₂ O ₃	8.57	8.48	Sm	3.34	
MnO	0.13	0.14	Eu	1.13	
MgO	7.77	7.58	Gd	3.58	
CaO	11.23	11.39	Tb	0.62	
Na ₂ O	3.09	3.10	Yb	2.13	
K ₂ O	0.37	0.37	Lu	0.31	
P ₂ O ₅	0.16	0.16	Th	2.43	
Total	100.56	100.05	Ta	0.53	
			Hf	2.44	
Ni	106	106			
Cr ^d	240	257			
Zn	60	62			
Ga	18	18			
Rb	4.6	4.8			
Sr	199	202			
Y ^e	27	27			
Zr ^f	102	108			
Nb	5	5			
Ba ^g	58	50			
La	7	6			
Ce	13	17			
Nd	11	—			

^a Values for standard basalt BOB-1 determined during this study.

^b Values for BOB-1 from Marsh et al., 1980. Major elements determined on fusion beads.

^c INAA values for standard W-1 determined at Bedford College during this study.

^d Not corrected for V interference.

^e Corrected for Rb interference.

^f Corrected for Sr interference.

^g Corrected for Ce interference.

roxene, and plagioclase, more-HYG elements include (most-HYG) Cs, Rb, Ba, Th, U, K, Ta, Nb, La, and Ce; the HYG elements include Sr, Nd, P, Hf, Zr, heavy REE, Ti, and Y (least-HYG). Values of *D* may of course vary according to the PTX conditions of the system; Sr and Eu, for example, can have *D* values exceeding one during plagioclase fractionation. Nevertheless, this broad grouping does assist in geochemical discussions, as it obviates the necessity of repetitious descriptions of trace-element behavior. Accordingly, the terminology has been used in this study.

It is also necessary to briefly refer to a further grouping of the incompatible trace elements—one based on their ionic structure. Thus, we may define those elements which have a low charge/radius ratio (the large-ion lithophile (LIL) elements): Cs, K, Rb, Ba, Th, U, Sr (La, Ce) and those which have a high charge/radius ratio (the high field-strength (HFS) elements): Ta, Nb, REE, P, Zr, Hf, Ti (see Pearce and Norry, 1979; Saunders, Tarney, Marsh et al., 1980; Saunders, Tarney, Weaver, 1980). This grouping is of value, because it broadly distinguishes between those elements generally considered to be mobile during hydrothermal alteration, either because of their low charge (K, Rb) or because of their ability to form complexes (U). Thus, the abun-

dances of Cs, K, Rb, U, and Sr in particular tend to be affected by halmyrolitic and hydrothermal activity (Hart, 1971; Hart et al., 1974; Mitchell and Aumento, 1977), and the analyzed values may not be primary. Many of the igneous units recovered during Leg 64 show evidence of secondary alteration, particularly where the unit was emplaced in wet sediments, in which case the unit appears to have undergone interaction with sediment pore waters (Gieskes et al., this volume). Accordingly, in the following discussion emphasis has been placed on those elements considered to be immobile during hydrothermal activity: the HFS element, Ti, Zr, Hf, Nb, Ta, Y, and, with more caution, the REE (Ludden and Thompson, 1979) and Th.

PASSIVE MARGIN TRANSECT: SITES 474 AND 475

The positions of Sites 474 and 475 are shown in Figure 2, along with Sites 482, 483, 484 and 485 which were occupied during Leg 65. Drilling at Site 474 recovered a suite of basaltic rocks that effectively provides a spatial and secular end-member for the ocean crust transect from the EPR. Site 475 unexpectedly resulted in recovery of basaltic rocks from basement, which is considered, on geophysical grounds, to be continental.

In the following site-by-site account, brief reference will be made to the petrography of each distinct igneous unit. Further details may be seen in the relevant site chapters. Wherever possible, the numbering of the igneous units will be kept the same for both the petrographical and geochemical descriptions.

Site 474

Site 474 (22°57.57.72'N; 108°58.84'W, 3022 m water depth) lies approximately 5 km to the east of the continental crust/oceanic crust boundary on magnetic anomaly 2" (3.2 m.y.; Larson et al., 1968). Two holes were drilled, but the first was abandoned after the heat probe jammed. Drilling in Hole 474A encountered the first of three possible sills at approximately 521 meters sub-

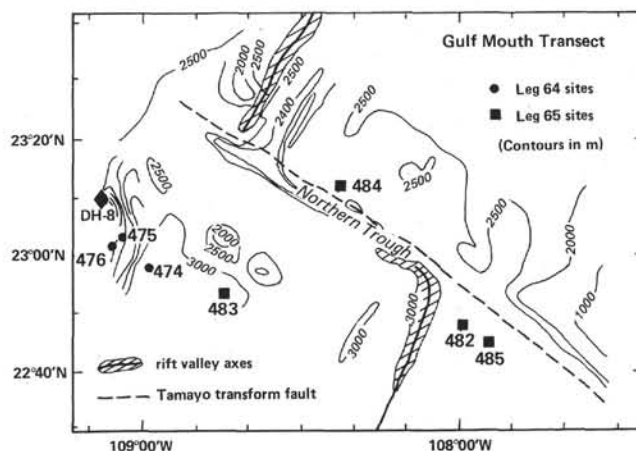


Figure 2. Bathymetric map of the mouth of the Gulf of California showing the location of Sites 474, 475, and 476 occupied during Leg 64 and Sites 482, 483, 484, and 485 occupied during Leg 65. (Dredge location DH-8 from Lewis et al. [1975].)

bottom and pillow basalts at 563 meters sub-bottom. A total of eight lithological units have been recognized by the shipboard party (Fig. 3); the main igneous rock types include olivine-rich dolerites and sparsely porphyritic to plagioclase-phyric basalts.

Unit 1 (5.5 m)

Unit 1 is a dolerite sill containing variable quantities of olivine (5–30%), plagioclase (5–15%), and red chrome spinel (trace) phenocrysts. There are noticeable concentrations of olivine phenocrysts, particularly in the lowermost one meter of the unit (Section 474-20-2), which suggest post-emplacment gravitational settling. Olivine-rich segregations do, however, occur throughout the unit, indicating perhaps that the magma was heterogeneous prior to emplacement. The olivines are almost entirely replaced by a green clay mineraloid, although the groundmass augite is quite fresh. Unit 1 intrudes sediments containing nannofossil assemblage NN16 to NN18 (above) and NN16 (below), indicating a maximum age of emplacement of ca. 1.8 m.y., which is significantly younger than the estimated age of the basement at this site (3.2 m.y.).

The analyses of the Unit 1 dolerite (Table 2) reflect the strong modal variation in mineralogy, with FeO/MgO ratios ranging from 0.67 to 1.42. Figure 4 may be used to emphasize several chemical variations within the unit (and within the other units of Hole 474A). Magnesium oxide, chromium, and nickel vary sympathetically with each other, and their variations are consistent with the heterogeneous distribution of (cumulus?) olivine and chrome spinel. In particular, MgO, Ni, and Cr have very high abundances in comparison with most of the other units in Hole 474A; parts of the unit are nearly picritic in composition. Equally, the dolerite contains abundant normative olivine and ranges from hypersthene to nepheline normative (Fig. 5). The HYG elements (e.g., Zr, Ti) exhibit negative correlations with MgO content, and several of the more-HYG elements have very low abundances (particularly K_2O , Nb, Ta, Th, Rb; Tables 2, 3). Ratios involving the HYG- and more-HYG elements are essentially constant throughout the unit (e.g., Zr/Y; Fig. 6), except where there is a possibility that an element may have been mobilized during hydrothermal or halmyrolitic activity (particularly K, Rb, Sr, Ba; Hart et al., 1974). Even so, the Ba/Zr (Fig. 7) and Sr/Zr (Fig. 8) ratios are nearly constant within the unit. The unusual geochemistry of Unit 1 is further illustrated by ratios of more-HYG elements versus HYG-elements. For example, the dolerite has very low Th/Hf ratios (0.01–0.05 based on the Bedford and Saclay data; Tables 3, 4; Fig. 9). The dolerite exhibits strong light-REE depletion, the degree of this depletion depending on whether the Bedford or Saclay data are considered; both laboratories show that the levels of La are very low. The Saclay data are plotted in Figure 10, and the very low La/Tb ratio ($La_N/Tb_N \sim 0.2$, where La_N is the chondrite-normalized value) is very distinct. Two samples from Unit 1, however, were determined for REE at Bedford; La was slightly higher ($La_N/Tb_N \sim 0.6$ and $La_N/Yb_N \sim 0.7$; Table 4; Fig. 11).

Unit 2 (8.0 m)

The presence of thermally altered sediments adjacent to its upper contact indicates an intrusive origin for Unit 2. Shipboard studies suggest that Unit 2 closely resembles the dolerite of Unit 1. This is particularly true of the upper part of the unit (Sections 474-41-5–474-42-2), which contains abundant olivine phenocryst, often in olivine-rich segregations (as much as 25% phenocrysts). Other phenocryst phases include (minor) plagioclase and chrome spinel. No phenocryst phases were seen in the lower part of the unit (Sections 474-42-3–474-42-5). As with Unit 1, alteration of the olivine is severe, and zeolite-filled fractures occur throughout.

Subsequent analytical work has verified the petrographic observations that Unit 2 has distinct upper and lower sections (see Table 2 and Fig. 3). The uppermost subunit, here designated 2a, is broadly and chemically comparable to Unit 1. This dolerite has high MgO, Cr, and Ni contents (Fig. 4) reflecting the high proportion of (cumulus?) olivine, and it is mildly nepheline normative (Fig. 5). The concentrations of the more-HYG elements are very low (Tables 3 and 4) and approach analytical detection limits. There is good agreement between the Bedford and Saclay data: both show extreme light-REE depletion (La_N/Tb_N [Saclay] ~ 0.3 , Fig. 10; La_N/Yb_N [Bedford] ~ 0.3 , Fig. 11). Th/Hf ratios (Fig. 9) are also very low (~ 0.01 – 0.04), and La/Ta ratios are very high (Fig. 12).

Subunit 2b comprises dolerite with a composition more typical of ocean ridge basalts: MgO, Ni, and Cr contents are much lower than in Subunit 2a (Figs. 3, 4). In many respects, Subunit 2b is comparable to Units 3 through 8 in Hole 474A. This is illustrated by the general abundances of Ni (Fig. 13), Cr and the HYG-elements, and by the hypersthene-normative character of the dolerite (Fig. 5). HYG and (particularly) more-HYG element abundances are higher than in Subunit 2a and Unit 1, resulting in significantly higher Th/Hf (Fig. 9) and La/Tb (Fig. 10; $La_N/Tb_N \sim 0.7$) ratios. Nevertheless, Unit 2b does have lower Th/Hf and higher La/Ta and Sr/Zr ratios than Units 3 through 8 (Figs. 9, 12, 8, respectively).

The observed differences in chemistry between Subunits 2a and 2b (and between Units 1 and 2) cannot be explained solely by intra-unit distribution of olivine and chrome spinel. The distribution of these minerals may have a significant effect on Mg, Ni, and Cr levels and absolute abundances of HYG elements, but it is unlikely that it could result in the observed variations in the more-HYG/HYG element ratios. We shall return to this point in a later section. These observations carry the necessary implication that Subunits 2a and 2b represent discrete, chemically distinct batches of magma.

Unit 3 (6.0 m)

The upper contact of Unit 3 was not recovered, so it has been impossible to ascertain whether the unit is intrusive in origin. Petrographically, Unit 3 is distinct from Units 1 and 2, being a coarse-grained, sparsely plagioclase-phyric ($\sim 5\%$, An_{60-70}) basalt. Olivine-rich

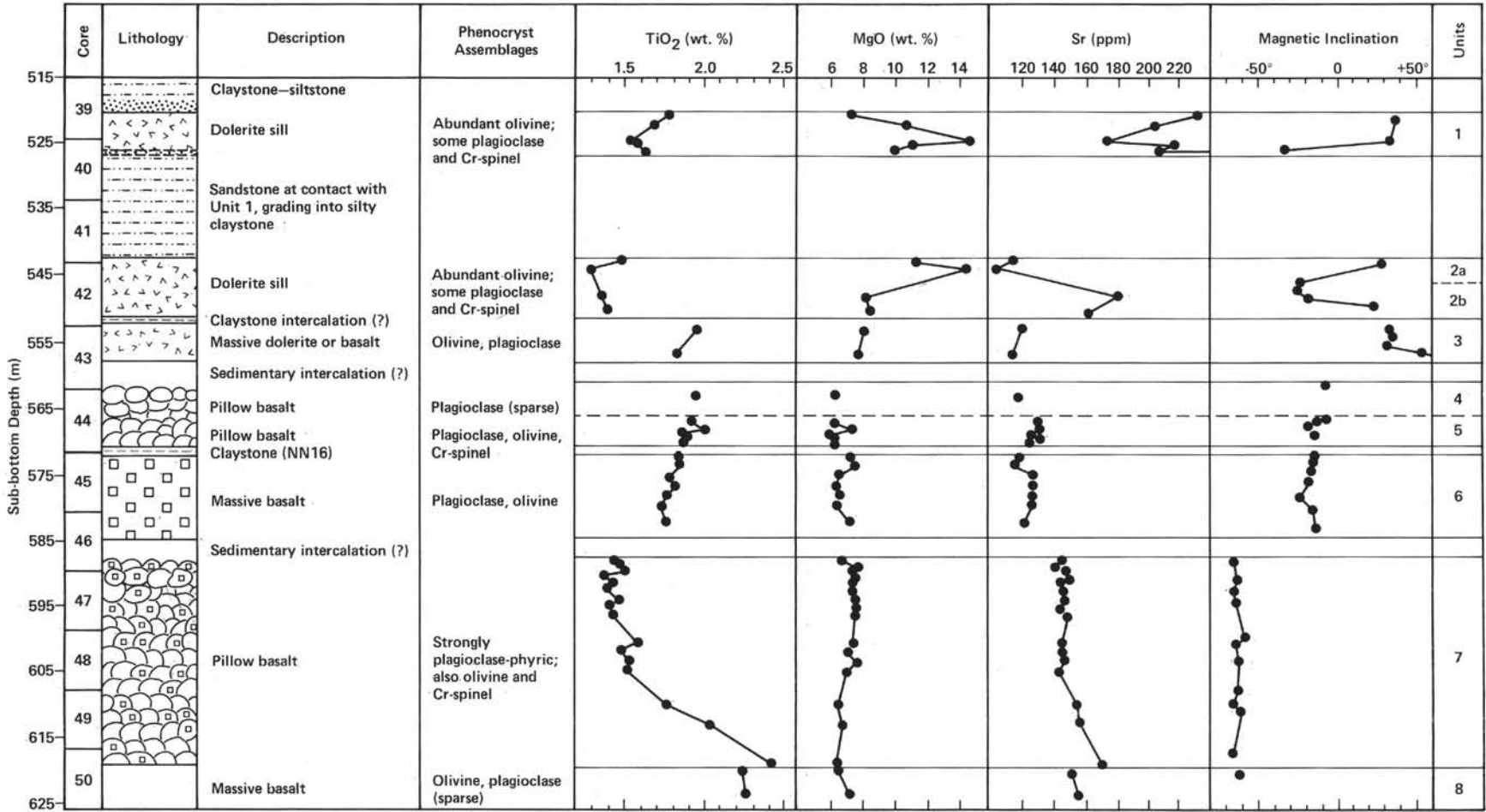


Figure 3. Downhole variations in lithology, magnetic inclination, and selected geochemical parameters, Hole 474A.

segregations do, however, occur at several intervals in Section 474-43-1, and calcite veining is found throughout the unit.

The basalt (Table 2) is hypersthene normative (Fig. 5), and its FeO/MgO ratios and Ni and Cr contents are more evolved than most samples from Units 1 and 2 (Fig. 4). In particular, Unit 3 has low Ni and Sr contents (Fig. 4, 8, 12). Conversely, the absolute contents of HYG and more-HYG elements are higher than in Units 1 and 2, with the exception of Zr in Unit 1. More-HYG/HYG element ratios are also generally higher in Unit 3 than in Units 1 and 2a (e.g., Th/Hf and La/Tb ratios; Figs. 9, 10). The chondrite-normalized REE pattern of Unit 3 is similar to that of Unit 1, showing strong light-REE depletion, although the middle REE/heavy REE ratio in Unit 3 is *lower* than in Unit 1 (Fig. 11). For example, the Sm_N/Yb_N ratio in Unit 3 is 1.0, and between 1.2 and 1.3 in Units 1 and 2a (Table 4). Similarly, the Zr/Y ratio is lower in Unit 3 than in either Unit 1 or Unit 2 (Fig. 6).

Unit 4 (4.0 m)

Unit 4 comprises moderately altered, aphanitic, sparsely plagioclase phyric basalt, which contains occasional small (1–2 mm) glomerocryst of olivine and plagioclase. In thin section, the groundmass is variolitic, indicating rapid cooling, and there are frequent aphanitic, cryptocrystalline selvages with traces of baked mudstone adhering to them. Clay- and zeolite-filled vesicles are common (15–20%; 0.2–1 mm in diameter). The basalt from Unit 4 is lithologically and texturally distinct from the overlying units, implying that this unit represents the highest level of true basement, rather than off-axis activity, at this site. Although Units 1 and 2 appear to be intrusive in origin, Unit 3 may well represent a massive flow unit. Nonetheless, Unit 4 does represent the first pillow basalt recovered at Site 474.

Only one sample from Unit 4 has been analyzed (Tables 2, 3). Although Unit 4 has a high FeO/MgO ratio (1.64), the levels of Ni, Cr, and Sr are not as high as in Unit 3 (Fig. 4). The basalt is hypersthene normative and may be considered a subalkaline tholeiite (Chayes, 1966). Absolute abundance of the HYG and more-HYG elements is higher than in Units 1 through 3, but this is probably a function of the degree of fractionation. More-HYG/HYG element ratios differ, however, from those observed in the dolerite of Units 1 through 3. The Th/Hf and La/Tb ratios are generally higher in Unit 4 than in Units 1 and 2 (Figs. 9, 10), although Zr/Y ratios are similar (Fig. 6). The Th/Hf ratios are higher in Unit 4 than in Unit 3. Note that on these plots, Unit 4 has ratios similar to those for Units 5 through 8. The absolute abundances of the mobile HYG-elements (K, Rb, Ba) are not significantly different from those in Units 1, 2, and 3 (allowing for fractionation): all are very low, similar to those in the N-type mid-ocean ridge basalts (MORB) of Sun et al. (1979). This is encouraging, as it suggests that introduction of these elements during low-temperature alteration by seawater has been minimal.

Unit 5 (4.0 m)

Unit 5 comprises fractured, plagioclase-phyric pillow basalt with numerous glassy selvages. Two generations of plagioclase phenocryst are present, the earliest consisting of large, zoned multicrystal aggregates as large as 5 mm in diameter (An_{80-90} ; 5% of the rock); the second comprises elongate phenocrysts as long as 2.5 mm in length (An_{70-80} ; ca. 30% of the rock). Olivine (~5%) and chrome spinel (trace) are also present, and the groundmass exhibits typical quench textures.

Slight chemical variation occurs within Unit 5: FeO/MgO ratios vary from 1.29 to 1.7 and Ni from 84 to 95 ppm. Zircon, however, is essentially invariant (Table 2; Figs. 3, 4). Although the basalt intrudes slightly into the quartz normative field on the basalt tetrahedron (Fig. 6), it is chemically similar to the basalts from Units 4 and 6. This is particularly true for the absolute abundances—and ratios—of the HYG and more-HYG elements: Y/Zr ~ 0.3 (Fig. 6), Ba/Zr ~ 0.2 (Fig. 7), Sr/Zr ~ 1 (Fig. 8), La_N/Tb_N ~ 0.7 (Fig. 10; Table 3), Th/Hf ~ 0.1 (Fig. 9), and La/Ta ~ 15 (Fig. 12). Consistency of these ratios between Units 4, 5, and 6 implies consanguinity of magmas.

Unit 6 (11.5 m)

Unit 6 is overlain by a thin sediment intercalation containing nannofossil assemblage NN16, which indicates an age for this sequence of about 3.2 m.y. This is in good agreement with the age of the basement at this site, as implied from magnetic anomaly data. The rock is a fresh, homogeneous, fine-grained dolerite and part of either a massive flow or a sill. It contains less than 5% plagioclase phenocrysts embedded in a slightly altered olivine-bearing, subophitic groundmass.

The analyses of the dolerite result in a tight cluster on most of the element- and oxide-variation diagrams (e.g., Fig. 4) and is caused by the limited chemical variation (e.g., FeO/MgO ranges from 1.31–1.50 ppm; Zr ranges from 119–123 ppm).

The rocks are hypersthene-olivine normative, although they contain slightly higher contents of Al_2O_3 than Units 1, 2a, 3, 4, and 5. Ratios and abundances of HYG and more-HYG elements are similar to those observed in Units 4 and 5 (see Tables 2, 3; Figs. 5–13).

Units 7 (31 m) and 8 (6.5 m; base not seen)

Unit 7 is the thickest unit drilled in Hole 474A, and the presence of abundant glassy selvages implies that it consists almost entirely of pillow basalt. An unusual feature of this unit is the occurrence of large (2–20 mm), partially resorbed and marginally zoned plagioclase megacrysts (An_{91} core; An_{80} rim), making up some 5% of the rock. Other phenocryst phases include smaller plagioclase laths (10%), olivine (Fo_{84-87} ; 5%) and chrome spinel. The groundmass shows good quench textures and is only very slightly altered (ca. 5% clay minerals).

Unit 7 grades down through a narrow amygdaloidal zone into Unit 8, which is at least 6.5 meters thick (drill-

Table 2. X-ray fluorescence analyses, Hole 474A.

Core Section	39	39	40	40	40	41	42	42	42	43	43	44	44	44	44	44	45	45	45	45	
Level (cm)	148	65	19	40	110	8	6	82	61	119	49	100	63	35	58	92	37	99	66	81	64
Unit	1	1	1	1	1	2a	2a	2b	2b	3	3	4	5	5	5	5	5	6	6	6	6
SiO ₂	48.2	45.9	44.8	48.1	45.8	46.9	44.5	48.8	48.5	49.1	48.9	48.8	49.3	49.3	49.3	49.4	49.6	48.8	49.0	49.6	49.2
TiO ₂	1.78	1.69	1.54	1.59	1.61	1.48	1.28	1.35	1.38	1.97	1.84	1.95	1.94	2.00	1.86	1.90	1.87	1.85	1.85	1.78	1.83
Al ₂ O ₃	15.6	15.9	14.7	14.1	15.6	15.2	16.6	16.7	16.7	15.1	15.4	15.5	15.7	15.5	15.7	15.8	16.1	16.0	15.7	16.1	16.2
tFe ₂ O ₃	11.15	10.48	11.13	10.26	11.19	11.10	10.77	9.68	9.74	10.58	10.83	11.58	10.83	10.44	11.37	11.19	11.13	11.16	10.94	10.78	10.83
MnO	0.21	0.17	0.16	0.17	0.19	0.21	0.17	0.16	0.15	0.17	0.17	0.23	0.22	0.20	0.18	0.18	0.18	0.17	0.17	0.17	0.14
MgO	7.07	10.86	14.90	11.17	10.01	11.42	14.87	8.28	8.44	8.09	7.87	6.34	6.25	7.26	6.03	6.32	6.25	7.30	7.51	6.65	6.50
CaO	11.17	10.75	9.27	10.21	11.40	9.74	9.59	11.64	11.50	11.56	11.64	12.10	12.05	11.45	11.91	11.74	11.62	11.29	10.92	11.59	11.53
Na ₂ O	3.01	2.78	2.37	2.66	2.91	2.56	2.47	2.78	2.78	2.62	2.69	2.56	2.63	2.62	2.64	2.54	2.61	2.65	2.49	2.69	2.77
K ₂ O	0.05	0.03	0.03	0.06	0.06	0.02	0.00	0.09	0.11	0.07	0.11	0.06	0.06	0.07	0.07	0.07	0.11	0.15	0.15	0.15	0.12
P ₂ O ₅	0.12	0.14	0.13	0.12	0.11	0.09	0.09	0.12	0.12	0.19	0.20	0.16	0.18	0.19	0.15	0.21	0.17	0.20	0.23	0.22	0.20
LOI	1.20	0.9	0.9	1.18	1.03	1.46	1.22	0.26	0.53	0.68	0.64	0.62	0.62	0.92	0.62	—	—	—	0.91	—	0.53
Total	99.64	99.60	99.89	99.63	99.89	100.19	100.07	99.81	99.96	100.20	100.23	99.86	99.83	99.93	99.85	99.39	99.56	99.64	99.87	99.75	99.79
Trace Elements (ppm)																					
Ni	346	243	463	607	345	487	522	97	102	75	66	88	94	95	85	84	84	76	78	83	88
Cr	502	367	580	829	486	822	797	216	214	246	224	230	227	218	222	209	197	209	188	195	192
Zn	69	62	59	74	63	62	57	57	56	76	70	81	79	76	78	73	72	71	65	78	68
Ga	19	19	17	18	18	17	18	17	22	210	19	22	19	21	21	20	19	19	19	21	18
Rb	<1	<1	<1	<1	1	<1	<1	1	<1	<1	1	<1	<1	2	<1	<1	<1	3	<1	2	1
Sr	232	205	175	217	208	114	106	182	164	121	115	129	131	132	127	132	127	119	119	128	129
Y	35	34	28	30	31	28	25	26	26	43	41	43	40	41	41	41	39	40	41	39	39
Zr	130	125	110	112	113	80	70	86	85	112	109	129	125	124	124	124	123	119	121	123	119
Nb	<1	<1	<1	<1	<1	<1	<1	2	2	3	4	5	5	5	3	6	5	4	4	5	4
Ba	44	45	64	31	33	11	22	12	14	30	25	19	30	36	33	25	29	35	37	36	31
La	5	6	6	6	6	4	4	6	5	8	8	8	8	9	9	9	7	8	8	10	8
Ce	15	12	12	11	8	<3	<5	10	11	15	14	18	14	19	17	16	15	12	17	17	17
Nd	12	13	11	11	11	8	9	11	10	13	13	14	14	15	15	14	13	13	13	13	14
Pb	<1	3	3	5	6	4	1	4	1	1	3	10	<1	2	2	3	5	1	3	5	5
Th	<1	2	1	<1	<1	2	<1	<1	5	<1	<1	<1	<1	<1	<1	<1	<1	<1	<1	2	2
Selected Ratios																					
Zr/Nb	>130	>125	>110	>112	>113	>80	>70	43	43	37	27	26	25	25	41	21	25	30	30	25	30
Ti/Zr	82	81	84	85	85	111	110	94	97	105	101	91	93	97	90	92	91	93	92	87	92
Y/Zr	0.27	0.27	0.25	0.27	0.27	0.35	0.36	0.30	0.31	0.38	0.38	0.33	0.32	0.33	0.33	0.33	0.32	0.34	0.34	0.32	0.33
Ce/Zr	0.12	0.10	0.11	0.10	0.07	<0.04	<0.07	0.12	0.13	0.13	0.13	0.14	0.11	0.15	0.14	0.13	0.12	0.10	0.14	0.14	0.14
Ba/Zr	0.34	0.36	0.58	0.28	0.29	0.14	0.31	0.14	0.16	0.27	0.23	0.15	0.24	0.29	0.27	0.20	0.24	0.29	0.31	0.29	0.26
(Ce/Y) _N	1.05	0.87	1.05	0.90	0.63	<0.26	<0.49	0.94	1.04	0.86	0.84	1.03	0.86	1.14	1.02	0.96	0.94	0.74	1.02	1.07	1.07
Fe/Mg	1.83	1.12	0.87	1.07	1.30	1.13	0.84	1.36	1.34	1.52	1.60	2.12	2.01	1.67	2.19	2.05	2.07	1.77	1.69	1.88	1.93
K/Rb	>415	>249	>249	>498	>498	>166	>25	747	>913	>581	913	>498	>498	291	>581	>581	>913	415	>1245	623	996
Ba/Sr	0.19	0.22	0.37	0.14	0.16	0.10	0.21	0.07	0.09	0.25	0.22	0.15	0.23	0.27	0.26	0.19	0.23	0.29	0.31	0.28	0.24
CIPW Norms																					
Q	0.0	0.0	0.0	0.0	0.0	0.0	0.0	0.0	0.0	0.0	0.0	0.0	0.0	0.0	0.0	0.2	0.0	0.0	0.0	0.0	0.0
Or	0.3	0.2	0.2	0.4	0.4	0.1	0.0	0.5	0.7	0.4	0.6	0.4	0.4	0.4	0.4	0.4	0.7	0.9	0.9	0.9	0.7
Ab	25.6	20.3	17.9	22.6	18.0	21.6	15.6	23.6	23.5	22.1	22.7	21.7	22.3	22.2	22.4	21.6	22.2	22.5	21.1	22.8	23.5
An	29.1	31.0	29.4	26.5	29.3	29.9	30.2	32.7	32.9	29.3	29.5	30.6	31.0	30.4	30.9	31.7	31.9	31.5	31.2	31.5	31.4
Ne	0.0	1.8	1.2	0.0	3.6	0.0	2.9	0.0	0.0	0.0	0.0	0.0	0.0	0.0	0.0	0.0	0.0	0.0	0.0	0.0	0.0
Di	21.1	17.5	12.7	19.0	21.6	14.4	13.4	19.8	19.0	21.8	21.9	23.4	22.8	20.6	22.5	21.0	20.5	19.1	17.6	20.2	20.2
Hy	5.8	0.0	0.0	8.6	0.0	6.4	0.0	5.9	4.5	13.4	10.0	13.4	15.3	16.6	15.5	18.0	17.8	12.8	19.2	15.3	13.2
Ol	10.3	22.0	31.6	15.8	19.9	20.3	31.2	11.9	13.4	5.5	7.8	2.8	0.8	2.0	0.8	0.0	0.1	6.2	2.2	2.5	3.7
Mt	1.9	1.8	1.9	1.8	1.9	1.9	1.9	1.7	1.7	1.8	1.9	2.0	1.9	1.8	2.0	2.0	1.9	1.9	1.9	1.9	1.9
Il	3.4	3.2	2.9	3.0	3.1	2.8	2.4	2.6	2.6	3.7	3.5	3.7	3.7	3.8	3.5	3.6	3.6	3.5	3.5	3.4	3.5
Ap	0.3	0.3	0.3	0.3	0.3	0.2	0.2	0.3	0.3	0.4	0.5	0.4	0.4	0.5	0.4	0.5	0.4	0.5	0.5	0.5	0.5

Note: Major (wt.%) and trace-element (ppm) analyses determined using a Philips PW1450 XRF spectrometer, at Birmingham University; tFe₂O₃ = total iron as Fe₂O₃; LOI = loss on ignition (determined during fusion-bead preparation); (Ce/Y)_N = chondrite-normalized Ce/Y ratios; CIPW norms determined using Fe₂O₃/FeO = 0.15.

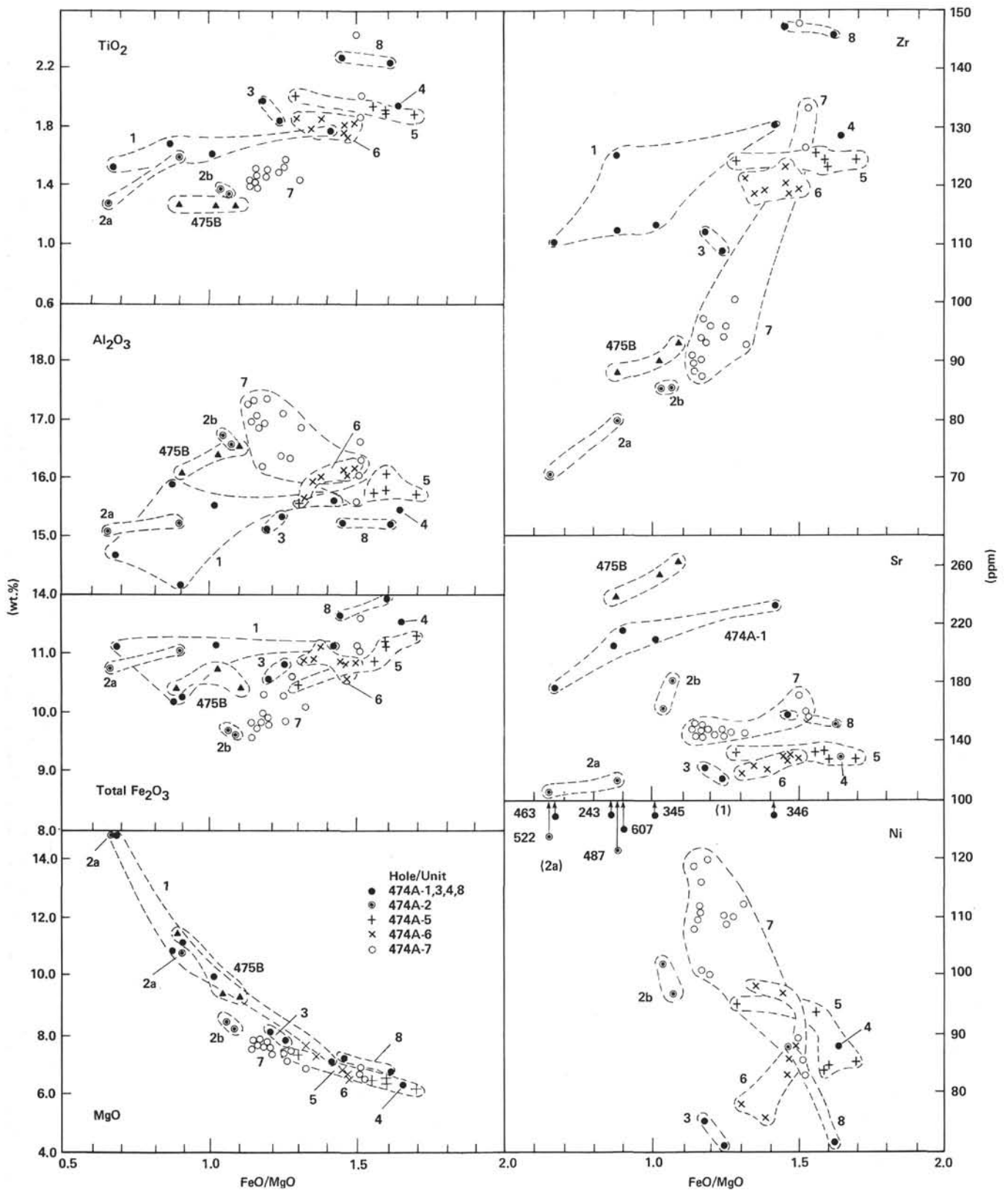


Figure 4. Variations in selected geochemical parameters versus FeO/MgO ratio for basic rocks recovered at Sites 474 and 475. (FeO represents total iron. Unit designations are the same as those defined in Figure 3. Analyses determined by XRF at Birmingham.)

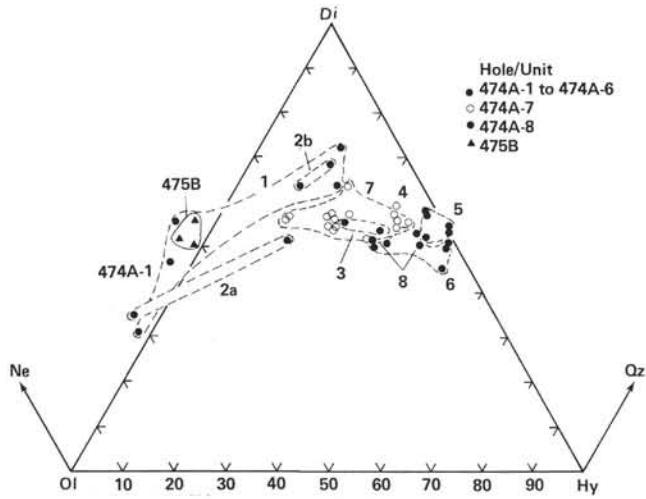


Figure 5. Basic rocks recovered at Sites 474 and 475 plotted on the normative nepheline(Ne)-diopside(Di)-olivine(Ol)-hypersthene (Hy) quartz (Qz) basalt tetrahedron. (Fe_2O_3/FeO ratio assumed to be 0.15. Analyses determined by XRF at Birmingham. Numbers refer to igneous units.)

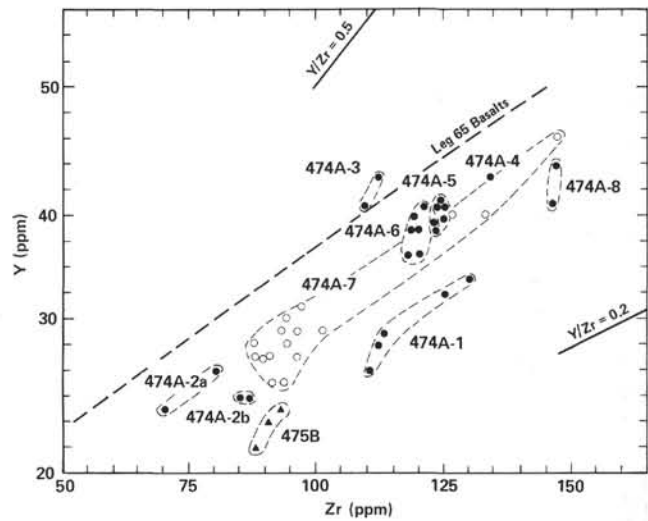


Figure 6. Y versus Zr for basic rocks recovered at Sites 474 and 475. (Trend for Leg 65 basalts from Saunders [in press]. Analyses determined by XRF at Birmingham. Symbols as in Fig. 5.)

ing stopped before the base was seen). The basalt of Unit 8 is sparsely plagioclase (5%) and olivine-phyric (5%), coarse-grained, and moderately altered. The absence of glassy selvages and the homogeneous nature of the lithology suggest that Unit 8 is probably a massive flow.

The basalt of Unit 7 is chemically quite varied, with the FeO/MgO ratio varying from 1.14 to 1.52 ppm, Ni from 120 to 83 ppm, and Zr from 87 to 133 ppm (Figs. 3, 4; Table 2). The contents of Al_2O_3 are high (as high as 17.3%), reflecting the presence of large feldspar phenocrysts. In terms of FeO/MgO ratio and abundances of HYG elements, most of Unit 7 is less evolved than Units 4 through 6 (Fig. 4), although there is a tendency for the basalt in the lowermost part of the unit (Sections

474-49-2-474-50-2) to show considerable HYG enrichment and concomitant Ni and MgO depletion. This can be seen in the downhole variation diagram (Fig. 3).

Unit 8 contains the most evolved basalts from Hole 474A; the FeO/MgO ratio reaches 1.62, Zr is as high as 147 ppm, and the other HYG-elements have sympathetically high levels. On most of the element variation diagrams, Unit 7 appears to grade into Unit 8 (see, for example, Figs. 4, 13), so the transitional lithological boundary between the two units appears to be mirrored by the chemistry.

On the plots of more-HYG and HYG elements, Units 7 and 8 exhibit colinearity, suggesting consanguinity of magmas. Unit 8 always lies at, and often overlaps with, the more fractionated members of Unit 7 (e.g., Figs. 6, 7, 8). Both units have the same La/Tb (Fig. 10), Th/Hf

Table 3. INAA results (Saclay) on selected samples, Hole 474A.

Core Section Interval (cm) Unit	39 4 65-67 1	41 ^a 6 8-10 2a	42 4 61-63 2b	43 3 49-51 3	44 1 100-103 4	44 2 63-65 5	45 5 40-42 6	46 1 110-112 6	46 2 26-29 7	47 2 46-48 7	47 4 140-143 7	48 1 101-103 7	49 3 133-136 7	50 4 1-4 8
Ni	260	509	115	78	97	103	117	113	128	150	123	122	72	112
Cr	394	714	244	243	241	231	226	226	275	255	260	278	173	234
Co	49.4	63.4	43.9	42.6	45.1	43.6	44.0	45.2	42.6	45.2	40.6	43.2	32.7	45.6
Sc	33.7	28.9	35.1	39.9	39.9	37.8	39.2	37.8	33.0	43.1	31.3	34.3	27.9	38.0
Ba	17	—	—	11	8	11	15	14	8	15	8	9	16	17
Sr	—	—	215	126	175	170	184	148	193	167	169	210	158	203
Cs	0.26	0.20	0.15	0.05	0.06	0.03	0.04	0.06	0.06	0.06	0.04	0.03	0.06	0.05
Rb	—	—	2.0	2.0	—	2.1	2.2	—	2.2	2.4	0.8	1.8	2.4	2.0
U	0.16	0.18	0.06	0.11	0.18	0.17	0.12	0.13	0.13	0.05	0.05	0.18	0.19	0.14
Th	0.04	0.01	0.09	0.20	0.36	0.33	0.33	0.33	0.24	0.23	0.24	0.27	0.30	0.43
Zr	134	81	77	99	154	119	128	143	88	109	82	124	93	161
Hf	2.98	2.39	2.26	3.12	3.52	3.30	3.17	3.34	2.54	2.52	2.40	2.78	2.78	3.80
Ta	0.06	0.01	0.13	0.20	0.33	0.31	0.30	0.31	0.24	0.31	0.23	0.28	0.31	0.42
Sb	0.02	—	0.02	—	—	—	—	0.02	0.02	0.01	0.01	—	—	0.01
La	1.07	1.13	3.11	3.32	4.88	4.49	3.54	4.80	3.69	3.76	3.65	3.74	4.64	4.96
Ce	10.0	6.8	8.9	10.0	14.4	13.8	12.6	12.0	9.3	9.6	9.2	12.5	10.2	16.4
Eu	1.53	1.26	1.22	1.45	1.69	1.56	1.48	1.55	1.19	1.22	1.14	1.26	1.22	1.75
Tb	0.80	0.65	0.66	0.83	1.19	0.95	0.87	0.85	0.65	0.71	0.68	0.77	0.75	1.01

Note: All values in ppm.
^a Average of two determinations.

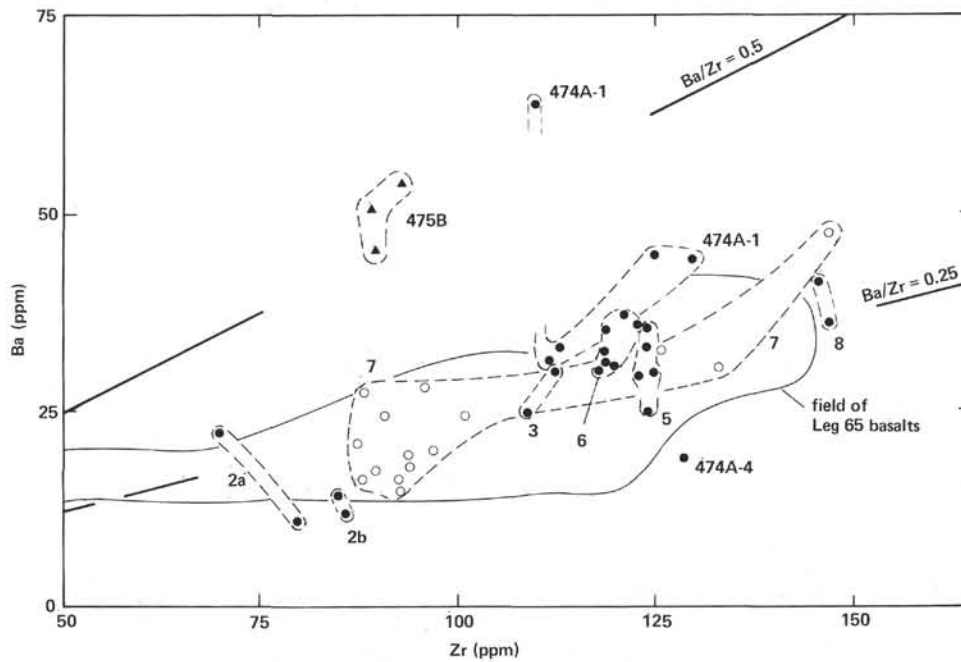


Figure 7. Ba versus Zr for basic rocks recovered at Sites 474 and 475. (Field for Leg 65 basalts from Saunders [in press]. Analyses determined by XRF at Birmingham. Symbols as in Fig. 5.)

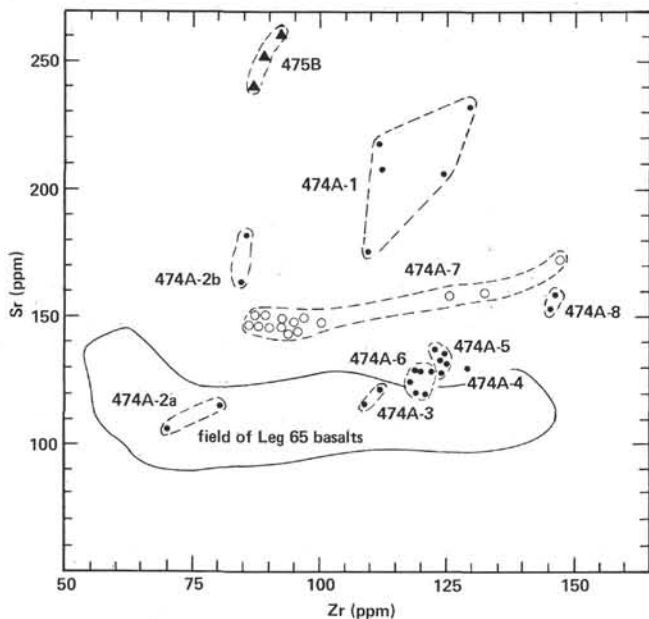


Figure 8. Sr versus Zr for basic rocks recovered at Sites 474 and 475. (Field for Leg 65 basalts from Saunders [in press]. Analyses determined by XRF at Birmingham. Numbers refer to igneous units.)

(Fig. 9), and La/Ta (Fig. 12) ratios, which in turn are indistinguishable from Units 4 through 6. Chondrite-normalized REE data for Units 7 and 8 are shown in Figure 11. Although the patterns show light-REE depletion ($La_N/Yb_N \sim 0.9$; Table 4), the depletion is not as great as in Units 1, 2a ($La_N/Yb_N \sim 0.3$), or 3 ($La_N/Yb_N \sim 0.6$). Unfortunately, full REE data are not available for Units 2b, 4, 5, and 6, but the La and Tb data in Tables 3 and Figure 10 indicate that Units 1 (La_N/Tb_N

Table 4. INAA results (Bedford) for selected samples, Hole 477A.

Core Section	39	40	42	43	48	50
Interval (cm)	148-150	19-21	6-8	119-121	101-103	1-4
Unit	1	1	2a	3	7	8
La	3.69	3.25	1.09	4.39	4.88	6.61 (4.96)
Ce	13.3	—	6.9	13.5	13.2	20.8 (16.4)
Nd	14.3	13.2	9.2	14.8	11.4	11.2
Sm	4.8	4.3	3.5	4.7	4.1	5.5
Eu	1.7	1.7	1.40	1.77	1.4	2.1 (1.75)
Tb	1.0	—	0.73	1.26	0.86	1.34 (1.01)
Tm	0.58	0.42	0.42	0.76	0.49	0.74
Yb	3.59	3.61	2.68	4.80	3.37	4.93
Lu	0.59	0.54	0.43	0.76	0.53	0.80
Th	0.17	0.12	0.10	0.41	0.32	0.58 (0.43)
Hf	3.27	—	2.49	3.54	2.84	—
Ta	0.09	0.03	n.d.	0.21	0.25	0.47 (0.42)
La_N/Yb_N	0.69	0.62	0.27	0.61	0.96	0.89
La/Ta	41	108	—	21	20	14
Th/Hf	0.05	—	0.04	0.12	0.11	— (0.11)

Note: Trace-element values in ppm; n.d. = not detected; La_N = chondrite-normalized La values; values in parentheses represent analyses done at Saclay (see Table 3) for comparison.

~ 0.2), 2a ($La_N/Tb_N \sim 0.3$), and 3 ($La_N/Yb_N \sim 0.6$) have lower La/Tb ratios than Units 4 ($La_N/Tb_N \sim 0.7$), 5 ($La_N/Tb_N \sim 0.75$), 6 ($La_N/Tb_N \sim 0.7-0.9$), 7 ($La_N/Tb_N \sim 0.8-1$), and 8 ($La_N/Tb_N \sim 0.8$). This is an important observation, as it suggests that the off-axis magmas (represented by Units 1, 2, and possibly 3) have lower La/Tb and La/Yb ratios than the ridge magmas (represented by Units 4-8). A similar variation also occurs in Th/Hf ratios (Fig. 9). This will be discussed more fully in the next section.

Site 474: Discussion

Before comparing the chemistry of the samples recovered from Hole 474A with basalts from the EPR (including Leg 65) and the MAR, it is necessary to assess

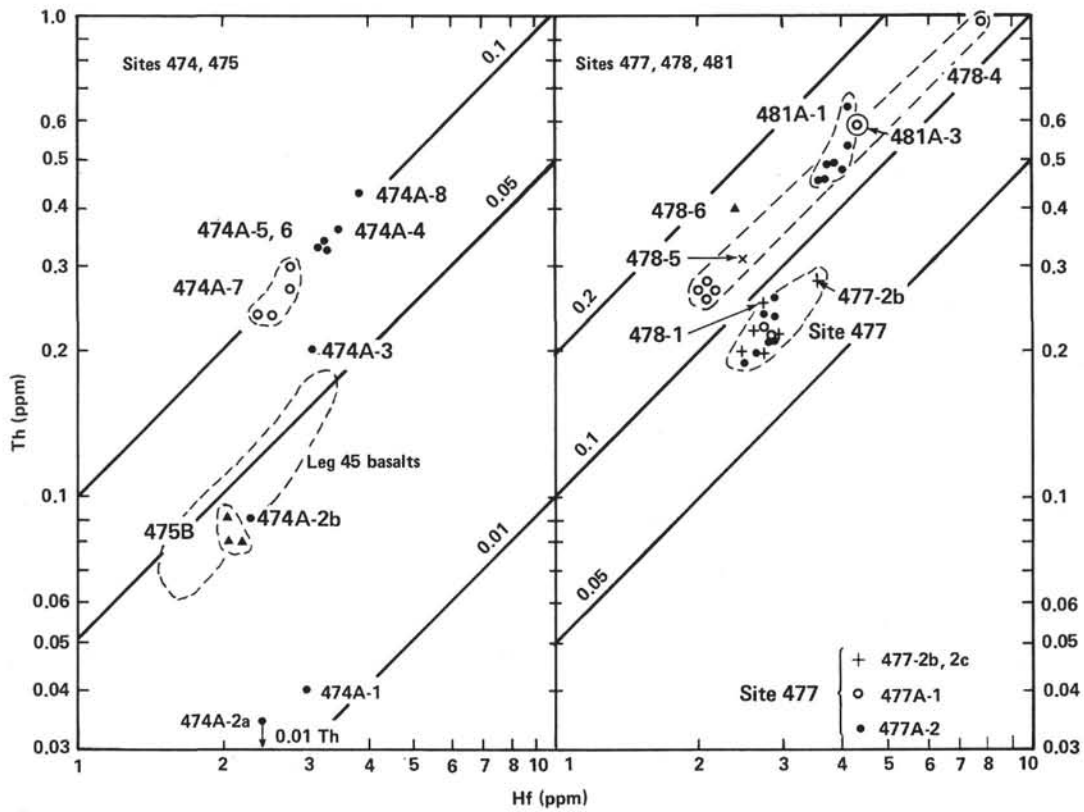


Figure 9. Th versus Hf for selected basic rocks recovered during Leg 64. (Analyses determined by INAA at Saclay. Leg 45 data from Bougault et al. [1978]. Numbers refer to igneous units.)

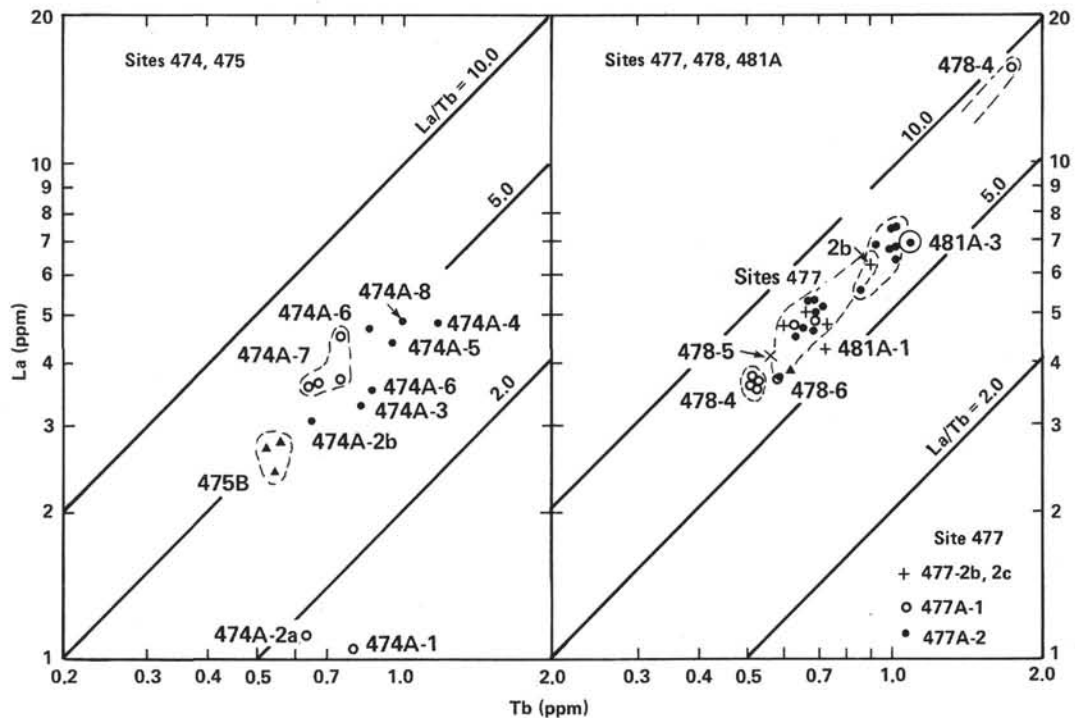


Figure 10. La versus Tb for selected basic rocks recovered during Leg 64. (Analyses determined by INAA at Saclay. Numbers refer to igneous units.)

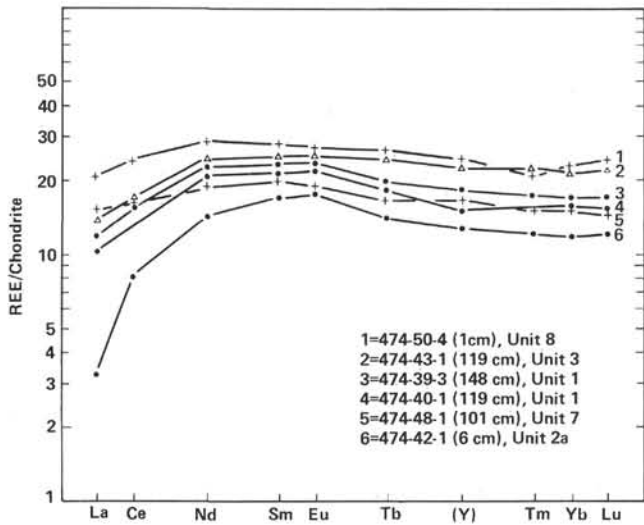


Figure 11. Chondrite-normalized REE data for basic rocks recovered at Site 474. (Analyses determined by INAA at Bedford College.)

more completely the interunit variations, some of which have been already mentioned. Certainly, the eight igneous units recovered at Site 474 are chemically diverse. For example, there is a greater range in the Zr/Y ratio in

the samples from Hole 474A than in the basalts recovered from the whole of Leg 65 (Fig. 5; Saunders, in press). Broadly speaking, the intrasite variations fall into two categories: those variations among basement (Units 4–8) and off-axis (Units 1, 2, and possibly 3) lithologies and those variations among units that comprise the basement. Initially, however, it is necessary to briefly outline the methodology involved in assessing interunit variations.

Perhaps the simplest variations are those that occur within a single unit. A typical example is Unit 1 of Hole 474A, where there are strong decreases in MgO, Ni, and Cr and antipathetic increases in the abundances of the HYG elements. The most convenient explanation for such variations would involve variable distribution of the phenocryst phases, olivine and Cr-spinel, with (cumulus?) olivine diluting the concentrations of the HYG elements. Such distributions may have resulted from post-emplacment crystal settling, but this is unlikely because there is not a significant increase in MgO, Cr, or Ni abundances toward the base of the sill. More likely, the magma had heterogeneous crystal concentrations prior to emplacement. The ratios involving the less-mobile HYG and more-HYG elements, however, are essentially constant throughout the unit (e.g., Zr/Y ratio;

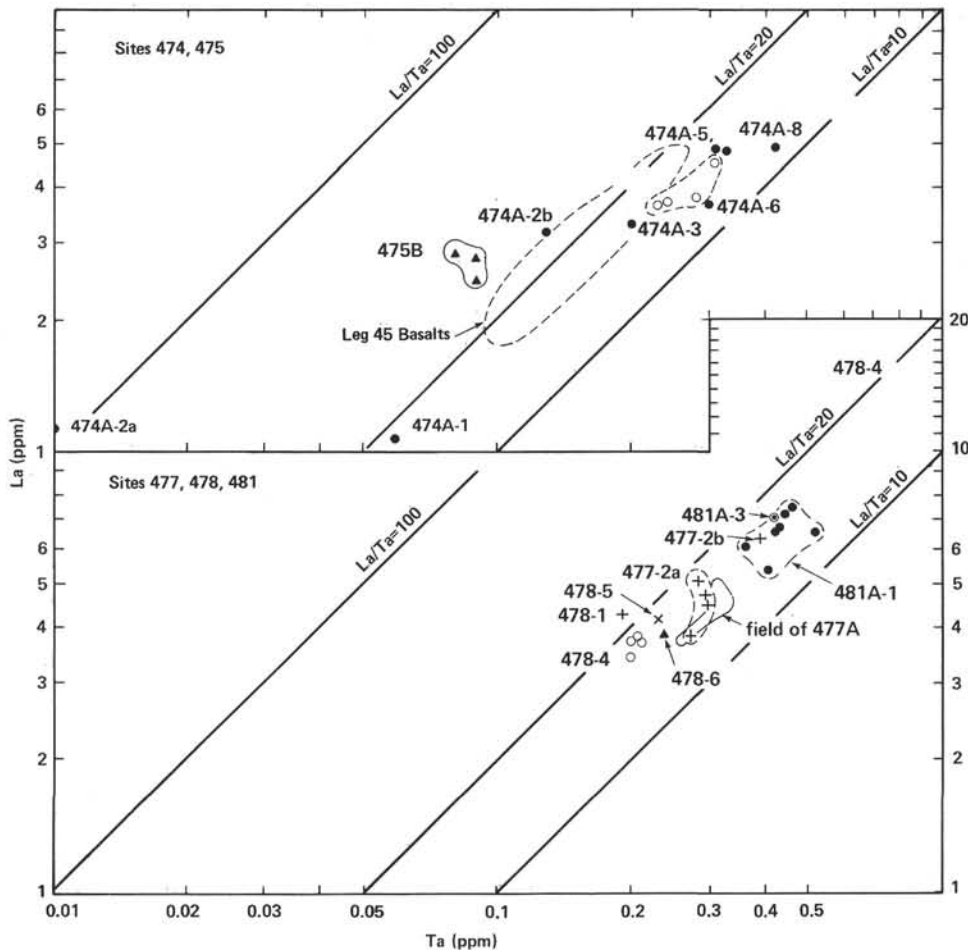


Figure 12. La versus Ta for selected basic rocks recovered during Leg 64. (Analyses determined by INAA at Saclay. Leg 45 data from Bougault et al. [1975]. Numbers refer to igneous units.)

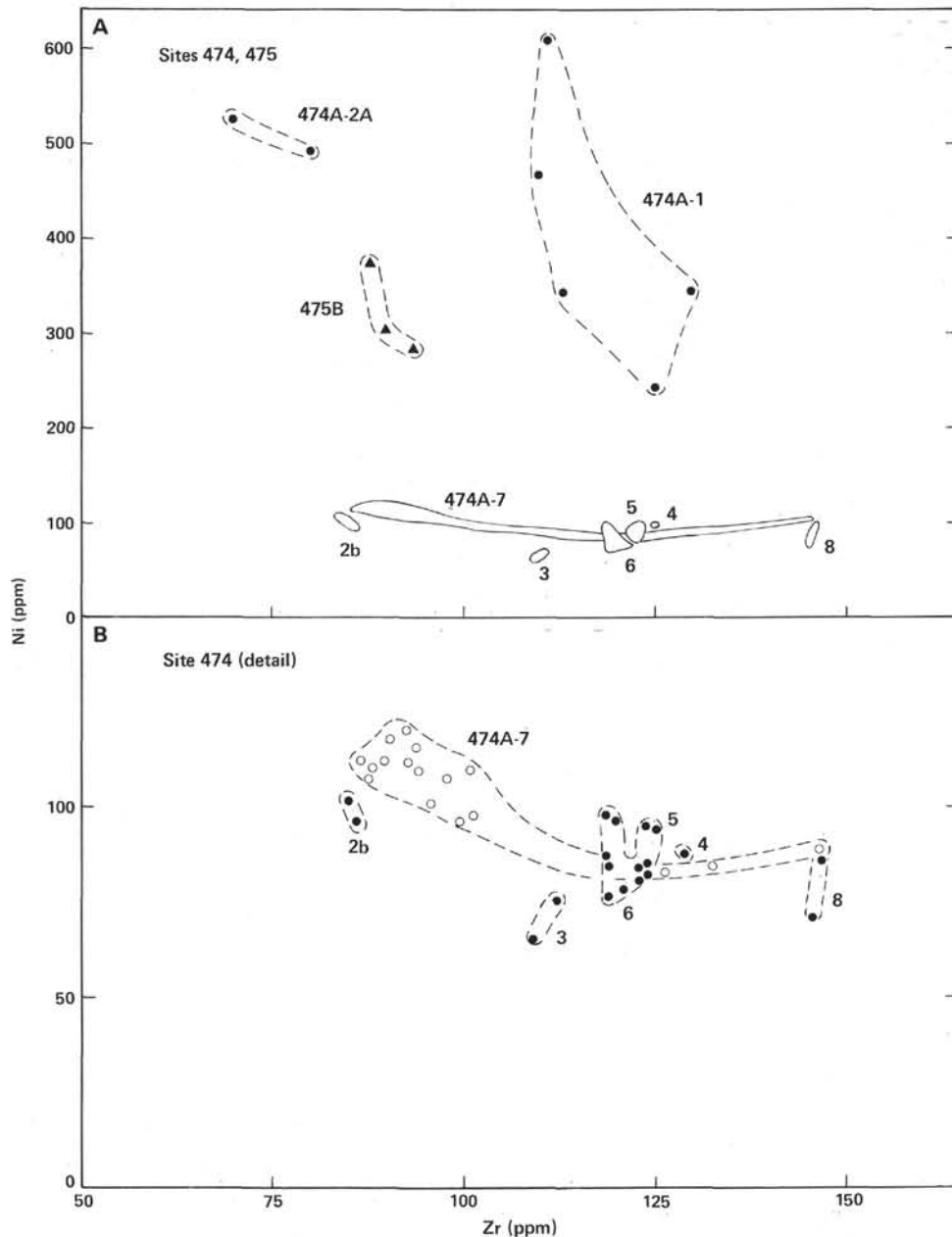


Figure 13. Ni versus Zr for basic rocks recovered at Sites 474 and 475. A. compressed abscissa to illustrate high Ni contents of 474A, Units 1 and 2a and Hole 475B. B. expanded abscissa to illustrate detail of other units recovered at Site 474. (Analyses determined by XRF at Birmingham. Symbols as in Fig. 5.)

Fig. 5). This is, of course, a function of definition: as stated earlier, HYG elements are those with bulk distribution coefficients (D) between 0.1–0.5, and more-HYG elements have D values of less than 0.01 (see Wood, Tarney et al., 1979). Thus, olivine and chrome spinel have very low distribution coefficients for most HYG elements (quantitative data are presented in Hanson, 1977 and Pearce and Norry, 1979), and so the removal (or addition) of these minerals will have no significant effect on the HYG/more-HYG ratios of the melt.

It is possible to extrapolate this line of reasoning to consider the interunit variations. If more-HYG/HYG ratios are significantly different between two units, it is possible to say with confidence that these units cannot

be directly related by closed-system/low-pressure fractional crystallization. Conversely, however, it is *not* possible to state with certainty that two or more units are related by fractional crystallization, unless all other constraints (including the relative times of emplacement and the occurrence of mineral phases necessary to complement major element modelling) are satisfied. If two units cannot be related by low-pressure fractional crystallization, it then becomes necessary to consider the progressively more complex processes of open-system fractionation (O'Hara, 1977), high-pressure fractionation (fractional crystallization or partial melting), dynamic partial melting (Langmuir et al., 1977), or source heterogeneity.

Units 1 and 2a are alkaline to subalkaline, both containing high MgO, Ni, and Cr contents and both having low more-HYG/HYG element ratios. Nevertheless, they cannot be directly related by closed system fractional crystallization. This is demonstrated in Figures 5, 9, 10, 11, and 12, which show that Unit 1 has higher Zr/Y, Th/Hf, La/Tb, La/Sm ratios and lower La/Ta ratios than Unit 2a. Although both units contain abundant (possibly cumulus) olivine and chrome spinel, it is likely that the parent melts were also magnesian, hence representing a high degree of melting of the source. Unfortunately, no fresh glass was recovered from these units.

It is equally difficult to relate Units 2b and 3 to Units 1 and 2a, the former having higher La/Tb and Th/Hf ratios. Unit 3 also has higher Th/Hf and lower La/Ta ratios than Unit 2. The only major differences in La/Ta ratio, however, are between Unit 2a ($La/Ta > 100$) and the other units of Hole 474A ($La/Ta \sim 15$), although Unit 2b has an La/Ta ratio of more than 20 (Fig. 12). Clearly, however, Units 2b and 3 cannot be related to each other or to Units 1 and 2a by closed-system fractionation.

The basement lithologies, represented by Units 4 through 8, are all subalkaline tholeiites with similar more-HYG/HYG element ratios. Thus La/Ta, Th/Hf, La/Tb, and Zr/Y ratios are essentially constant throughout all four units. In particular, Units 4, 5, and 6 are chemically very similar (e.g., Fig. 4), indicating consanguinity of magma types; these three units may well represent products from the same magma chamber. Units 7 and 8 may be related in a similar fashion, Unit 8 being a more evolved equivalent of Unit 7 (Figs. 4, 8, 13). The rhythmic basement stratigraphy (alternating pillow lavas and massive flows) is mirrored by the chemistry: the pillow lavas of each cycle appear to be chemically related to each underlying flow. Detailed modeling is required, however, before this can be stated with any confidence.

Perhaps the most important feature of the igneous samples recovered at Site 474 is the contrast in chemistry between the basement (or axis) sequence and the off-axis sequence. Units 1 and 2 are generally less fractionated, with lower more-HYG/HYG element ratios than Units 4 to 8. This is illustrated most clearly on the chondrite-normalized REE plot (Fig. 11). It will be apparent from the foregoing discussion that such variations could not be produced by closed system low-pressure fractionation even if the axis and off-axis sequences were contemporaneous. In fact, Units 1 and 2 postdate Units 4 through 8 by as many as 1.4 m.y., which, based on a 3 cm/y. half-spreading rate (Larson, 1972), implies emplacement as far as 40 km from the main spreading axis.

Similar compositional variations have been reported for the lava piles in Iceland (Gibson et al., 1976) and, in particular, the Troodos Massif, Cyprus (Smewing et al., 1975; Smewing and Potts, 1976). In Troodos, the upper pillow lavas (off-axis sequence) tend to be more basic and HYG-element depleted than the underlying axis sequence lavas. Smewing and Potts (1976), using REE data, have invoked an incremental partial melting model to derive both the axis sequence and the upper

pillow lavas from a compositionally homogeneous source. They suggest that the axis sequence lavas were formed by approximately 10% batch melting of a more-HYG element depleted mantle source followed by varying degrees of fractional crystallization. The upper pillow lavas were then produced by subsequent partial melting increments of the residue at higher levels in the mantle further from the spreading axis. Incremental partial melting (Shaw, 1970), however, has in general proved difficult to correlate with observed trace-element variations. As little as 2 to 3% partial melting will leave behind a residue too depleted to give rise to basalts with realistic abundances of HYG elements. To circumvent this problem, Langmuir et al. (1977) developed a model (continuous melting) whereby a small proportion of the liquid generated during incremental melting remains in equilibrium with the residue as melting proceeds, thus preventing the residue from becoming too rapidly depleted in HYG elements. Dynamic melting, which combines continuous melting with batch melting, can produce liquids with a larger range of trace-element ratios from a single source than batch melting. More important, continuous melting can produce second-stage liquids with more-HYG/HYG ratios *lower* than the initial source (Langmuir et al., 1977).

Wood (1979) has refined Smewing et al.'s (1976) model for the evolution of the Troodos lavas and has suggested that the dynamic partial melting model could better explain the observed differences in REE distributions between the axis sequence and the upper pillow lavas. Similarly, we would suggest that dynamic partial melting would produce the differences in REE patterns observed between the axis and off-axis sequences recovered from Hole 474A. We feel, however, that it is unlikely that dynamic partial melting alone could produce the variations in more-HYG/more-HYG element ratios (eg., La/Ta) observed between Unit 2a and the other units of Hole 474A. Resorting to some degree of mantle heterogeneity is necessary in order to explain such differences.

Recent comprehensive studies of basalts being erupted along ocean ridges, particularly along the MAR, have shown that two chemically and isotopically distinct magma types are being produced: normal, depleted mid-ocean ridge basalts (N-type MORB; Sun et al., 1979), which have low more-HYG/HYG element ratios (e.g., Th/Hf < 0.1; Rb/Sr < 0.01 [Schilling, 1971; Frey et al., 1974; Wood et al., 1979a; Bougault et al., 1980; Tarney, Wood et al., 1979, Tarney et al., 1980]); low $^{87}\text{Sr}/^{86}\text{Sr}$ ratios (0.7023–0.7027 [Hart, 1971]) and high $^{143}\text{Nd}/^{144}\text{Nd}$ ratios (0.5131–0.5133 [De Paulo and Wasserburg, 1976; O'Nions et al., 1977]); and enriched, or E-type MORB, which are typically erupted on ridge segments with positive heat flow and depth anomalies and which have high more-HYG/HYG element ratios (e.g., Th/Hf > 0.2; Rb/Sr \sim 0.04 [Hart et al., 1973; Wood, Tarney et al., 1979, Wood, Joron et al., 1979; Tarney, Saunders et al., 1979; Tarney, Wood et al., 1979; Tarney et al., 1980]). In addition, E-type MORB have higher $^{87}\text{Sr}/^{86}\text{Sr}$ ratios (0.7027–0.7035 [White et al., 1976]) and lower $^{143}\text{Nd}/^{144}\text{Nd}$ ratios (< 0.5131 [O'Nions et al.,

1977)) than N-type MORB. The E-type MORB are erupted on many ocean islands and at certain segments along the MAR (e.g., 45°N), often in association with N-type MORB; and in a spatial sense E-type and N-type MORB tend to be gradational (e.g., along the Reykjanes Ridge; see Tarney, Wood et al., 1979).

Even in the absence of isotopic data, the basalts recovered from Hole 474A are chemically similar to N-type MORB. They all have low more-HYG/HYG element ratios and very low contents of more-HYG elements. This is illustrated on Fig. 15, where the data for Units 2a and 7 are plotted on a mantle-normalized diagram, with examples of N-type and E-type MORB (Sun et al., 1979; Wood, Joron et al., 1979). Unit 7 compares favorably

with N-type MORB, although the anomalously high level of Cs may be a result of low-temperature interaction between the basalt and seawater. The dramatic depletion of several more-HYG elements (Th, Ta) in Unit 2a is shown in Fig. 15, but again we feel that the high levels of Cs, Rb, K, and Ba result from interaction of the dolerite with seawater or sediment porewater and are not primary abundances. This post-emplacement effect is even more noticeable in the dolerite and gabbro sills recovered from the Guaymas Basin sites, where hydrothermal circulation clearly played an important role.

There is as yet no consensus on the nature of suboceanic mantle heterogeneity, but Tarney et al. (1980) have

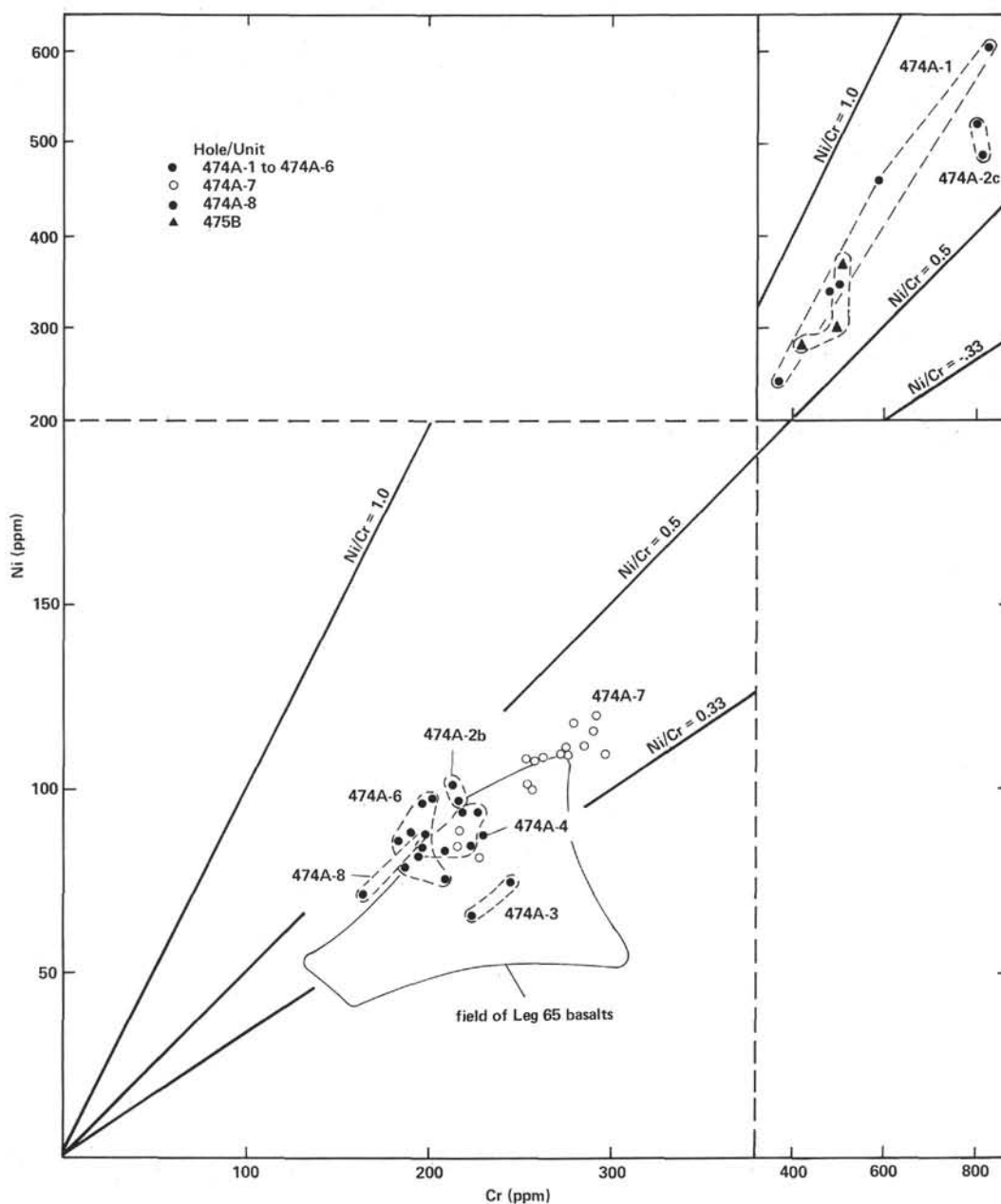


Figure 14. Ni versus Cr for basic rocks recovered at Sites 474 and 475. (Analyses determined by XRF at Birmingham. Symbols as in Fig. 5.)

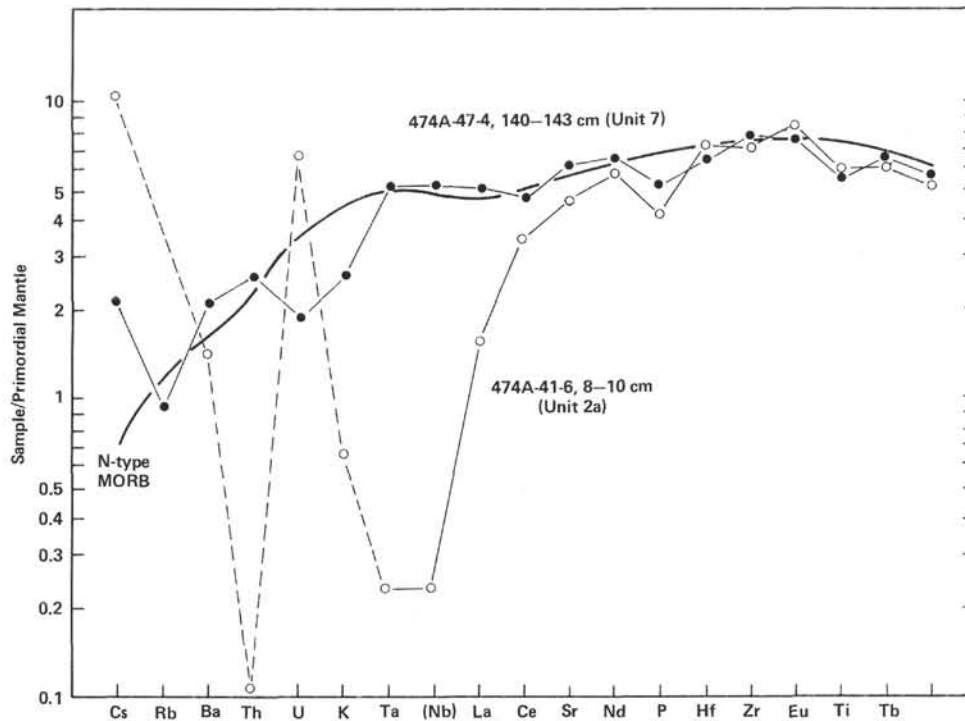


Figure 15. Data from Units 2a, Hole 474A, and 7, Hole 474A, plotted on a mantle-normalized diagram with an N-type MORB. (Normalizing values and data for N-type MORB from Wood et al. [1979b]. Cs, Rb, Th, U, Ta, La, Ce, Lu, Tb determined by INAA at Saclay; others determined by XRF at Birmingham.)

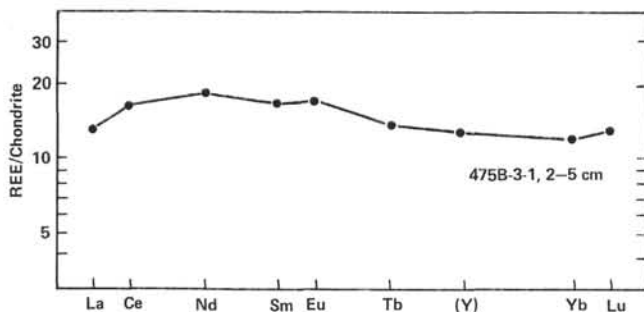


Figure 16. Chondrite-normalized REE data for basalts recovered at Site 475. (Analyses determined by INAA at Bedford College.)

proposed a model whereby a depleted refractory host mantle is variably veined by alkalic, more-HYG enriched melts derived in turn from a deep mantle source. This model is to some extent inspired by the work of Lloyd and Bailey (1975), Hanson (1977), and Frey et al. (1978) who have invoked similar metasomatizing fluids to explain the enriched chemistry of oceanic and continental alkalic basalt suites. The veined mantle model has the advantage of allowing derivation of chemically diverse magmas from the same mantle source. In the present case, we would envisage that the mantle giving rise to the axis magmas (Units 4–8) contained a small (~0.5%) component of alkalic veins with low La/Ta ratios (~11; Tarney et al., 1980). During partial melting beneath the spreading center (ca. 10–20% melting; Sun et al., 1979), these veins would completely melt, with a proportion of depleted host mantle, to produce the

magmas that eventually gave rise to Units 4 through 8. Melting of the veins will selectively deplete the bulk mantle in those elements most highly concentrated in the veins (Ta, Nb, Th, Cs, Rb, K) thus changing the La/Ta and La/Th ratio of the *bulk source*. Remelting of this now depleted, veinless mantle could then produce Unit 2a with its very high La/Ta ratios. Note, however, that the Ta/Th ratio remains constant throughout *all* of the units of Hole 474A (cf. Fig. 27).

The similarity of La/Ta ratios between Units 4 through 8 and N-type MORB (15–20) implies that most N-type MORB may be derived from a source containing a small component of alkalic, more-HYG/element-enriched veins. This is not inconsistent with the veining model of Tarney et al. (1980), which, to satisfy isotopic constraints, requires that the veining be a continuous and still occurring event.

It is necessary to briefly compare the Site 474 samples with basalts recovered closer to the EPR during Leg 65; more detailed comparisons will be presented elsewhere (Saunders, in press). The Leg 65 samples analyzed at Birmingham and Bedford are essentially N-type MORB (e.g., Rb/Sr ~ 0.01, La_N/Yb_N ~ 0.5, Zr/Nb ~ 40, La/Ta ~ 20), and for comparative purposes trends or fields of Leg 65 are given on several of the diagrams in this chapter. In general, the Leg 65 basalts are more depleted in more-HYG elements than the axis sequence from Hole 474A (comparisons with the off-axis sequence are not relevant at this stage). This is demonstrated by the slightly lower Zr/Y ratios (Fig. 6) and generally lower La/Sm and La/Yb ratios in the Leg 65 basalts (based

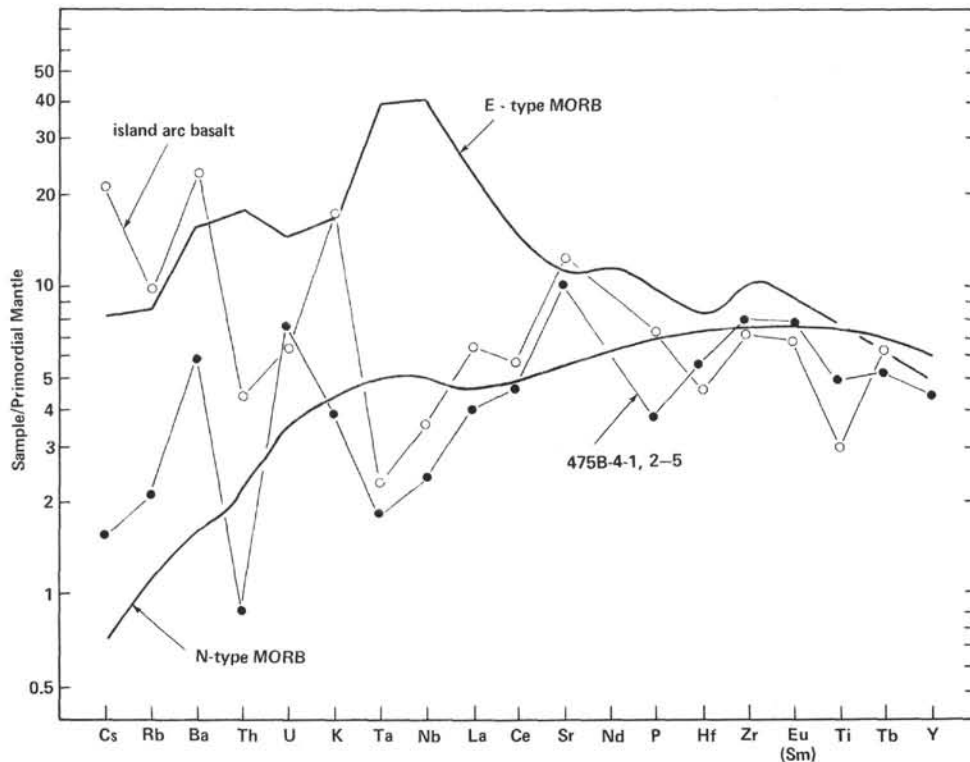


Figure 17. Analysis of basalt from Site 475 plotted on a mantle-normalized diagram with an N-type MORB, an E-type MORB, and an island-arc basalt for comparison, Site 475. (Normalizing values and data for N-type MORB are from Wood et al. [1979b]. Island-arc basalt is from sample 456A-13-1, 23–26 cm recovered from the Mariana Ridge during DSDP Leg 60 [Wood et al., in press]. E-type MORB is from Tarney et al. [1980].)

on the Bedford data, Hole 474A, Units 4–8 has $La_N/Yb_N \sim 0.9$, whereas the Leg 65 basalts generally have $La_N/Yb_N = 0.4-0.6$. In addition, the Leg 65 basalts have higher Ti/Zr ratios (100–130) than the axis lavas from Hole 474A (80–110; Saunders, in press). These differences could be reasonably explained by variable degrees of partial melting, and recourse to mantle heterogeneity may not be necessary.

Finally, none of the basalts from either of the off-axis or axis sequences of Site 474 appear to contain any component of orogenic basalt chemistry. Many back-arc basin basalts do appear to be transitional in chemistry between MORB and the adjacent arc magmas (e.g., Gill, 1976; Saunders and Tarney, 1979; Weaver et al., 1979; Saunders, Tarney, and Weaver, 1980), suggesting involvement of large-ion lithophile (LIL) element-enriched fluids in the formation of the back-arc basalts. It has been proposed that these fluids are derived from the adjacent subduction zone. Orogenic basalts are typically quartz normative (although they may be olivine-hypersthene or rarely nepheline normative), have a low abundance of Ni and Cr, and have high LIL (e.g., K, Rb, Ba, Sr, Th)/high field strength (HFS; e.g., Ti, P, Zr, Nb, Ta) element ratios (Jakes and White, 1972; Ringwood, 1974; Dixon and Batiza, 1979; Hawkesworth et al., 1979; Saunders, Tarney, Marsh et al., 1980). Although some primitive island-arc tholeiites may be light-REE depleted (Hawkesworth et al., 1977) most orogenic basalts have $La_N/Yb_N > 1$, again unlike the Site 474 samples.

Those elements that show relative enrichment in orogenic magmas—i.e., the LIL elements—are of course also those elements whose abundances are most likely to be affected during alteration of basalt by seawater. The interpretation of trace-element patterns in altered basalts and dolerites may therefore be rather subjective, and in this context it is necessary to reconsider the distribution of LIL and HFS elements in Units 1 and 2a (Fig. 15). The high abundances of several LIL elements relative to Ta has been interpreted as being caused by seawater alteration of Ta-depleted (and indeed originally Cs-, Rb-, K-, Th-, Ba-, and U-depleted) melt. It is unlikely that these dolerites represent orogenic magmas, because of their low Th/Ta ratios (cf. the pattern for an orogenic basalt in Fig. 17); Th appears to be one of the few LIL elements not easily mobilized during seawater alteration of basaltic rocks.

Site 475

Site 475 lies in a slope basin approximately 21 km southeast of the tip of Baja California (Fig. 2), a position selected to delineate the continent/ocean crust transition. The site lies on a continuation of the northeasterly trend of Cabrillo Seamount (Fig. 2), from which granites, granodiorites, and quartz diorites have been recovered (Shepard, 1964; Moore et al., 1978; Fornari et al., this volume). Drilling at neighboring Site 476 recovered calc-alkaline granite (Saunders and Fornari, this volume), but Lewis et al. (1975) dredged basalt from a location (DH-8 on Fig. 2) northwest of the site.

Three holes were drilled at Site 475. The first was abandoned after penetrating a sequence of diatomaceous silty clays, zeolite-bearing clays, and finally an early Pliocene(?) conglomerate. Hole 475A yielded a small amount of dolomitic limestone. Drilling in Hole 475B (23°3.36'N; 109°3.57'W, 2593 m water depth), and was more successful: basalt was encountered at 76 meters sub-bottom, and coring continued for an additional 20 meters before the hole had to be abandoned. Unfortunately, absence of sediment from immediately above the basalt means that accurate dating is not possible, but by extrapolation from Hole 475, the basalt may be early Pliocene.

The basalt is extensively fractured, with occasional fresh glassy selvages and quench textures indicating subaqueous extrusion. The presence of brown-stained, weathered rims on several fragments, however, suggests that the basalt may have been in the form of cobbles prior to drilling.

All of the basalt recovered at Hole 475B is mineralogically similar and may be considered as a single type. It contains approximately 10% anhedral to euhedral olivine phenocrysts (0.2–2.0 mm; FO_{87}) and trace amounts of chrome spinel phenocrysts. No vesicles are present, and alteration in the centers of the cobbles is very slight.

Three samples of the basalt were analyzed. The results are presented in Tables 5 (XRF), 6 (INAA, Saclay), and 7 (INAA, Bedford). The samples have similar chemical compositions, which corroborates the petrographical observation that the basalt belongs to a single unit. The data have been plotted with those from Hole 474A. Immediately obvious are the high contents of MgO, Ni, and Cr in the Hole 475B basalt. In this respect they resemble Units 1 and 2a of Hole 474A, but there is a much lower content of phenocryst olivine in the Hole 475B basalt. Ratios of FeO/MgO are low (Fig. 4), and the basalts are slightly nepheline normative (Fig. 5). Note also that the basalt has Ni/Cr ratios similar to those of Unit 1, Hole 474A (Fig. 14).

The contents of the HYG and more-HYG elements are generally low, reflecting the unfractionated nature of the basalts. The Y/Zr (Fig. 6) and La/Tb (Fig. 10) ratios of the Hole 475B basalts are similar to those from Units 4 through 8 (Hole 474A), and although the La_N/Yb_N ratio is greater than one, the basalts still exhibit relative light-REE depletion ($La_N/Sm_N = 0.8$; Fig. 16). The REE data (Fig. 16) suggest that sample 475B-3-1, 2–5 cm has a slight positive europium anomaly. This may be real and would correlate with the high Sr content; but in the absence of plagioclase phenocrysts could not be the result of crystal accumulation.

Not all of the ratios of HYG and more-HYG elements are similar to those found in Units 4 through 8 from Hole 474A. For example, Ba and Sr (and to a lesser extent K_2O and Rb) contents are higher than in most fresh basalts from Hole 474A or from Leg 65, as shown on the plots of Ba versus Zr (Fig. 7) and Sr versus Zr (Fig. 8). Also, the basalt from Hole 475B has low Th/Hf (0.06; Fig. 9) and high La/Ta (29; Fig. 12) ratios, indicating relative depletion in Th and Ta.

Table 5. X-ray fluorescence analyses, Hole 475B.

Core Section Level (cm)	2 01 2	3 01 2	4 01 2
SiO ₂	47.2	47.2	46.8
TiO ₂	1.29	1.33	1.27
Al ₂ O ₃	16.4	16.6	16.2
tFe ₂ O ₃	10.72	10.44	10.31
MnO	0.14	0.14	0.21
MgO	9.47	8.66	10.68
CaO	11.18	11.56	11.48
Na ₂ O	2.75	2.90	2.76
K ₂ O	0.14	0.17	0.12
P ₂ O ₅	0.08	0.09	0.08
LOI	0.69	1.26	—
Total	100.11	100.32	99.88
Trace Elements (ppm)			
Ni	302	286	377
Cr	492	419	509
Zn	70	68	68
Ga	19	20	19
Rb	3	4	<1
Sr	253	261	239
Y	24	25	22
Zr	90	93	88
Nb	1	2	2
Ba	46	54	52
La	4	6	5
Ce	9	12	10
Nd	9	11	10
Pb	6	3	<1
Th	3	2	<1
Selected Ratios			
Zr/Nb	90	47	44
Ti/Zr	86	86	87
Y/Zr	0.27	0.27	0.25
Ce/Zr	0.10	0.13	0.11
Ba/Zr	0.51	0.58	0.59
(Ce/Y) _N	0.92	1.18	1.12
Fe/Mg	1.31	1.40	1.12
K/Rb	387	353	>996
Ba/Sr	0.18	0.21	0.22
CIPW Norms			
Q	0.0	0.0	0.0
Or	0.8	1.0	0.7
Ab	22.1	21.4	18.6
An	32.0	31.6	31.4
Ne	0.6	1.6	2.6
Di	18.6	20.4	20.3
Hy	0.0	0.0	0.0
Ol	19.7	17.3	21.1
Mt	1.9	1.8	1.8
Il	2.4	2.5	2.4
Ap	0.2	0.2	0.2

Note: See Table 1, note.

Site 475: Discussion

The basalt recovered at Site 475 has high MgO, Ni, and Cr contents, which suggest that the composition is not far removed from a primary mantle melt. This is supported to some extent by the high forsterite content (FO_{87}) of the olivine phenocrysts. The low modal olivine

Table 6. INAA results (Saclay) on selected samples, Hole 475B.

Core Section Interval (cm)	2 1 2-5	3 1 2-5	4 1 2-5
Ni	337	299	412
Cr	407	364	460
Co	54.8	53.4	59.8
Sc	29.1	30.1	28.6
Ba	36	43	45
Sr	—	319	—
Cs	0.27	0.27	0.03
Rb	2.5	3.2	1.8
U	—	0.1	0.21
Th	0.09	0.08	0.08
Zr	88	112	86
Hf	2.10	2.22	2.06
Ta	0.09	0.09	0.08
Sb	0.04	0.04	0.02
La	2.45	2.77	2.85
Ce	9.9	11.0	9.3
Eu	1.12	1.11	1.15
Tb	0.56	0.57	0.53

Note: All values in ppm.

Table 7. INAA results (Bedord) on a selected sample, Hole 475B.

Core Section Interval (cm)	3 1 2-5
La	4.32
Ce	14.5
Nd	11.8
Sm	3.4
Eu	1.41
Tb	0.72
Yb	2.70
Lu	0.45
Th	0.15
Hf	2.36
Ta	0.15
La _N /Yb _N	1.07
La/Ta	29
Th/Hf	0.06

Note: Trace-element values in ppm.

phenocryst content indicates that the whole-rock analysis reasonably represents the liquid composition, and this has been confirmed by subsequent microprobe analysis of the glassy selvages (Fornari et al., this volume, Pt. 2). In addition, the absence of plagioclase phenocrysts and negative europium anomalies—suggesting that no plagioclase fractionation has occurred—means that the Sr/HYG element ratio may also reflect the parental melt ratio.

An unusual feature about this basalt is that although it is mildly alkaline in its major element chemistry, it has very low abundances of the more-HYG elements (e.g., Th, Ta, La, Ce), even when compared to N-type MORB. This is illustrated in Fig. 17, where Sample 475B-4-1, 2-5 cm is plotted with N- and E-type MORB and an

island-arc basalt on a mantle-normalized diagram (see Site 474 discussion). The differences between the Site 475 basalt and N-type MORB become immediately obvious: The former has high La/Ta and La/Th ratios caused by low values of Ta and Th. In addition, the Hole 475B basalt has significantly higher Sr/La, Ba/La, and U/La ratios than N-type MORB. While it is not possible to completely rule out alteration of the basalt by seawater (note that although most of the fragments have weathered rims, these were carefully avoided during sampling), the tight clustering of the data points on the biaxial plots strongly indicates that this is not an important factor. Therefore, the relatively high abundances of at least Sr and Ba, and possibly also U, may be primary. In some ways the Hole 475B basalt resembles island-arc basalts: high La/Ta, La/Nb, Sr/La, and Ba/La ratios. In other respects, however, the comparison breaks down: low Th/Ta and Th/La ratios, low abundances of many of the LIL elements (Cs, Rb, K, Th), and high Ni and Cr contents. Of course, the two lines on Figure 17 for N-type MORB and island-arc basalts hardly represent *all* depleted ocean ridge or orogenic basalts, respectively, but they do indicate the salient features of the two magma "types" (e.g., Joron and Treuil, 1977; Wood, Joron et al., 1979b; Sun et al., 1979; Tarney et al., 1980).

To explain the unusual geochemistry of the Hole 475B basalts, we may invoke two processes: (1) mixing of chemical components of N-type and orogenic basalts, which occurred during magma mixing or because of a complex mantle source chemistry; and (2) derivation of the basalt from a depleted mantle source (perhaps similar to the source of N-type MORB) and subsequent contamination of the magma during ascent through continental crust. Bearing in mind the tectonic setting of Site 475, both of these processes must be considered.

As mentioned in the Site 474 discussion, island-arc and destructive continental margin magmas typically have high LIL/HFS element ratios (e.g., Th/Ta, K/Zr ratios). On the mantle-normalized plot, this is shown by relative enrichments of the elements Cs through K and Sr and depletion in Ta, Nb, Zr, Hf, and Ti (Fig. 17). The enrichment of the LIL elements is probably a result of their selective removal from the dehydrating subducted oceanic lithosphere (Hawkesworth et al., 1979; Saunders et al., 1980), whereas the depletion of the HFS elements probably results from their immobilization in both the subducted crust and overlying mantle wedge (Wood, Joron, Treuil et al., 1979; Saunders et al., 1980a). Site 475 certainly is closely adjacent to a calc-alkaline province—the neighboring Hole 476 recovered a calc-alkaline granite (Saunders and Fornari, this volume, Pt. 2)—so the potential for involvement of sub-orogenic belt mantle is present. Whether or not orogenic magma was being produced in southern Baja California during the Pliocene is more contentious: it would appear that active subduction had stopped several million years before (Dickinson and Snyder, 1979). Therefore, we feel that actual magma mixing is improbable. More likely, the Hole 475B basalt has been derived from a mantle source, which has an overall depleted chemistry

similar to the N-type MORB source but which contains a small but *variable* component of mantle involved in Mesozoic-Tertiary subduction zone activity. This is a model similar to that described for back-arc basalts from Bransfield Strait, Antarctica (Weaver et al., 1979), from the Scotia Sea (Saunders and Tarney, 1979), and from some western Pacific marginal basins (Tarney et al., in press). Indeed, Penguin Island, which is a Recent off-axis volcano in Bransfield Strait, and lies on continental crust, has erupted primitive basalts with several of the characteristics of the Site 475 basalt: it is nepheline normative, has similar low contents of the HFS elements, and has high LIL/HFS element ratios. Penguin Island basalt does have a La_N/Yb_N ratio of 4, but this was attributed by Weaver et al. (1979) to the fractionation effect of residual garnet: the source probably has a La_N/Yb_N ratio of less than one.

Derivation of the Hole 475B basalt from a mantle source similar to that of N-type MORB, followed by assimilation of small quantities of continental crust, is an alternative (but not mutually exclusive) model, but it does not readily explain the depletion in Ta and Th. Assimilation of calc-alkaline-type material should not result in an absolute decrease in Ta and should result in enhancement of Th values (see for example the Th contents in the Site 476 granite; Saunders and Fornari, this volume, Pt. 2; Saunders, Tarney, Marsh et al., 1980). It is possible that the mantle source for the Hole 475B basalt is depleted in Ta relative to N-type MORB source—which may simply reflect the lack of comprehensive data on MORB—but the absence of enrichment of Th is less easily explained. We feel that until more data are available on other Tertiary basalt suites from Baja California and until Sr and Nd isotopes are determined on the 475B basalts, the case for crustal contamination must remain open. Nevertheless, the suggestion that the Site 475 basalts have been derived from a depleted, N-type MORB source concurs with the proposal of Dickinson and Snyder (1979) that a no-slab window (and hence by inference a predominantly 'Pacific-type' mantle) has underlain this region of Baja California for several million years.

GUAYMAS BASIN TRANSECT—SITES 477, 478 AND 481

The Guaymas Basin, situated approximately midway along the Gulf of California, contains two short segments of spreading axis separated by a 20-km-long transform fault (Fig. 18). The basin is characterized by rapid sedimentation rates which, combined with high rates of ocean floor spreading (~ 3 -cm/y. half rate; Larson, 1972), have resulted in an unusual seismic and magnetic crustal structure. A two-layer solution, involving intercalation of Oceanic Layers 1 and 2, better fits the data than the normal three-layer oceanic crust model (Phillips, 1964; Lawver et al., 1975; Lawver and Hawkins, 1978).

Sites 477 and 481 are in the southern and northern rifts, respectively, whereas Site 478 is on the basin floor, approximately 12 km northwest of the southern rift (Fig. 18). Igneous rocks were recovered at all three sites

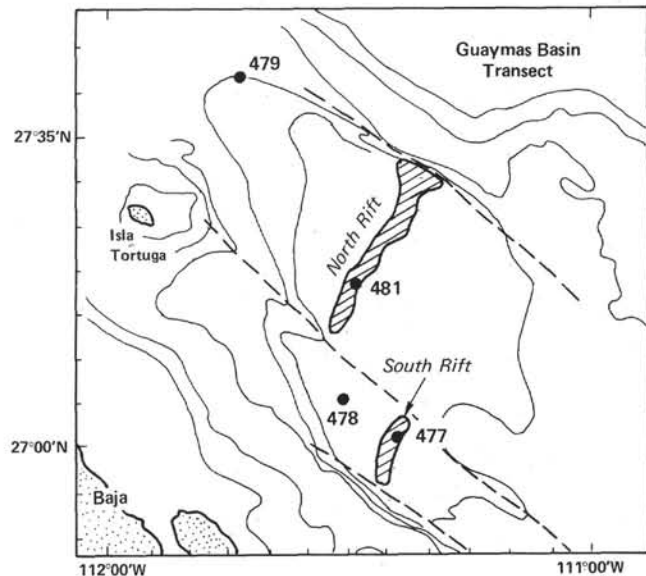


Figure 18. Map of the Guaymas Basin showing the location of Sites 477, 478, 479, and 481 and major tectonic features.

in the basin, and the usual lithology comprised basaltic, doleritic, or even gabbroic sills intruded in sediments; unequivocal basaltic flows were not drilled. The results of the drilling thus provide a striking confirmation of the conclusions drawn from the geophysical surveys.

Site 477

Three holes were drilled in the southern rift of the Guaymas Basin. Hole 477 ($27^{\circ}01.85'N$; $111^{\circ}24.02'W$, 2003 m water depth) was drilled and continuously cored to a depth of 191 meters before it had to be abandoned. Pebbles of basalt (Unit 1), with glassy rinds and baked-clay selvages, were recovered in Core 477-7; no samples were taken for analysis. A dolerite sill (Unit 2) was cored between 58 and 100 meters sub-bottom.

In Hole 477A, a dolerite sill complex (Units 1, 2) was encountered at 34 meters sub-bottom and cored until its base was reached at 60 meters sub-bottom. These sills, and that in Hole 477, were emplaced in diatomaceous turbidites, which have been hydrothermally altered both above and below the intrusions. Some of the alteration is undoubtedly related to the emplacement of the sills (Einsele et al., 1980), but the very high heat flow recorded at this site must be caused by further active intrusion at a relatively shallow depth. This concurs with the estimated age of the entire section drilled—sediments and intrusions are Quaternary to Recent ($\leq 50,000$ y., if accepted spreading rates are used).

Hole 477B was drilled for 4.6 meters using the hydraulic piston corer, and only sediments were recovered. It will not be considered further here.

Hole 477

Unit 2 (42.0 m)

Unit 2 comprises feldspar-phyric to aphyric dolerite, and consequently the shipboard party divided the unit

into three subunits on the basis of the presence or absence of feldspar phenocrysts (Fig. 19). Unit 2a consists of the uppermost 0.2 meters of dolerite recovered in Sections 477-7, CC through 477-9-1 (14 cm). It is a friable, water-permeated, coarse-grained dolerite containing abundant (as much as 15%) plagioclase (An_{60-70}) phenocrysts, and is mineralogically and texturally indistinguishable from the upper portion of Unit 2c. The groundmass or interstitial material in the dolerite has been completely replaced by green clay minerals, many of which have been removed during subsequent hydrothermal activity. Thus, even though the major constituent minerals (olivine, clinopyroxene, plagioclase) are fresh, no samples were analyzed.

Unit 2b is an aphyric dolerite of which only 0.5 meters were recovered in Sections 477-9-1 (15 cm) through 477-10-1 (15 cm). Its total thickness is not known. As with the dolerite of Unit 2a, the rock is friable and permeated by water, although one sample was taken for analysis.

Unit 2c forms the major part of Unit 2, representing about 11.6 meters of recovery and having a total thickness of approximately 30 meters (Fig. 19). It is texturally and mineralogically variable, ranging from strongly feldspar-phyric (as much as 30% plagioclase phenocrysts; Table 8) to more sparsely feldspar-phyric and having coarse-grained basaltic (lower margin) to coarse-grained doleritic (almost gabbroic in the center of the unit) textures. Plagioclase phenocrysts range in size from 1 to 5 mm, and the groundmass olivine and pale brown augite ranges from 0.5 to 4 mm; the olivine is subordinate to the augite in both size and abundance. There is an apparent slight increase in modal olivine content in the lower part of Unit 2c, an observation not supported by subsequent chemical analysis. The interstices between the individual mineral grains are filled with soft, pale green clay minerals as in Units 2a and 2b, and again the individual mineral grains are unaltered. As much as 15% of the rock may comprise these secondary alteration materials.

The analyses of dolerite from Hole 477 are given in Tables 9, 10, and 11. All of the samples are subalkaline tholeiites (Fig. 20), but Unit 2b has lower MgO (6.95%) and Ni (48 ppm) contents and a higher FeO/MgO ratio than Unit 2c (Figs. 19, 21). The Al_2O_3 content of Unit 2c is significantly higher than that of Unit 2b, which is consistent with the higher-modal plagioclase content of the former unit. The abundances of the HYG and more-HYG elements increase systematically from Unit 2c to 2b (e.g., Zr and TiO_2 in Fig. 21), but ratios involving more-HYG and HYG elements remain essentially constant between the two units (e.g., Y/Zr, Fig. 22; Ba/Zr, Fig. 23; La/Sm, and La/Yb, Fig. 24). Indeed, the chondrite-normalized REE patterns of the two units are remarkably similar (Fig. 24). Although the La_N/Tb_N ratios (e.g., Fig. 10) are slightly greater than 1, the La_N/Sm_N ratios are in fact less than 1; i.e., the dolerites are relatively light-REE depleted. In addition, the Th/Hf (~0.08; Fig. 9) and La/Ta (~15; Fig. 12) ratios demonstrate low abundances of Th and Ta, and the analyses in Tables 9 through 11 indicate that other more-HYG elements (e.g., Cs, Rb, K) also have low

levels similar to N-type MORB. The dolerites from both units, however, have high Sr contents which may in part be a result of alteration by seawater or sediment porewaters; but the tight clustering of the data points indicates that the values may be primary. To what extent the primary Sr levels represent liquid compositions is also unknown although the consistently high Sr levels in sparsely plagioclase-phyric samples suggests that the effect of cumulus plagioclase is minor. Cumulus plagioclase would of course have the combined effect of diluting the concentration of many HYG elements and enhancing the concentration of Sr. In the absence of positive Eu anomalies, however, it is not possible to assess the importance of plagioclase accumulation.

The similarity of the more-HYG/HYG element ratios and the form of the chondrite-normalized REE patterns of Units 2b and 2c suggest that the units have been derived from the same parental magma by low-pressure fractional crystallization. Removal of plagioclase alone, however, while increasing the abundances of the HYG elements, does not explain the lower levels of Ni and MgO in Unit 2b. This requires the removal of olivine from Unit 2c, and even though olivine is present in these dolerites, it could not be ascertained whether it is a phenocryst or groundmass phase. Removal of approximately 30% crystals (plagioclase and olivine) from Unit 2c would produce a magma with the trace-element characteristics of Unit 2b.

Hole 477A

Unit 1 (7.0 m)

Only 1.7 meters of Unit 1 were recovered (Fig. 19). The upper chill zone is preserved as fresh, glassy selvages with roopy surfaces in Section 477-1-1 and consists of 80% quenched groundmass containing 5% each of olivine and plagioclase phenocrysts (Table 12). Down-hole, the quenched basalt becomes progressively plagioclase-rich and coarser grained to form a plagioclase-phyric, medium-grained (intergranular) dolerite. The samples from Unit 1 are relatively fresh, containing less than 5% secondary clay minerals.

Unit 2 (14.5 m)

The bulk-density log indicates that a sedimentary intercalation occurs between Units 1 and 2. The upper margin of Unit 2 is indicated by a glassy selvage and aphanitic groundmass textures in Section 477A-2-1. The basalt contains as much as 15% large (as large as 10 mm) plagioclase phenocrysts, a modal percentage that does not change significantly as the basalt grades down-hole into dolerite and gabbro (Table 12). Further down-hole, however, in Section 477A-3-3, the dolerite/gabbro becomes increasingly olivine-rich, but near the bottom of Section 477A-3-3 the rock abruptly reverts to a plagioclase-phyric dolerite. Unit 2 contains two vesicular zones, schematically represented in Fig. 19. The first, between Sections 477A-2-2 (20 cm) and 477A-2-3 (66 cm), contains up to 6 modal percent vesicles, 0.75 to 5.0 mm in diameter, which are invariably unfilled. The second occurs in Sample 477A-3-1, 65–105 cm and contains up to 14% 1 mm diameter vesicles.

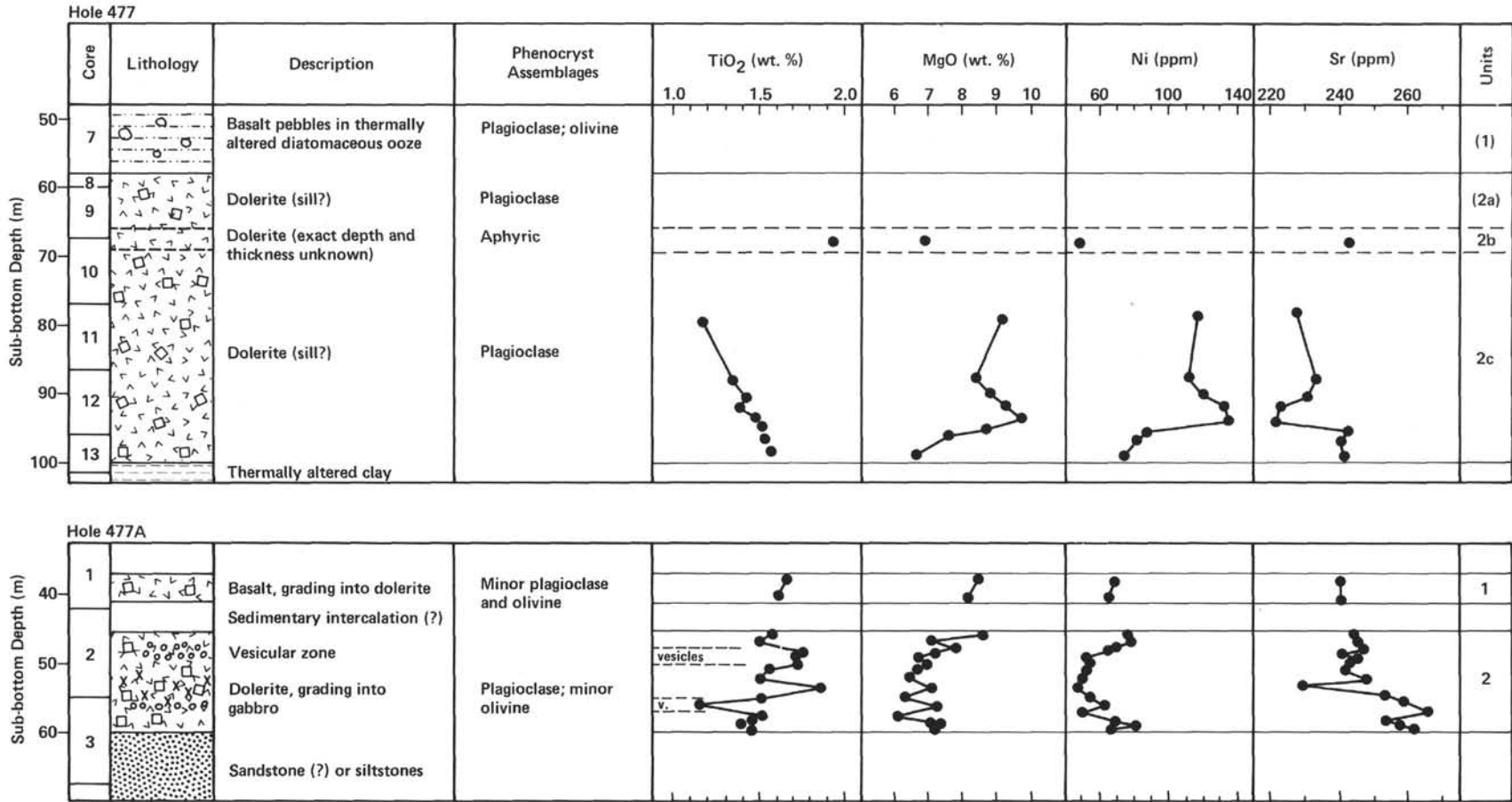


Figure 19. Downhole variations in lithology and selected geochemical parameters, Holes 477 and 477A. (Analyses determined by XRF at Birmingham.)

Table 8. Representative modal analyses of dolerites (%), Hole 477.

Core Section	9	9	11	12	12	13
Interval (cm)	13	32	43	110	45	52
Unit	2a	2b	2c	2c	2c	2c
Plagioclase (phenocrysts)	13.2	—	29.0	7.7	26.0	20.0
Plagioclase (groundmass)	44.3	50.4	35.3	47.2	27.0	31.0
Clinopyroxene	17.2	28.6	15.3	17.2	12.0	13.0
Olivine	6.4	3.1	6.3	11.4	11.0	14.0
Titanomagnetite	4.0	7.3	3.6	2.8	11.0	11.0
Clay minerals	10.9	6.5	7.2	11.5	13.0	11.0
Zeolite	—	0.3	—	—	—	—
Cavity	3.9	3.7	3.2	2.2	—	—

Note: Analyses determined using at least 600 point counts per sample. The distinction between phenocryst and groundmass plagioclase is problematic because of the seriate textures in the more coarse-grained samples.

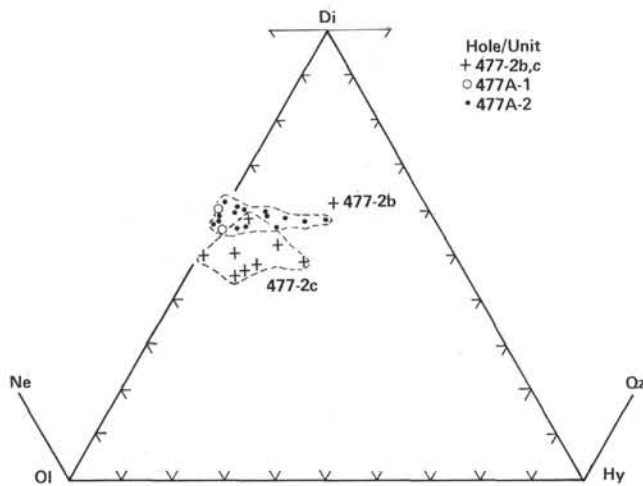


Figure 20. Basic rocks recovered at Site 477 plotted on the normative basalt tetrahedron. ($\text{Fe}_2\text{O}_3/\text{FeO}$ ratio assumed to be 0.15. Analyses determined by XRF at Birmingham.)

There are no significant, systematic down-hole variations in the chemistry of the Hole 477A samples (Fig. 19). Indeed, the two units are essentially indistinguishable: Both comprise subalkaline tholeiites, which tend toward the olivine/diopside boundary, with some samples entering the nepheline-normative field (Fig. 20). Both units, and particularly Unit 2, have high Al_2O_3 contents (approaching 19%; Table 13), which almost certainly reflect the high content of plagioclase phenocrysts (as in Unit 2c, Hole 477), since the natural glasses have significantly lower Al_2O_3 contents (Fornari et al., this volume). Within Units 1 and 2 there is a steady decrease in MgO and Ni with increasing FeO/MgO ratio and a concomitant increase in the abundances of HYG and more-HYG elements (e.g., Zr ; Fig. 21). More-HYG/HYG element ratios remain essentially constant, however, throughout the two units and are the same as the ratios observed in the Hole 477 samples (Tables 13–15; Figs. 22–26). This is shown particularly well by the

chondrite-normalized REE patterns for Site 477 (Fig. 24), where the constant La_N/Sm_N and La_N/Yb_N ratios strongly suggest a common parental magma for the units of both holes. Note that Sample 477A-3-1, 86–88 cm has a slight positive Eu anomaly, indicating the presence of cumulus plagioclase, which is consistent with its high Al_2O_3 and low TiO_2 and Zr contents. Sample 477A-3-1, 86–88 cm is, however, from the lowermost vesicular zone, although the upper vesicular zone in Unit 2 tends to have higher contents of the HYG elements (see Fig. 19). The Sr content of Sample 477A-3-1, 86–88 is, however, no higher than in many of the other samples from this unit.

Other ratios involving HYG and more-HYG elements, which remain constant throughout Units 1 and 2 and throughout Holes 477 and 477A, are Th/Hf (~ 0.07 ; Fig. 9), La/Ta (15–18; Fig. 12) and Th/Ta (~ 0.75 ; Fig. 27). Again, these values are similar to those observed in N-type MORB (Joron and Treuil, 1977; Bougault et al., 1980; Tarney et al., 1980), although the high Sr/Zr ratio in all of the Site 477 samples is atypical of N-type MORB. As in the dolerites from Hole 477, the similarity of the Sr/Zr ratios between aphyric and plagioclase-phyric samples suggests that the effects of cumulus plagioclase are minor.

Site 477: Interhole Correlations

There are no obvious lithological criteria to correlate the units of Holes 477 and 477A. Similarly, the occurrence of both plagioclase-rich and plagioclase-poor dolerites and basalts in both holes makes correlation using petrographic criteria very difficult. The chemical data strongly suggest that the units of both holes could easily be derived from a common parental magma involving varying degrees of low-pressure fractional crystallization of plagioclase and olivine. This in turn suggests that the units were emplaced at approximately the same time, and that it is the mode of sill emplacement (into poorly consolidated sediments) that has led to the sills being laterally discontinuous.

A discussion of the Site 477 data with respect to their regional setting will be presented after the petrology and geochemistry of the basalts from Sites 478 and 481 are described.

Site 478

Site 478 is 12 km northwest of the southern active rift in the Guaymas Basin. It lies on basement estimated from spreading rates to be about 400,000 yr. old. Available seismic data suggest that the acoustic basement at Site 478 is contiguous with that in the rift zone, and one of the objectives was to compare the geology and processes of an off-axis region with those observed at Site 477.

A total of 464 meters was drilled, comprising mainly diatomaceous ooze and mud intruded by massive dolerite sills. Thermal aureoles are well developed, and alteration effects are visible several tens of meters above some of the sills. On the basis of shipboard petrographic studies, six lithological units have been recognized (Fig. 28). Although the hole was abandoned while basalt was

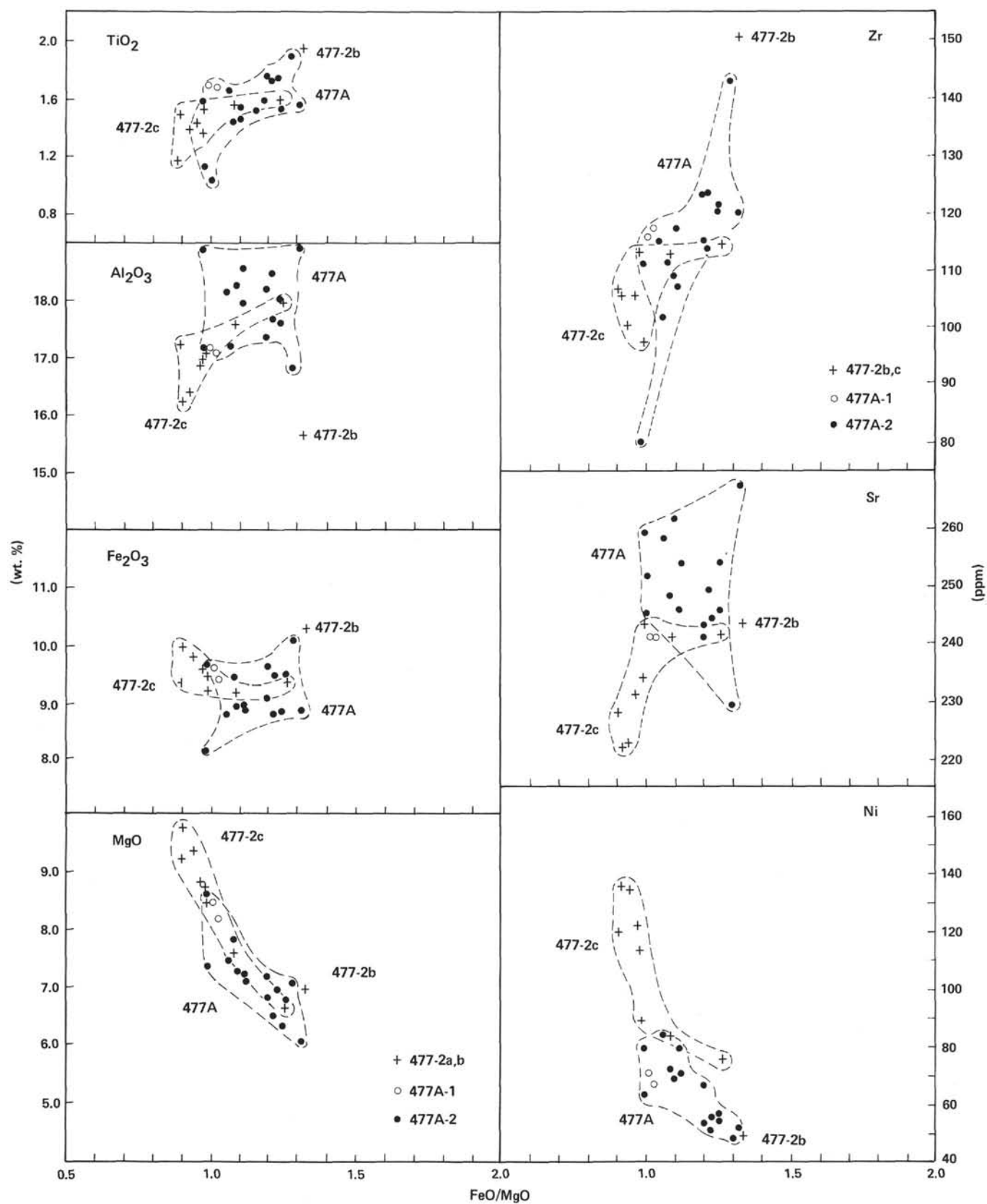


Figure 21. Variations in selected geochemical parameters versus FeO/MgO ratio for basic rocks recovered at Site 477. (FeO represents total iron. Analysis determined by XRF at Birmingham. Numbers refer to igneous units.)

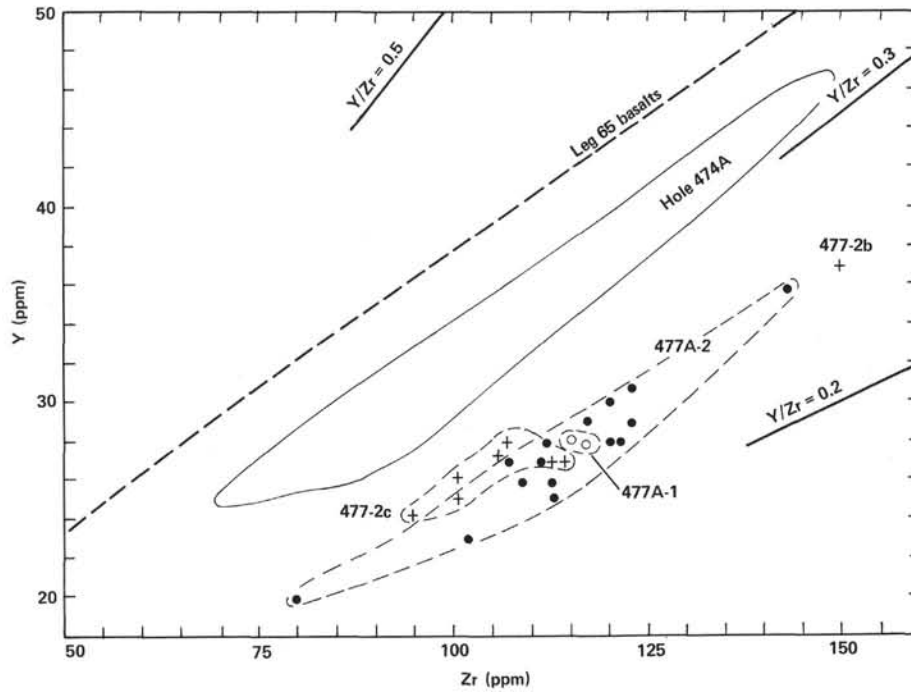


Figure 22. Y versus Zr for basic rocks recovered at Site 477. (Fields for Site 474 rocks taken from Fig. 6. Analyses determined by XRF at Birmingham.) Symbols as in Figure 21.

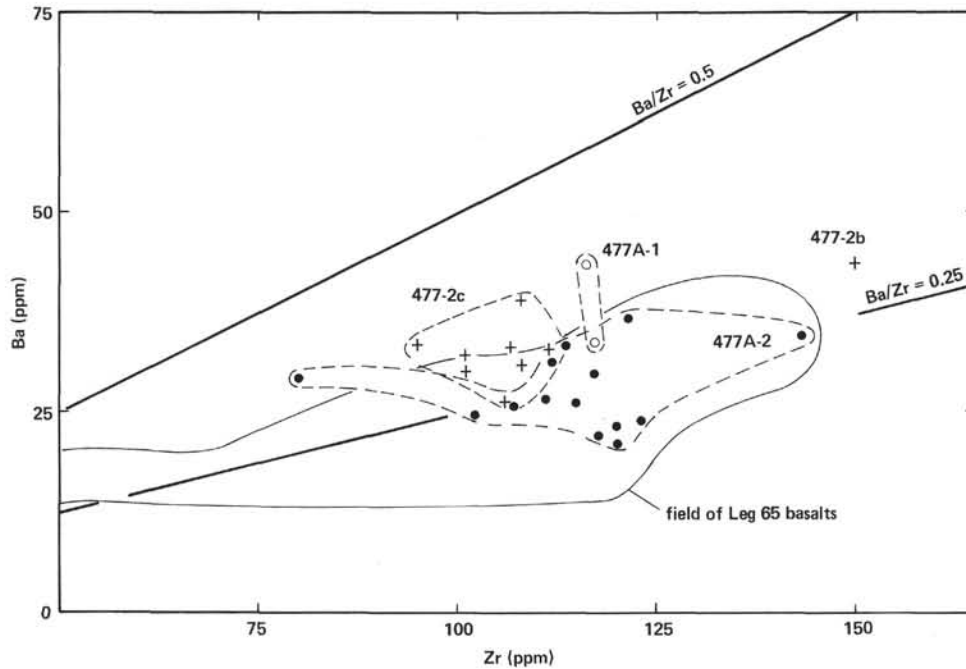


Figure 23. Ba versus Zr for basic rocks recovered at Site 477. (Field for Leg 65 basalts from Saunders [in press]. Analyses determined by XRF at Birmingham.) Symbols as in Figure 21.

still being drilled, it is unlikely that true basement was reached (see site chapter, Site 478).

Units 1 (10.5 m) and 2 (1.5 m)

Unit 1 comprises a medium-grained aphyric basalt, which contains approximately 10% clay minerals. Unit 2 (separated from Unit 1 by a 1-m-thick sedimentary intercalation) is a fine-grained, partially vesicular aphyric

basalt, again showing evidence of slight alteration. The cored sections and logging data indicate that Units 1 and 2 have thermally altered the sediments as high as 38 meters above Unit 1. Only one sample from Unit 1 has been analyzed; none was taken from Unit 2.

The sample from Unit 1 is one of the more evolved basalts recovered at Site 478. It has an FeO/MgO ratio of 1.2 and higher contents of TiO₂ (1.74%), Zr (102

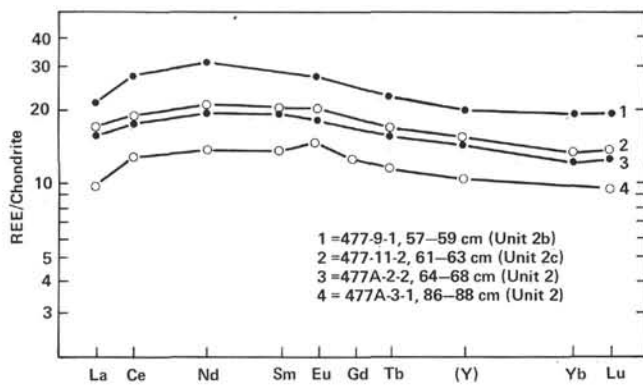


Figure 24. Chondrite-normalized REE data for basic rocks recovered at Site 477. (Analyses determined by INAA at Bedford College.)

ppm), and other HYG elements than samples from Units 4 through 6 (Tables 16, 17; Fig. 29). In addition, it has lower contents of MgO, Ni, Cr (Figs. 29, 30) and Sr (Fig. 31). In general, the basalt has an N-type MORB chemistry, being a subalkaline tholeiite (Fig. 32) with a La_N/Tb_N ratio of 0.9 (Fig. 10), $Y/Zr \sim 0.3$ (Fig. 33), $Th/Hf \sim 0.09$ (Fig. 9), $La/Ta \sim 22$ (Fig. 12), and $Th/Ta \sim 1.3$ (Fig. 27).

Unit 3 (4.5 m)

Only 20 cm of this unit have been recovered; it is an aphyric basalt with clay-, calcite- and pyrite-lined vesicles. No samples were taken for analysis.

Unit 4 (112.5)

This is the thickest internally consistent igneous body sampled during Leg 64, and the presence of a well-developed thermal aureole above its upper contact indicates that it is intrusive in origin. The quenched zone, while not glassy, is aphyric—a texture apparently maintained throughout the unit. The top of the unit consists of sparsely vesicular, coarse-grained basalt down to Section 478-41-1 (80 cm), and from this interval to Section 478-53-4, Unit 4 is doleritic to gabbroic in texture. Discrete textural changes occur throughout this section and are principally related to the occurrence of poikilitic clinopyroxene-plagioclase glomerocrysts, gabbroic xenoliths, and vertical and horizontal zones of alteration associated with silica and clay-filled veins. It is thought that the glomerocrysts are post-emplacement cooling features and not pre-emplacement crystal aggregates. Olivine is rare and comprises at most 5% of the rock, and although some primary olivine may have been replaced by clay minerals, no persistent pseudomorphing was observed. Brown to green clay minerals and amorphous to clear, fibrous zeolites account for between 10 and 50% of the rock. Fresher dolerite occurs between Cores 478-50 and 478-53.

Gabbro xenoliths, as much as 10 cm across, occur sporadically in Core 478-42 and abundantly in Core 478-51. Their mineralogy typically comprises intermediate plagioclase (An_{50-58}), clinopyroxene ($Wo_{43}En_{44}Fs_{12}$), and ilmenite, but no olivine was seen. As much as 20% clay minerals may be present. Some of the xenoliths

(e.g., Section 478-42-2 [116 cm]) show clear evidence of cumulate texture, with distinct layering of plagioclase crystals.

Unit 4 has been intensively analyzed (Table 16) to monitor any downhole variations in chemistry, although the absence of any unequivocal phenocryst phases in the thin sections suggests that *in situ* gravitational settling played an insignificant role. There is a slight decrease in TiO_2 and an antipathetic increase in Ni contents as the center of the sill is approached (Fig. 28). This may reflect slight variations in initial magma composition. Larger variations occur at the top of the unit, between Cores 478-41 and 478-42, particularly in the contents of HYG elements. The cause of these variations is not clear but may be the result of movements of late-stage mesostatic fluids.

The dolerite and basalt from Unit 4 has a primitive chemistry, containing 7.75 and 9.5 wt.% MgO and 80 and 140 ppm Ni (Fig. 29). As shown in Figure 28, there are antipathetic variations between Ni content and HYG-element contents (e.g., Ni and Zr; Fig. 30), and in plots of HYG and more-HYG elements the broad spread of data points generally indicates the various incompatible element ratios of the unit. Thus, the Y/Zr ratio (Fig. 33) is about 0.2, lower than in Unit 1 of Hole 478 (0.3) and significantly lower than in the Leg 65 basalts (~ 0.35). Correspondingly, both the La_N/Tb_N (1.12; Fig. 10) and Th/Hf (0.12; Fig. 9) ratios are significantly higher in Unit 4 than in Unit 1, whereas La/Ta ratios are lower in Unit 4 (< 20 ; Fig. 12). The Ti/Zr ratios ($\sim 60-80$) of Unit 4 are similar to those observed in samples from Site 477, but significantly lower than those from Site 474 ($Ti/Zr \sim 80-110$) and from Sites 482 through 485 of Leg 65 (100-130) (Saunders, in press).

Chondrite-normalized REE data for Unit 4 are presented in Figure 34; the raw data are given in Table 18. The patterns for the dolerite remain parallel, although absolute REE abundances vary. The La_N/Yb_N ratios are over one, but La_N/Sm_N ratios are slightly less than one. Note that the REE patterns are remarkably similar in shape to those of the basalts and dolerites recovered at Site 477.

The Sr and Ba data for Site 478 are plotted against Zr in Figures 31 and 35, respectively. Units 4 through 6 from Site 478 have high Sr/Zr ratios—unlike Unit 1 but similar to the samples recovered at Site 477. It is not possible to ascertain to what extent these high Sr abundances are the result of secondary alteration, but as in the Site 477 samples, the data points lie in reasonably tight clusters. The same, however, cannot be said for Ba (Fig. 35). There is considerable scatter in the distribution of Ba *without* any sympathetic variation in Zr, which strongly indicates that Ba levels have been affected by postcrystallization processes, probably involving exchange with sediment porewaters. Thus, we feel that the high Ba/Zr ratios (0.5-1.0) in the Site 478 samples are the result of secondary processes. The high Sr/Zr ratios may also be secondary, but we feel that this is unlikely because of the tight clustering of the data points and because the similarity of the Sr/Zr ratios to

Table 9. X-ray fluorescence analyses, Hole 477.

Core Section	9	11	12	12	12	12	12	13	13
Interval (cm)	57	61	49	70	39	76	46	53	146
Unit	2b	2c	2c	2c	2c	2c	2c	2c	2c
SiO ₂	49.8	48.3	49.0	48.6	48.0	48.1	48.1	49.3	48.7
TiO ₂	1.92	1.17	1.35	1.41	1.39	1.48	1.52	1.53	1.58
Al ₂ O ₃	15.7	17.2	17.0	16.9	16.4	16.2	17.1	17.5	17.9
tFe ₂ O ₃	10.25	9.33	9.21	9.57	9.76	9.97	9.49	9.19	9.32
MnO	0.17	0.14	0.15	0.16	0.15	0.16	0.15	0.14	0.14
MgO	6.95	9.20	8.45	8.86	9.35	9.75	8.75	7.60	6.65
CaO	11.70	11.61	11.44	11.28	11.01	10.87	11.45	11.51	11.89
Na ₂ O	3.11	2.79	2.75	2.82	2.76	2.76	2.77	3.00	3.05
K ₂ O	0.20	0.18	0.17	0.16	0.18	0.23	0.19	0.22	0.20
P ₂ O ₅	0.33	0.24	0.22	0.21	0.23	0.25	0.21	0.23	0.21
LOI	—	0.14	—	—	—	0.33	—	—	—
Total	100.13	100.28	99.78	99.98	99.29	100.10	99.68	100.20	99.64
Trace Elements (ppm)									
Ni	48	118	113	121	134	135	88	83	75
Cr	213	239	221	215	234	217	203	196	234
Zn	61	52	60	59	54	58	58	54	55
Ga	24	17	18	15	17	16	21	19	21
Rb	<1	1	<1	<1	3	1	<1	<1	1
Sr	243	228	234	231	223	222	243	241	242
Y	37	28	24	26	25	27	27	27	27
Zr	150	107	95	101	101	106	113	112	114
Nb	5	3	3	4	3	4	4	4	4
Ba	43	33	33	32	30	26	39	33	31
La	9	7	6	6	8	6	7	7	8
Ce	19	14	13	15	14	17	10	16	17
Nd	16	12	11	11	12	12	12	12	12
Pb	6	2	2	6	4	5	3	3	3
Th	1	4	1	<1	2	1	4	<1	<1
Selected Ratios									
Zr/Nb	38	36	32	25	34	27	28	28	29
Ti/Zr	77	66	85	84	83	84	81	82	83
Y/Zr	0.25	0.26	0.25	0.26	0.25	0.25	0.24	0.24	0.24
Ce/Zr	0.13	0.13	0.14	0.15	0.14	0.16	0.09	0.14	0.15
Ba/Zr	0.29	0.31	0.35	0.32	0.30	0.25	0.35	0.29	0.27
(Ce/Y) _N	1.26	1.23	1.33	1.42	1.38	1.55	0.91	1.46	1.55
Fe/Mg	1.71	1.18	1.26	1.25	1.21	1.19	1.26	1.40	1.63
K/Rb	>1660	1494	>1411	>1328	498	1909	>1577	>1826	1660
Ba/Sr	0.18	0.14	0.14	0.14	0.13	0.12	0.16	0.14	0.13
CIPW Norms									
Q	0.0	0.0	0.0	0.0	0.0	0.0	0.0	0.0	0.0
Or	1.2	1.1	1.0	0.9	1.1	1.4	1.1	1.3	1.2
Ab	26.3	23.5	23.3	23.9	23.5	23.3	23.5	25.3	25.9
An	28.1	33.8	33.6	32.9	32.1	31.2	33.6	33.6	34.7
Ne	0.0	0.0	0.0	0.0	0.0	0.0	0.0	0.0	0.0
Di	22.6	17.9	17.7	17.6	17.4	17.1	17.8	17.8	18.9
Hy	7.8	0.5	7.8	4.6	4.1	3.5	2.6	4.8	1.7
Ol	6.9	17.8	11.1	14.4	16.1	17.3	15.4	11.3	11.6
Mt	1.8	1.6	1.6	1.7	1.7	1.7	1.7	1.6	1.6
Il	3.6	2.2	2.6	2.7	2.7	2.8	2.9	2.9	3.0
Ap	0.8	0.6	0.5	0.5	0.5	0.6	0.5	0.5	0.5

Note: See Table 1, note.

those at Site 477, where alteration was less severe (e.g., Ba/Zr ratios at Site 477 are constant and are similar to those observed in the Leg 65 basalts; Fig. 23).

One sample (Sample 478-51-3, 49–52) of a gabbro xenolith was analyzed from Core 478-51; the results are included in Tables 16, 17, and 18. The geochemistry of the gabbro is significantly different from that of the enclosing dolerite; MgO, Ni, and Cr contents are much lower, and the FeO/MgO ratio and HYG element contents are much higher. For example, Zr (324 ppm) is approximately four times higher than in the dolerite. Although the absolute abundances of HYG elements vary, however, the incompatible element ratios of the gabbro and dolerite are similar. Thus, Y/Zr (Fig. 33),

Th/Hf (Fig. 9), La/Ta (Fig. 12) and Th/Ta (Fig. 27) ratios remain constant between the dolerite and gabbro. The La/Tb ratio increases slightly in the gabbro as does the La_N/Yb_N ratio (Table 18; Figs. 10, 34). Notice that the gabbro has a slight negative europium anomaly (Fig. 34), suggesting plagioclase removal, and that the absolute Sr content of the gabbro is similar to that in the dolerite (Fig. 31)—again indicating plagioclase fractionation. The Ti/Zr ratio of gabbro (39) is significantly lower than that of the dolerite (~60–80), indicating fractionation of ilmenite or titanomagnetite.

The general similarity of the more-HYG/HYG ratios in the dolerite and gabbro indicates that the two rock types are closely related, possibly by low-pressure frac-

Table 10. INAA results (Saclay) for selected samples, Hole 477.

Core Section	9 1	12 1	12 4	12 5	13 2
Interval (cm)	57-59	49-52	76-80	46-50	146-150
Unit	2b	2c	2c	2c	2c
Ni	56	140	149	102	93
Cr	207	174	254	208	157
Co	40.3	45.1	46.3	39.2	40.1
Sc	46.6	32.9	31.1	31.1	33.5
Ba	15	21	16	10	12
Sr	277	291	282	275	272
Cs	0.08	0.07	0.21	0.04	0.03
Rb	2.9	—	2.2	—	—
U	0.16	0.08	—	0.07	0.09
Th	0.28	0.19	0.22	0.20	0.22
Zr	179	99	116	93	115
Hf	3.57	2.48	2.61	2.68	2.82
Ta	0.39	0.27	0.28	0.29	0.30
Sb	0.02	0.02	0.01	0.01	0.02
La	6.22	3.86	5.07	4.79	4.63
Ce	16.5	11.3	11.3	10.8	12.6
Eu	1.35	0.94	1.32	1.28	1.00
Tb	0.90	0.62	0.68	0.60	0.74

Note: All values in ppm.

Table 11. INAA results (Bedford) for selected samples, Hole 477.

Core Section	9 1	11 2
Interval (cm)	57-59	61-63
Unit	2b	2c
La	7.1	5.28
Ce	23.4	15.2
Nd	19.1	12.5
Sm	—	4.01
Eu	2.19	1.41
Tb	1.18	0.82
Yb	4.31	2.67
Lu	0.66	0.43
Th	0.45	0.32
Hf	4.53	2.57
Ta	0.46	0.31
La _N /Yb _N	1.1	1.32
La/Ta	15	17
Th/Hf	0.10	0.12

Note: Trace-element values in ppm.

tional crystallization. Removal of olivine, clinopyroxene, feldspar, and a titanium-bearing minor phase from a melt of the composition of the dolerite of Unit 4 could produce the composition observed in the gabbro xenolith. Such a process would have no significant effect on most more-HYG element ratios, although, depending on the relative quantities of feldspar and pyroxene removed, it could cause slight fractionation of the REE (clinopyroxene has $K_{D}^{xtal/liquid}$ values > 1), leading to increased La_N/Yb_N ratios. Therefore, the gabbro xenoliths appear to represent high-level differentiates, possibly formed at the top of a subridge magma chamber. Clearly, the cumulate textures observed in several thin sections were not significant in the analyzed xenolith, because cumulus plagioclase/pyroxene would be ex-

Table 12. Representative modal analyses, Hole 477A.

Core Section	2 1	2 2	2 2	2 3	2 4	3 1	3 1	3 2	3 4
Level (cm)	45	10	28	48	85	58	89	20	130
Unit	2	2	2	2	2	2	2	2	2
Plagioclase (phenocrysts)	26	16	14	17	17	32	57	68	21
Plagioclase (groundmass)	36	38	39	38	39	25	*	*	44
Clinopyroxene	18	15	9	16	17	23	22	19	19
Olivine	8	9	14	4	15	6	4	6	5
Opaques	9	13	9	12	10	10	3	5	6
Clay Minerals	3	9	6	9	2	4	5	—	—
Vesicles	—	—	6	4	—	—	14	2	2

Note: Analyses determined using at least 600 point counts per sample. The distinction between phenocryst and groundmass plagioclase is often problematic because of the seriate textures in the more coarse-grained samples; * = Values included in phenocryst-plagioclase contents.

pected to result in positive Eu anomalies and low abundances of the HYG elements (cf. Saunders et al., 1979).

Units 5 (4.5 m) and 6 (4.0 m)

Aphyric and sparsely plagioclase-phyric basalt was recovered in Core 478-54 and, on the basis of textural changes, has been divided into two units, 5 and 6. The contact between Unit 5 and the overlying dolerite of Unit 4 was not recovered, but the slight variation in the bulk-density record suggests that the two units are adjacent and not separated by a sedimentary intercalation. Indeed, Unit 5 may be the more rapidly chilled margin of Unit 4. Unit 5 is chilled against Unit 6.

The basalts of Units 5 and 6 are petrographically very similar, both being essentially aphyric, although Unit 6 contains rare ($< 1\%$ of the rock) resorbed plagioclase phenocrysts. Groundmass olivine was not found, although the small grain size makes identification difficult. Both basalts are altered, with as much as 50% of the rock comprising a mesostasis now replaced by clay minerals, zeolites, and possibly by calcite. No vesicles are present.

Three samples were taken from Unit 5 and four from Unit 6 for XRF analysis (Table 16), and one sample from each unit was analyzed at Saclay (Table 17). Both units consist of subalkaline tholeiites (Fig. 32). Unit 5 is chemically indistinguishable from the dolerite of Unit 4, having similar major-element contents (Table 16, Fig. 29) and generally overlapping the field of Core 478-4 on the HYG/HYG plots (e.g., Y/Zr, Fig. 33; Sr/Zr, Fig. 31). Ratios of more-HYG and HYG elements are essentially constant between Units 4 and 5 (e.g., La/Tb, Th/Hf, La/Ta, Th/Ta ratios; Figs. 9, 10, 12, 27). Even the Ni/Zr ratios are the same in Units 4 and 5 (Fig. 30). These observations support the earlier suggestion that Unit 5 is a fine-grained equivalent—possibly the chilled margin—of Unit 4.

Three of the samples from Unit 6 are also chemically similar to Units 4 and 5, having similar abundances and ratios of Ni and the HYG elements, although Al₂O₃ contents are noticeably lower. One sample (Sample 478-54-4, 2-4 cm), however, has significantly higher con-

Table 13. X-ray fluorescence analyses, Hole 477A.

Core Section Level (cm) Unit	1 1 35 1	1 1 145 1	2 1 7 2	2 1 47 2	2 1 00 2	2 2 64 2	2 3 27 2	2 3 46 2	2 4 22 2	2 4 85 2	3 1 15 2	3 1 35 2	3 1 86 2	3 2 17 2	3 3 37 2	3 4 113 2	3 5 106 2
SiO ₂	49.0	48.7	48.7	49.0	48.7	49.0	49.4	49.0	49.0	49.1	49.0	49.5	48.7	49.1	48.9	49.0	48.8
TiO ₂	1.67	1.62	1.59	1.50	1.63	1.76	1.72	1.71	1.57	1.50	1.88	1.51	1.14	1.53	1.45	1.39	1.46
Al ₂ O ₃	17.2	17.1	17.3	18.0	17.2	17.4	17.6	17.6	18.2	18.4	16.8	18.0	18.9	18.9	18.6	18.2	18.2
Fe ₂ O ₃	9.52	9.40	9.52	8.89	9.40	9.66	9.41	9.49	9.06	8.78	10.15	8.79	8.08	8.85	8.86	8.78	8.90
MnO	0.14	0.15	0.15	0.15	0.14	0.15	0.15	0.15	0.14	0.14	0.16	0.14	0.13	0.14	0.14	0.13	0.14
MgO	8.50	8.24	8.65	7.17	7.83	7.23	6.75	6.92	6.80	6.50	7.10	6.35	7.31	6.02	7.15	7.49	7.25
CaO	11.91	12.03	12.04	12.00	11.71	11.81	11.91	11.99	12.17	12.21	11.84	12.04	12.81	12.14	12.25	12.12	12.21
Na ₂ O	2.96	3.03	2.91	2.87	2.97	3.10	2.95	2.98	3.01	2.97	3.14	2.93	2.82	2.98	2.97	2.90	2.95
K ₂ O	0.15	0.22	0.14	0.25	0.23	0.25	0.21	0.18	0.22	0.21	0.25	0.24	0.12	0.22	0.22	0.19	0.20
P ₂ O ₅	0.20	0.22	0.14	0.21	0.22	0.23	0.18	0.18	0.21	0.19	0.26	0.20	0.12	0.19	0.20	0.19	0.21
LOI	+0.32	0.18	—	+0.34	—	—	+0.42	—	—	+0.11	+0.52	—	0.12	+0.30	—	+0.31	—
Total	101.21	100.85	101.21	100.06	100.05	100.58	100.18	100.23	100.44	100.04	100.57	99.67	100.20	100.16	100.74	100.35	100.36
Trace Elements (ppm)																	
Ni	70	66	78	79	72	66	54	55	53	50	48	55	63	51	70	82	69
Cr	207	201	250	248	194	191	204	197	201	192	212	188	220	134	191	195	190
Zn	57	58	61	54	58	60	60	61	50	49	65	55	40	55	55	50	51
Ga	20	19	19	18	19	17	18	18	22	20	22	23	21	27	21	17	20
Rb	<1	<1	<1	<1	2	1	<1	<1	1	<1	<1	2	<1	<1	<1	<1	2
Sr	241	241	245	246	248	241	246	244	243	249	229	254	259	267	254	258	262
Y	28	28	27	27	28	29	30	31	26	25	36	28	20	28	29	23	26
Zr	116	117	111	107	112	123	120	123	115	113	143	121	80	120	117	102	109
Nb	4	4	4	3	3	4	3	4	4	4	5	4	3	3	5	5	5
Ba	44	34	27	26	32	22	21	24	27	34	35	37	29	23	30	25	31
La	6	6	5	7	7	9	7	8	9	7	9	8	6	7	8	7	7
Ce	16	15	15	16	16	15	17	16	15	15	18	15	10	15	14	14	11
Nd	13	12	11	13	13	13	15	13	12	11	14	11	9	13	12	10	11
Pb	<1	5	5	6	4	5	2	<1	1	1	3	1	5	<1	3	6	3
Th	<1	<1	<1	<1	2	4	<1	<1	<1	<1	<1	2	<1	2	<1	<1	1
Selected Ratios																	
Zr/Nb	29	29	28	36	37	31	40	31	29	28	29	30	27	40	23	20	22
Ti/Zr	86	83	86	84	87	86	86	83	82	80	79	75	85	76	74	82	80
Y/Zr	0.24	0.24	0.24	0.25	0.25	0.24	0.25	0.25	0.23	0.22	0.25	0.23	0.25	0.23	0.25	0.23	0.24
Ce/Zr	0.14	0.13	0.14	0.15	0.14	0.12	0.14	0.13	0.13	0.13	0.13	0.12	0.13	0.13	0.12	0.14	0.10
Ba/Zr	0.38	0.29	0.24	0.24	0.29	0.18	0.17	0.20	0.23	0.30	0.24	0.31	0.36	0.19	0.26	0.25	0.28
(Ce/Y) _N	1.40	1.32	1.36	1.46	1.40	1.27	1.39	1.27	1.42	1.47	1.23	1.32	1.23	1.32	1.19	1.50	1.04
Fe/Mg	1.30	1.32	1.28	1.44	1.39	1.55	1.62	1.59	1.55	1.57	1.66	1.61	1.28	1.70	1.44	1.36	1.42
K/Rb	>1245	>1826	>1162	>2075	955	2075	>1743	>1494	1826	>1743	>2075	996	>996	>1826	>1826	>1577	830
Ba/Sr	0.18	0.14	0.11	0.11	0.13	0.09	0.09	0.10	0.11	0.14	0.15	0.15	0.11	0.09	0.12	0.10	0.12
CIPW Norms																	
Q	0.0	0.0	0.0	0.0	0.0	0.0	0.0	0.0	0.0	0.0	0.0	0.0	0.0	0.0	0.0	0.0	0.0
Or	0.9	1.3	0.8	1.5	1.4	1.5	1.2	1.1	1.3	1.2	1.5	1.4	23.3	1.3	1.3	1.1	1.2
Ab	24.7	24.0	23.7	24.3	25.1	26.1	24.9	25.2	25.4	25.1	26.4	24.9	23.3	25.2	24.9	24.5	24.9
An	32.7	32.0	33.4	35.4	32.9	32.5	34.0	34.1	35.4	36.3	30.8	35.3	38.3	37.6	36.4	35.9	35.8
Ne	0.0	0.7	0.3	0.0	0.0	0.0	0.0	0.0	0.0	0.0	0.0	0.0	0.3	0.0	0.0	0.0	0.0
Di	19.8	20.9	20.1	18.5	19.3	19.8	19.5	19.6	19.0	18.7	21.2	19.0	19.7	17.4	18.4	18.6	18.9
Hy	0.6	0.0	0.0	4.1	1.6	0.9	5.8	3.1	1.4	2.9	0.6	6.8	0.0	3.9	0.0	2.1	0.4
Ol	15.2	14.8	15.9	10.6	13.6	12.9	8.5	10.7	11.7	10.0	12.8	6.9	12.9	8.9	13.4	12.5	13.2
Mt	1.6	1.6	1.6	1.5	1.6	1.7	1.6	1.6	1.6	1.5	1.8	1.5	1.4	1.5	1.5	1.5	1.5
Il	3.1	3.1	3.0	2.8	3.1	3.3	3.3	3.2	3.0	2.8	3.6	2.9	2.2	2.9	2.7	2.6	2.8
Ap	0.5	0.5	0.3	0.5	0.5	0.5	0.4	0.4	0.5	0.4	0.6	0.5	0.3	0.4	0.5	0.4	0.5

Note: See Table 1, note.

Table 14. INAA results (Saclay) for selected samples, Hole 477A.

Core Section Interval (cm) Unit	1 1 35-39 1	1 1 145-147 1	2 2 0-2 2	2 2 64-68 2	2 4 85-87 2	3 1 35-37 2	3 ^a 2 17-19 2	3 4 116-118 2	3 5 106-108 2
Ni	83	80	103	72	66	69	64	104	85
Cr	229	156	201	214	215	214	140	210	205
Co	38.5	38.2	41.3	38.9	36.9	37.5	35.5	41.5	39.5
Sc	32.8	33.8	42.9	34.5	33.0	33.6	28.1	32.1	32.4
Ba	23	12	14	14	18	16	17	11	14
Sr	299	299	279	268	288	295	307	299	296
Cs	0.06	0.05	0.05	—	0.03	0.02	0.09	—	0.02
Rb	—	—	2.3	—	1.6	1.6	1.8	—	—
U	0.15	0.12	0.07	0.09	—	0.11	0.13	0.07	0.08
Th	0.23	0.22	0.21	0.24	0.20	0.25	0.24	0.19	0.21
Zr	127	128	125	118	118	134	117	115	118
Hf	2.72	2.81	2.83	2.93	2.66	2.91	2.78	2.50	2.81
Ta	0.31	0.32	0.40	0.32	0.30	0.32	0.31	0.26	0.29
Sb	—	—	0.02	—	0.02	0.01	0.01	—	0.01
La	4.76	4.70	5.13	5.28	4.52	5.05	4.97	3.71	4.46
Ce	10.7	13.3	13.7	12.3	11.4	12.7	12.5	10.6	12.9
Eu	1.30	1.00	1.34	1.28	1.43	1.33	1.24	1.19	1.34
Tb	0.68	0.69	0.70	0.68	0.68	0.72	0.68	0.58	0.63

Note: All values in ppm.

^a Average of three determinations.

Table 15. INAA results (Bedford) for selected samples, Hole 477A.

Core Section	2	3
Interval (cm)	64-68	86-88
Unit	2	2
La	5.55	3.26
Ce	16.1	11.1
Nd	12.9	8.7
Sm	4.2	2.8
Eu	1.56	1.15
Gd	—	3.4
Tb	0.86	0.61
Yb	2.99	—
Lu	0.47	0.33
Th	0.33	0.24
Hf	3.01	2.09
Ta	0.33	0.22
La _N /Yb _N	1.25	1.0 ^a
La/Ta	17	15
Th/Hf	0.11	0.11

Note: Trace-element values in ppm.

^a Interpolated Yb value.

centrations of HYG and more-HYG elements and lower Ni contents than either Unit 4 or Unit 5. Nevertheless, HYG/HYG element ratios are constant within Unit 6 and again similar to Unit 4 (e.g., Y/Zr; Fig. 33), suggesting that the units may be related by fractional crystallization involving olivine and plagioclase. In thin sec-

tion, both Units 5 and 6 can be seen to be extensively altered, and this is reflected in their chemistry by the variable distribution of Rb and Ba. Note also that Unit 6 has higher contents of Th—as demonstrated by higher Th/Ta and Th/Hf ratios—which may be a primary characteristic but which could also be caused by severe alteration.

Hole 478: Interunit Variations

Mineralogically, Units 1, 4, and 5 are all aphyric, although Unit 6 contains sporadic resorbed plagioclase phenocrysts. This similarity is reflected in the chemistry, Units 4, 5, and most of Unit 6 being chemically indistinguishable from one another. The HYG/HYG and more-HYG/HYG element ratios are essentially constant throughout these units. We have suggested the Unit 5 is the more rapidly cooled marginal equivalent of Unit 4, and that the more evolved sample from Unit 6 is related to Units 4 and 5 by low-pressure fractional crystallization involving olivine and plagioclase. The general absence of phenocrysts of these minerals indicates, however, that fractionation occurred in sub-ridge magma chambers. The adjacent positions of Units 4, 5, and 6 in the lithological column does not preclude their derivation from a common parental magma. Unit 5 is chilled against Unit 6, suggesting that Unit 6 was subject to considerable temperature rise during the emplacement of Unit 5 and the massive Unit 4. This provides a causative mechanism for the high degree of alteration in the Unit 6 basalt.

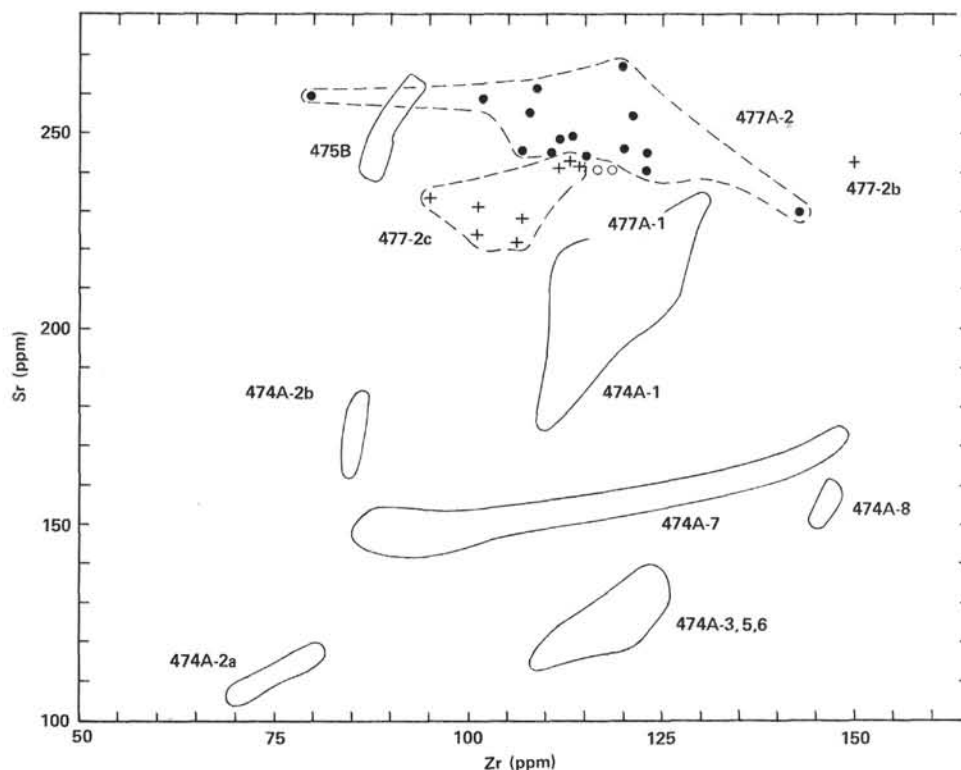


Figure 25. Sr versus Zr for basic rocks recovered at Site 477. (Fields for Site 474 and Site 475 rocks taken from Fig. 8. Analyses determined by XRF at Birmingham. Numbers refer to igneous units.)

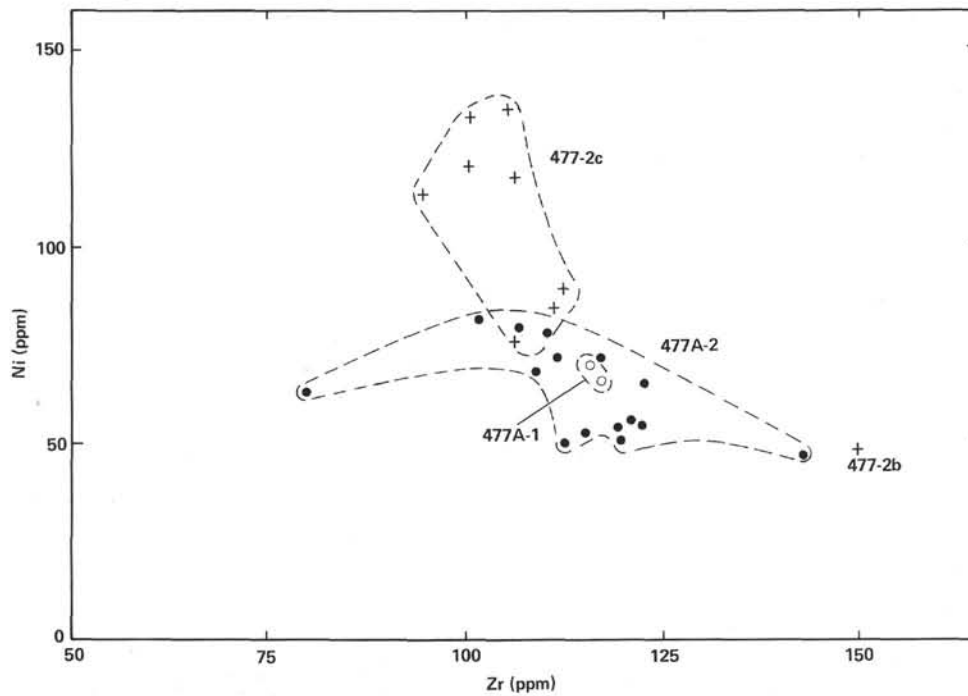


Figure 26. Ni versus Zr for basic rocks recovered at Site 477. (Analyses determined by XRF at Birmingham. Numbers refer to igneous units.)

Unit 1, however, has lower more-HYG/HYG element ratios than Units 4, 5, and 6, which effectively rules out derivation of all of the units from a common parental magma source by various degrees of closed-system/low-pressure fractional crystallization. Rather, appeal must be made to differing degrees of partial melting of the mantle source or perhaps open-system fractional crystallization (O'Hara, 1977). There is, however, no necessity to invoke mantle heterogeneity to explain the slight interunit variations in more-HYG/HYG element ratios.

Site 481

Site 481 (27°15.18'N; 11°30.46'W, 1998 m water depth) lies at the southwestern end of the northern actively spreading rift in the Guaymas Basin (Fig. 18). It is in an area of high but variable heat flow, analogous to Site 477, although the average heat flow is generally lower than that at Site 477. Two holes were drilled at this site: Hole 481, drilled with the Serocki-Storms-Cameron piston corer, contained only sediments, and Hole 481A contained 364 meters of turbiditic mass flow deposits and several groups of sills. On the basis of shipboard petrographic studies and down-hole logging data, four main igneous lithological units have been recognized, the uppermost of which has been subdivided into 18 subunits (Fig. 36).

Unit 1 (28 m, including intercalated sediments)

A total of eighteen separate igneous subunits has been identified in Unit 1, and many of these are separated by thin, indurated sedimentary intercalations (see Site 481 site chapter). Most of the subunits are intrusive, and both upper and lower contacts are against sediments or older igneous rocks. Mineralogically, the subunits of Unit 1 are practically indistinguishable, either

being aphyric (Subunits 1-2, 1-8-1-11, 1-15, 1-16), containing minor (<5%) plagioclase microphenocrysts (Subunits 1-1, 1-12-14, 1-17, 1-18) or containing minor (<5%) plagioclase and altered olivine microphenocrysts (Subunits 1-3-1-7). The groundmass exhibits considerable variation in texture, ranging from variolitic through intersertal to doleritic and even gabbroic in the centers of some subunits (e.g., Subunit 1-10). Alteration of some of the subunits is locally quite severe, resulting in replacement of olivine by clay minerals and of mesostasis by clay minerals and calcite. Calcite veining is common.

There are a few basalt/basalt contacts which allow positive identification of the emplacement sequence of several intrusions. These show that Subunit 1-7 intrudes Subunit 1-6, Subunit 1-10 is chilled against Subunit 1-11, Subunit 1-15 is chilled against Subunit 1-16 and that narrow, opaque-rich basaltic veins (not sampled) cut Subunits 1-13 through 1-18.

Fourteen samples were selected from the freshest portions of Unit 1 and analyzed by XRF (Table 19) and INAA (Tables 20, 21). The downhole plot (Fig. 36) demonstrates the chemical variation within Unit 1: Zr, for example, ranges from 123 to 189 ppm in Subunit 1-10 alone, although Zr levels of between 144 and 171 ppm are more normal. The TiO₂ content varies sympathetically, and Ni varies antipathetically with Zr, as expected. Generally, Unit 1 has higher total iron contents and FeO/MgO ratios than other basaltic rocks from the Guaymas Basin (Fig. 29), although Ni contents are not as low as expected in such relatively "evolved" samples (see, for example, Fig. 30). The samples all have a subalkaline tholeiite chemistry (Fig. 32).

Ratios involving immobile HYG and more-HYG elements are approximately constant throughout the unit.

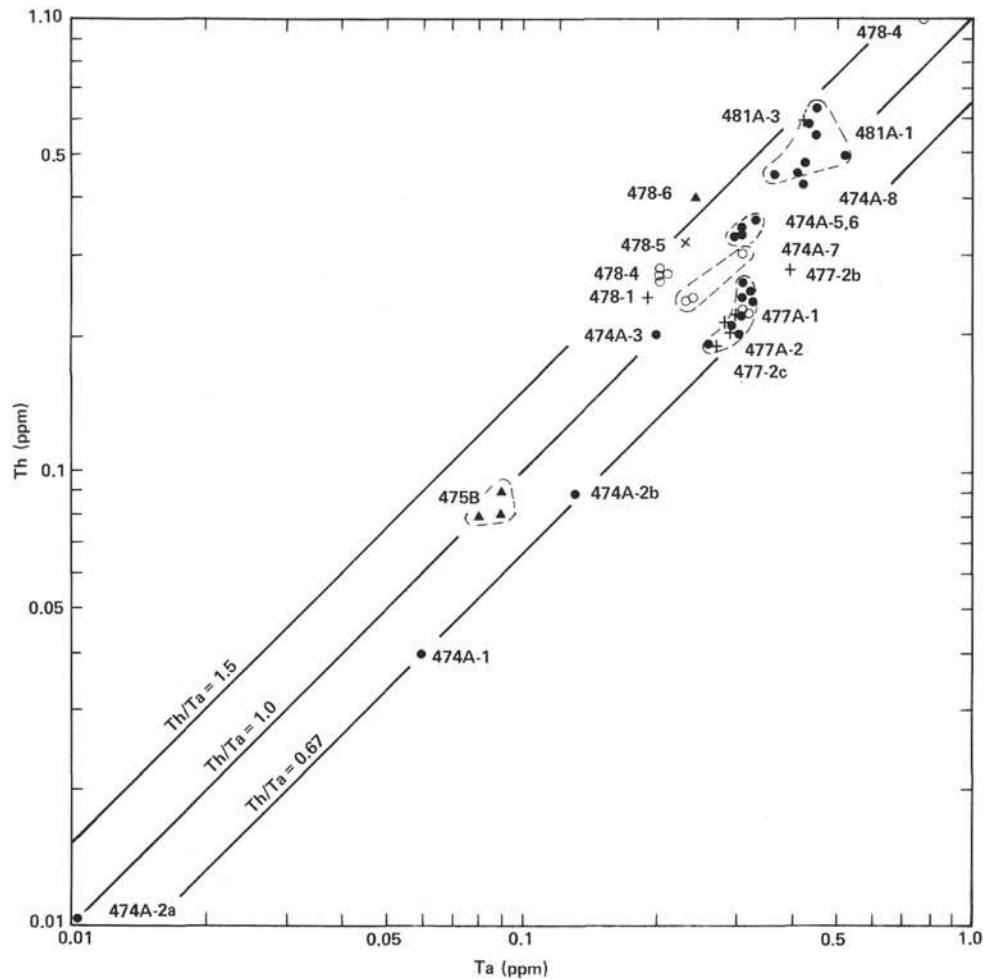


Figure 27. Th versus Ta for selected samples recovered during Leg 64. (Analyses determined by INAA at Saclay. Numbers refer to igneous units.)

The Y/Zr content is approximately 0.25, similar to Subunits 478-4 and 478-5, although Section 481A-1-10 has a slightly higher, but remarkably constant, Y/Zr ratio (Fig. 33). The ratios of La/Tb are constant and similar to those observed in Holes 477, 477A, and 478 (Fig. 10), and the form of the chondrite-normalized REE patterns is the same as that noted in other samples from the Guaymas Basin (i.e., $La_N/Yb_N > 1$, $La_N/Sm_N < 1$; Figs. 24, 34, 37). No europium anomalies have been observed. The Th/Hf ratios are constant within the unit and similar to those of Cores 478-4 and 478-5 but higher than those at Site 477 (Fig. 9). The La/Ta (~ 15 ; Fig. 12) and Th/Ta ($\sim 1-1.5$; Fig. 27) ratios are also constant and similar to those from Sites 477 and 478.

Abundances of the more mobile elements K, Rb, and Ba are erratic, suggesting post-emplacement interaction with sediment porewaters. Note, however, that Subunit 1-10 has a high but constant Ba/Zr ratio, which may be primary (Fig. 35). As in the basalts from Sites 477 and 478, levels of Sr are higher than those in the Leg 65 basalts (Fig. 31), and again the tight clustering of data points indicates that these abundances may be primary.

The wide range in HYG element abundances in Subunit 1-10 must reflect either *in situ* chemical differentiation—the more evolved sample (Sample 481A-15-3, 271–115 cm) being a gabbro from the center of the subunit—or changing magma composition during emplacement. Notice, however, that Ni does not change with increasing Zr content, suggesting that olivine fractionation did not play an important role (indeed, the subunit is aphyric). We feel that the varying HYG abundances were produced as the subunit slowly cooled and as mesostatic (HYG-element enriched) fluids migrated towards the center of the unit. The gabbroic portion of the unit is very coarse grained, containing acicular pyroxene crystals as much as 30 mm long. Note that a mean composition of the more depleted sample and the mesostasis-enriched gabbroic portion is similar to other samples from Unit 1.

Unit 2 (4.8 m)

Only two pieces of aphanitic, aphyric vesicular basalt were recovered from Unit 2. Neither of these has been analyzed.

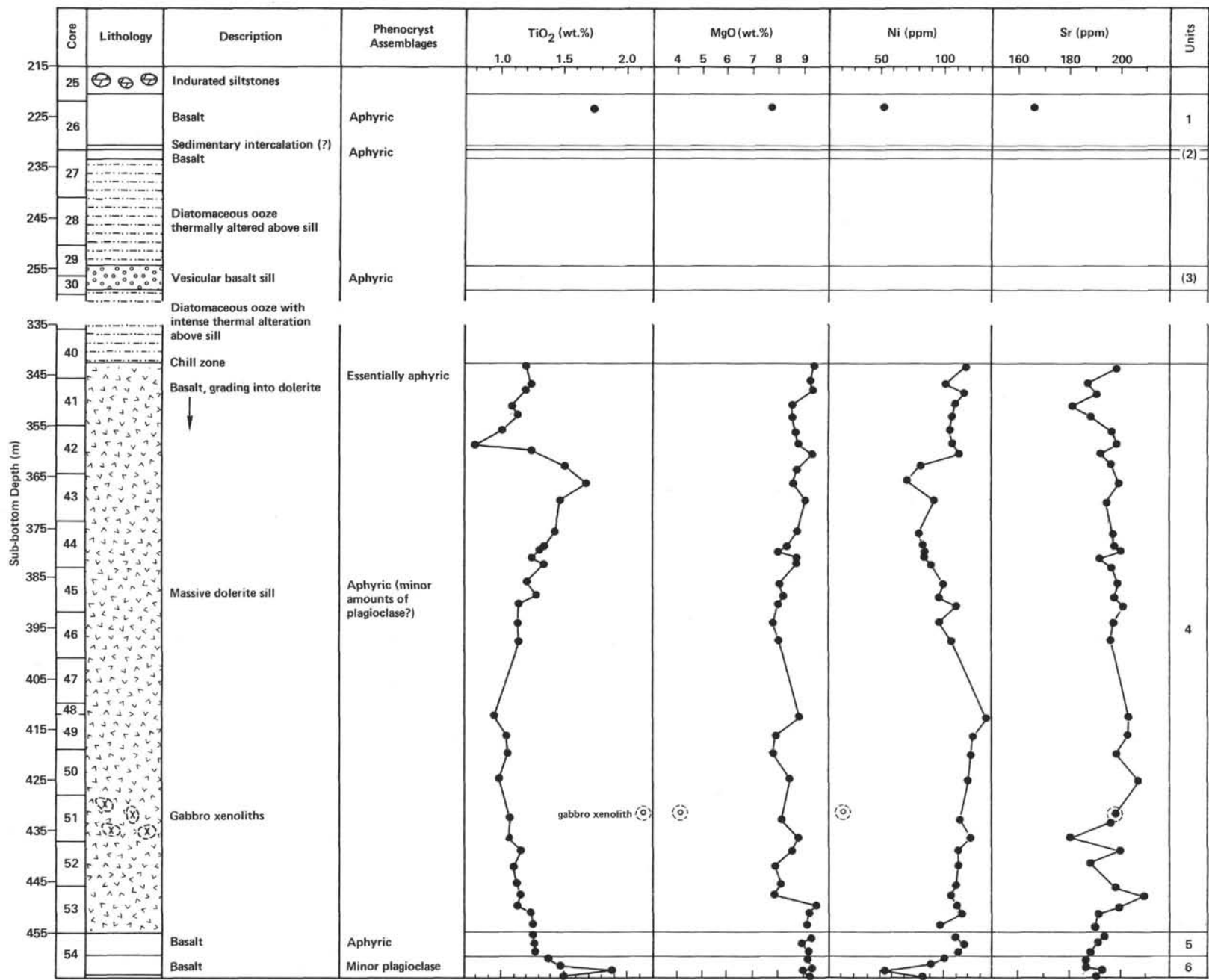


Figure 28. Downhole variations in lithology and selected geochemical parameters, Hole 478.

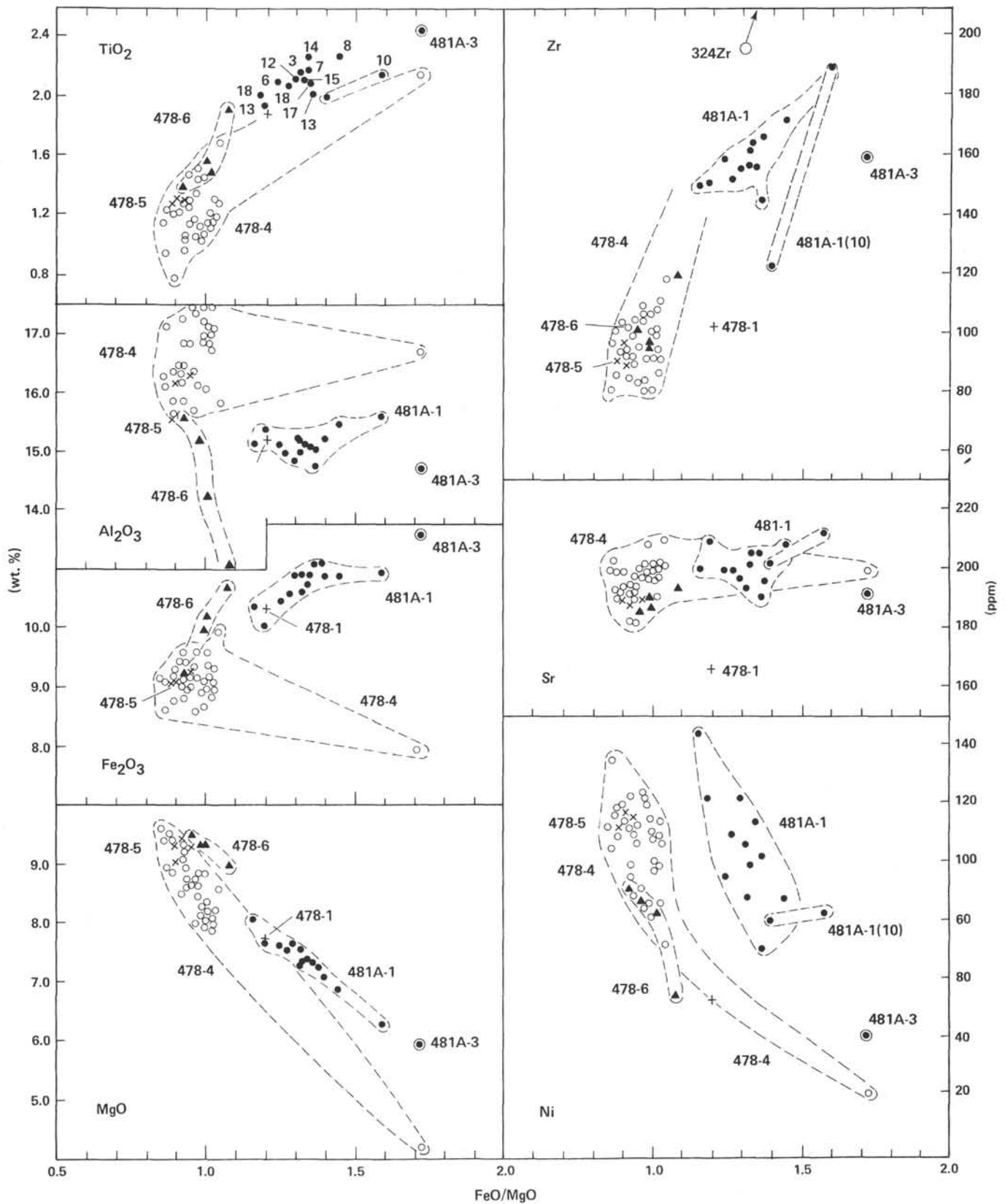


Figure 29. Variations in selected geochemical parameters versus FeO/MgO ratio for basic rocks recovered at Sites 478 and 481. (FeO represents total iron. Analyses determined by XRF at Birmingham. Numbers without hole designations in TiO₂ box refer to subunits of Unit 481A-1.)

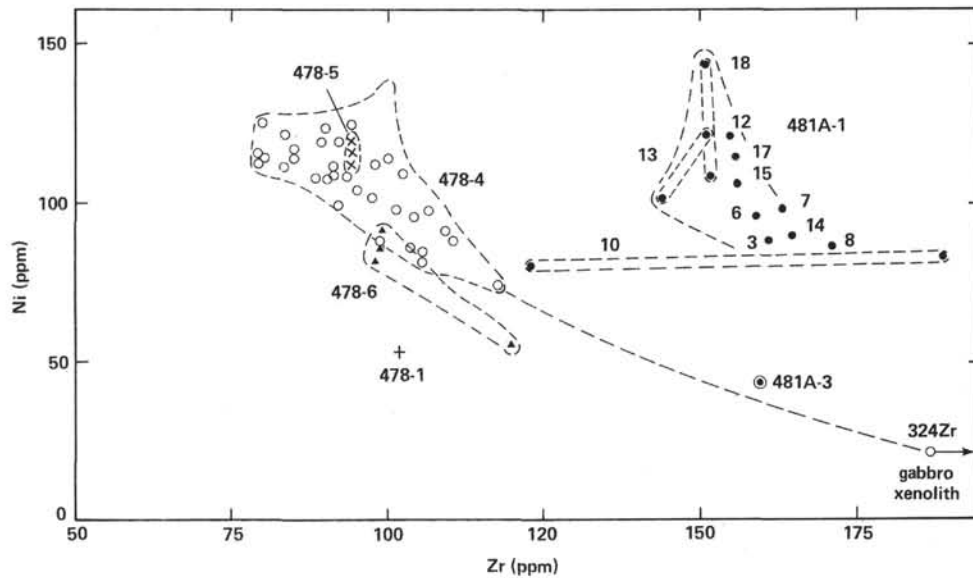


Figure 30. Ni versus Zr for basic rocks recovered at Sites 478 and 481. (Analyses determined at Birmingham by XRF. Numbers 3-18 refer to subunits of Unit 481A-1.)

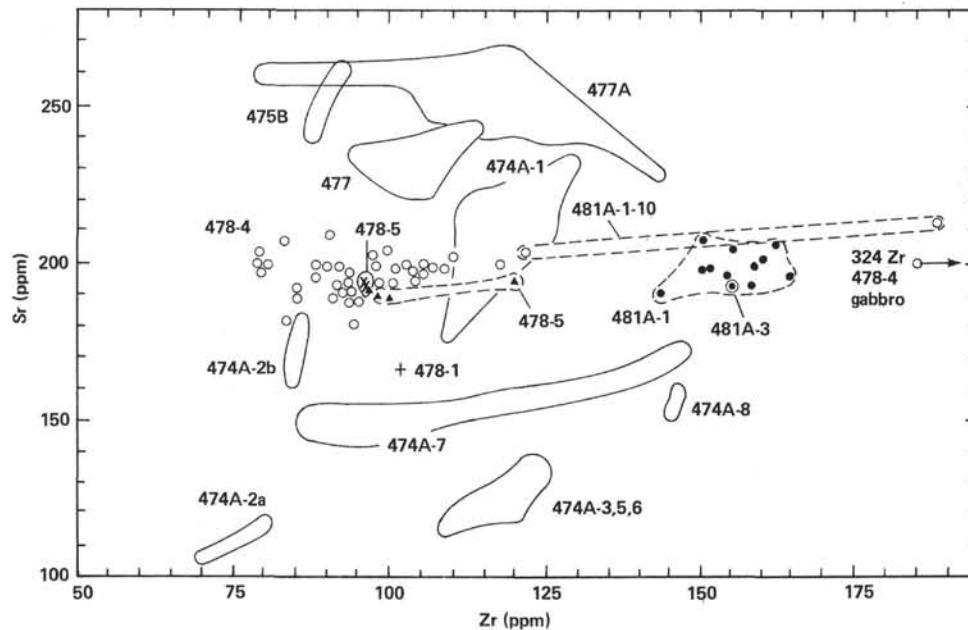


Figure 31. Sr versus Zr for basic igneous rocks recovered at Sites 478 and 481. (Fields for Sites 474, 475, and 477 from Figs. 8, 25. Analyses determined by XRF at Birmingham.)

Unit 3 (13.2 m)

The top of Unit 3 is marked by a devitrified chill zone below a sequence of thermally altered varved sediments. Only 20 cm of Unit 3 were recovered, comprising five pieces of aphanitic, sparsely plagioclase-phyric, vesicular basalt. The groundmass exhibits typical variolitic-to-hyalopilitic quench textures and is only slightly altered. Occasionally, the vesicles are filled or lined with calcite and/or zeolites and pyrites.

One sample from Unit 3 has been analyzed (Tables 19, 20). It is a subalkaline tholeiite (Fig. 32) with a low Al_2O_3 (14.7%) and high Fe_2O_3 (11.6%) content and

high FeO/MgO ratio (1.7) compared with the other samples from Hole 481A (Fig. 29). Accordingly, it has low MgO and Ni contents and moderately high contents of HYG elements. Ratios of immobile HYG and more-HYG elements are similar to those in Core 481-1; Y/Zr is slightly higher (Fig. 33), but the Th/Hf (Fig. 9), La/Tb (Fig. 10), La/Ta (Fig. 12), and Th/Ta (Fig. 27) ratios are indistinguishable. On both major- and trace-element grounds, Unit 3 appears to be a more evolved equivalent of Unit 1, both units perhaps having been derived from a common parental magma. The Zr content of the Unit 3 basalt is, however, anomalously low (e.g., Figs. 29, 33). This may be experimental error, because

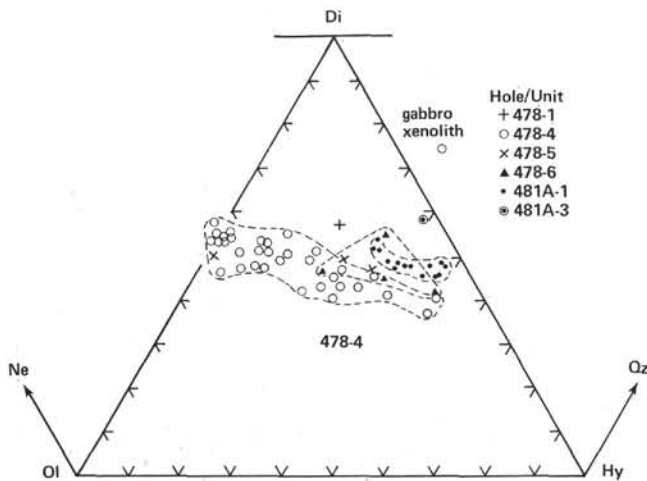


Figure 32. Basic rocks recovered at Sites 478 and 481 plotted on the normative basalt tetrahedron. ($\text{Fe}_2\text{O}_3/\text{FeO}$ ratio assumed to be 0.15. Analyses determined by XRF at Birmingham.)

the Saclay data give a value of 199 ppm (Table 20)—significantly higher than the XRF value (159 ppm), even correcting for interlaboratory bias.

GUAYMAS BASIN TRANSECT—DISCUSSION

The samples recovered at Sites 477, 478, and 481 in the Guaymas Basin exhibit many chemical similarities, particularly when the chemical diversity in one hole at the mouth of the Gulf—Hole 474A—is borne in mind. The HYG and more-HYG element ratios remain essentially constant within each site, but significant differences do occur *among* sites. This is particularly true for Th/Hf and Th/Ta ratios, which are higher at Sites 478 and 481 than at Site 477 (Figs. 9, 27). The La/Ta and La/Tb ratios, however, remain constant among all

three sites, as does the slope of the chondrite-normalized REE patterns.

From detailed studies of trace element behavior in basaltic suites from the MAR Bougault et al. (1980) consider that changes in La/Ta, Th/Ta, and perhaps Th/Hf ratios among different suites indicate compositional variations in the mantle source. Slight but significant differences between the partition coefficients of Th and Hf means that the Th/Hf ratio may be changed during partial melting processes. This chapter, however, reveals that La/Yb ratios remain remarkably constant throughout most of the Guaymas Basin samples, suggesting that varying degrees and conditions of partial melting are less important than source heterogeneity; i.e., if the Th/Hf ratios can be changed by different degrees of partial melting, why are the La/Yb ratios *not* changed? We are therefore led to the conclusion that the mantle source feeding Sites 478 and 481 was compositionally different, in Th/Hf and Th/Ta ratios, from that feeding Site 477.

The regularity of the chondrite-normalized REE patterns is not restricted to the samples recovered at Site 477, 478, and 481. Tortuga Island, a seamount lying to the northwest of the Guaymas Basin, is on oceanic crust estimated to be 1.7 m.y. old. The most primitive basalt recovered by Batiza et al. (1979) from Tortuga Island (Sample 2-20), and taken by them to represent the parental basaltic liquid, has a chondrite-normalized REE pattern virtually identical to those reported in this chapter (Fig. 37). In addition, the Tortuga Island basalts have Sr contents similar to the Guaymas Basin samples. Thus, Sample 2-20 ($\text{FeO}/\text{MgO} = 1.05$; Ni = 91 ppm), containing 245 ppm Sr and having a Sr/Ce ratio of 18, compares favorably with Sample 477-12-5, 46–50 cm ($\text{FeO}/\text{MgO} = 0.98$; Ni = 88 ppm), which contains 243 ppm Sr and has a Sr/Ce ratio of 23 (see Tables 13, 14

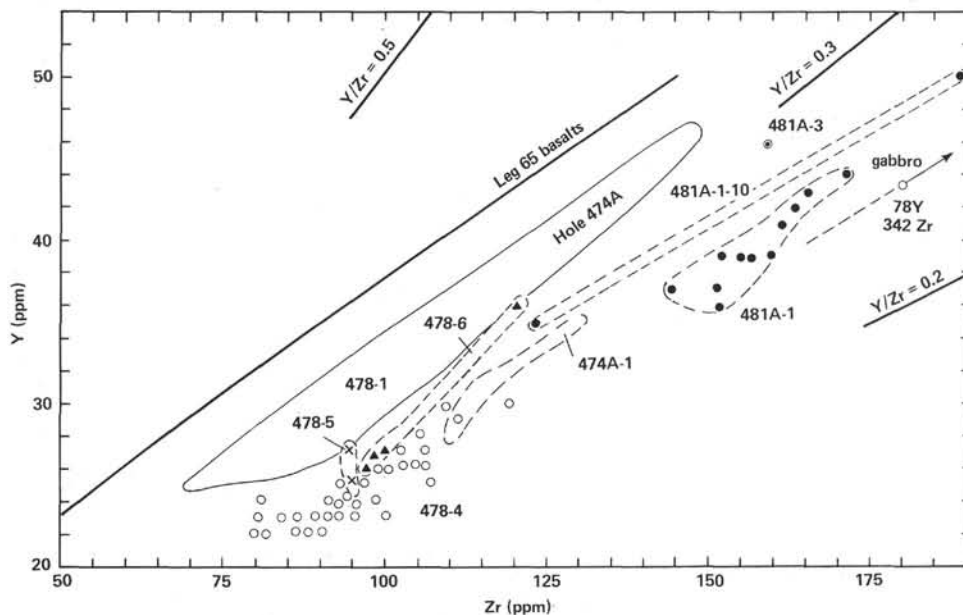


Figure 33. Y versus Zr for basic igneous rocks recovered at Sites 478 and 481. (Fields for Sites 474 from Fig. 6. Analyses determined by XRF at Birmingham.)

and data in Batiza et al., 1979). This is a useful comparison, because it implies that the high Sr contents in the Guaymas Basin samples are indeed primary. In addition, Basalt 2-20 has a low initial $^{87}\text{Sr}/^{86}\text{Sr}$ ratio (0.70245; Batiza et al., 1979), indicating that the high Sr contents in the Tortuga Islands suite are not a result of seawater interaction.

LEG 64: DISCUSSION

The samples recovered at Sites 477, 478, and 481 in the Guaymas Basin and the basalts from Tortuga Island are broadly similar in chemistry to N-type MORB, having La_N/Sm_N ratios of less than one, Th/Hf ratios between 0.07 and 0.15, La/Ta ratios between 15 and 20, and Th/Ta ratios between 0.7 and 1.5 (Kay et al., 1970; Bougault et al., 1978; Joron et al., 1980; Sun et al., 1979). In detail, however, N-type MORB, as defined by Wood et al. (1979c) and based on the data in Bougault et al. (1978) and Joron et al. (1980), have Th/Hf ratios of less than 0.1. This may of course reflect the lack of comprehensive data on N-type MORB; there are few available data from the EPR, for example. Nevertheless, the basaltic samples from Sites 478 and 481 have higher Th/Hf and Th/Ta ratios than the basaltic rocks from Sites 477, 474, and Leg 65. All of the Guaymas Basin samples have higher La/Yb, La/Sm, Th/Hf, and Sr/HYG element and lower Ti/Zr ratios than the Leg 65 basalts recovered during dredging operations at the mouth of the Gulf (Terrell et al., 1979) or from elsewhere along the EPR (e.g., Kay et al., 1970; Thompson et al., 1976; Hart, 1976). Note that the basalt from Site 475 also has high Sr/HYG element ratios and chondrite-normalized REE patterns similar to the Guaymas Basin samples.

It is therefore relevant at this stage to compare the Guaymas Basin samples with basalts recovered from elsewhere along the EPR. In Figure 38, data from Site 477 are plotted on a mantle-normalized diagram with basalts from Site 474 (basement) and Site 483 (Leg 65; Saunders, in press) at the mouth of the Gulf and a "typical" N-type MORB. Basalts from Site 483, located approximately 52 km west of the EPR, provide a more valid comparison with the Guaymas Basin samples than the older Site 474 basement. All of the samples in Figure 38 exhibit relative depletion of the elements Rb to La, although the depletion is more marked in the basalt from Site 483. The positive Sr anomaly in the sample from Section 477A-3-2 (17 cm) emphasizes the high Sr contents in the Guaymas Basin samples, although the negative Sr anomaly in the Site 483 basalt is probably a result of plagioclase fractionation. In addition, the samples from the Guaymas Basin have consistently lower Ti/Zr ratios than those from Site 474 and Leg 65.

It is unlikely that the consistently higher La/Sm, Th/Hf, and Sr/HYG element ratios and lower Ti/Zr ratios in the samples from the Guaymas Basin and Tortuga Island are caused solely by conditions of partial melting being different from those operating elsewhere along the EPR. Rather, we feel that these variations reflect different mantle source chemistries.

Several important conclusions may be drawn from the data obtained during this study. The broad overall depletion in more-HYG elements relative to HYG elements observed in *all* of the samples suggests the Gulf region has been underlain by Pacific Ocean "N-type" mantle at least since the Gulf began opening. This concurs with the tectonic reconstruction of Dickinson and Snyder (1979) which proposes that a no-slab window—and hence, by inference, predominantly Pacific-type mantle—underlay the entire region from ca. 5 m.y. ago. The differences in source chemistry between the samples from the mouth of the Gulf and those from the Guaymas Basin are probably explained by the mixing of the EPR-type mantle source with a component of subcontinental mantle—although the low initial $^{87}\text{Sr}/^{86}\text{Sr}$ ratios reported in the Tortuga Island basalts imply that the subcontinental mantle component is very minor. Alternatively, the high Sr contents may have been introduced by a residual calc-alkaline component left within the mantle region during Mesozoic and Tertiary subduction-related magmatic activity. Again, the low $^{87}\text{Sr}/^{86}\text{Sr}$ ratios imply that this component must be very minor.

The suggestion that Pacific-type oceanic mantle has underlain the region from about 5 m.y. ago concurs with the proposal that the ensialic Site 475 basalts were derived from an N-type source followed by minor contamination with continental crust. An analogous situation is found in the Tertiary Hebridean province of Scotland, where basalts have been derived from a depleted mantle source and subsequently variably contaminated by crustal material (Thompson et al., 1980).

Interesting comparisons can be made between the Gulf of California and two marginal basins that have developed as a consequence of rifting of an active continental margin, viz., the "rocas verdes" marginal basin ophiolite complex in southern Chile (Dalziel et al., 1974) and Bransfield Strait, northern Antarctic Peninsula (Weaver et al., 1979). The rocas verdes complex stretches from near Cape Horn northward to about 49°S and represents a narrow marginal basin that opened in the Late Jurassic and which had closed again by the Middle Cretaceous. Field evidence suggests that the basin was widest in the south, in the vicinity of Tortuga Island (Chile), and narrowed progressively toward the north at Sarmiento. It is possible that it existed as a series of enechelon basins, perhaps not unlike those in the Gulf of California (see Dalziel, in press). Geochemical studies of the southern Chile basaltic rocks (Saunders et al., 1979; Stern, 1979, 1980) have shown that those in the north, at Sarmiento, have relatively enriched geochemical characteristics (e.g., $\text{Ce}_N/\text{Yb}_N \sim 2$), whereas those in the south—at Tortuga, where the basin was widest—have depleted geochemical features typical of N-type MORB. On the other hand, the basalt dykes flanking the Tortuga complex have enriched geochemical features similar to those at Sarmiento. Stern (1979, 1980) considered that much of the difference in basalt chemistry could be explained by the dynamic melting model of Langmuir et al. (1977). Thus the first-stage melts generated at the start of opening of the basin had rela-

Table 16. X-ray fluorescence analyses, Hole 478.

Core Section Level (cm) Unit	26	40	41	41	41	41	42	42	42	42	43	43	44	44	44	44	44	45	45	45	46
SiO ₂	49.4	49.7	49.1	49.6	49.1	49.2	49.4	47.7	49.1	49.1	49.0	48.8	48.8	48.9	48.4	48.7	49.4	48.4	48.4	48.9	48.3
TiO ₂	1.74	1.20	1.24	1.20	1.09	1.14	1.01	0.79	1.25	1.51	1.68	1.48	1.44	1.35	1.30	1.24	1.43	1.20	1.28	1.13	1.13
Al ₂ O ₃	15.2	15.7	16.0	15.8	16.8	16.8	16.5	16.4	16.2	16.0	15.8	15.9	16.1	16.4	16.7	16.4	15.6	17.0	16.8	16.9	17.0
tFe ₂ O ₃	10.35	9.19	9.09	9.25	8.90	9.00	8.98	8.75	9.51	9.51	9.94	9.44	9.59	9.15	9.29	9.10	9.32	9.13	9.31	8.93	8.79
MnO	0.16	0.14	0.15	0.13	0.14	0.14	0.14	0.14	0.15	0.14	0.14	0.14	0.15	0.14	0.15	0.14	0.15	0.14	0.15	0.15	0.14
MgO	7.75	9.45	9.35	9.40	8.60	8.62	8.70	8.80	9.35	8.85	8.60	9.15	8.80	8.45	8.10	8.82	8.75	8.10	8.30	8.05	7.80
CaO	11.52	10.86	10.87	10.18	11.05	11.25	11.05	10.34	10.25	11.06	11.02	11.07	10.35	10.98	11.13	10.79	10.75	11.25	11.10	11.15	11.12
Na ₂ O	2.94	2.26	2.56	2.47	3.03	2.86	2.84	3.02	2.72	2.85	2.89	2.64	3.09	3.08	3.06	2.98	2.67	3.06	3.04	3.15	3.14
K ₂ O	0.09	0.20	0.20	0.24	0.31	0.22	0.20	0.31	0.30	0.16	0.15	0.11	0.29	0.24	0.23	0.14	0.26	0.24	0.26	0.27	0.23
P ₂ O ₅	0.18	0.19	0.17	0.18	0.14	0.15	0.40	0.18	0.18	0.20	0.21	0.20	0.20	0.19	0.18	0.17	0.20	0.17	0.17	0.14	0.16
LOI	0.47	—	—	1.26	—	—	—	3.74	—	—	—	0.90	—	—	1.63	—	—	—	—	—	2.92
Total	99.84	98.82	98.77	99.74	99.15	99.38	99.17	100.17	98.95	99.41	99.46	99.84	98.77	98.85	100.13	98.47	98.51	98.71	98.88	98.84	100.73
Trace Elements (ppm)																					
Ni	53	119	104	119	111	109	107	109	113	84	73	95	81	86	87	88	91	101	98	111	97
Cr	204	249	243	226	228	227	251	221	225	237	215	230	228	224	207	221	167	221	197	261	223
Zn	61	44	45	46	48	49	51	48	50	56	56	49	50	44	52	48	50	48	50	59	46
Ga	18	14	17	18	18	12	11	14	0	22	17	16	19	20	20	16	24	18	17	19	19
Rb	<1	2	4	3	2	3	2	2	4	1	2	<1	3	2	4	2	3	3	4	4	2
Sr	166	199	188	191	182	189	197	199	193	197	200	195	198	198	201	193	198	200	198	202	198
Y	32	23	25	23	23	23	22	26	26	30	26	28	27	26	29	26	30	26	27	24	25
Zr	102	90	96	93	84	92	89	103	101	106	118	105	106	104	111	99	109	98	102	98	107
Nb	3	2	3	4	4	2	2	3	3	2	5	4	2	2	3	2	4	3	4	2	3
Ba	42	90	75	57	37	45	51	65	41	257	51	60	81	37	45	40	41	43	42	41	43
La	7	8	8	7	5	7	7	7	7	8	8	7	8	6	6	5	8	6	8	5	5
Ce	13	14	14	12	13	11	11	13	13	16	16	15	19	15	12	16	17	12	15	12	13
Nd	12	11	11	10	10	11	9	11	12	13	13	14	14	11	12	12	13	10	12	10	12
Pb	4	1	6	<1	1	2	1	1	2	2	2	<1	4	2	2	<1	3	<1	<3	7	3
Th	1	2	4	<1	<1	3	<1	<1	2	4	<1	1	2	<1	<1	1	1	<1	<1	<1	1
Selected Ratios																					
Zr/Nb	34	45	32	23	21	46	45	34	34	53	24	26	53	52	37	50	27	33	26	48	36
Ti/Zr	102	80	77	77	78	74	68	46	74	85	85	85	81	78	70	75	79	73	75	69	63
Y/Zr	0.31	0.26	0.26	0.25	0.27	0.25	0.25	0.25	0.26	0.25	0.25	0.27	0.25	0.25	0.26	0.26	0.28	0.27	0.26	0.24	0.23
Ce/Zr	0.13	0.16	0.15	0.13	0.15	0.12	0.12	0.13	0.13	0.15	0.14	0.14	0.18	0.14	0.11	0.16	0.16	0.12	0.15	0.12	0.12
Ba/Zr	0.41	1.00	0.78	0.61	0.44	0.49	0.57	0.63	0.41	2.42	0.43	0.57	0.76	0.36	0.41	0.40	0.38	0.44	0.41	0.42	0.40
(Ce/Y) _N	1.00	1.50	1.38	1.28	1.39	1.17	1.23	1.23	1.23	1.51	1.31	1.32	1.73	1.42	1.02	1.51	1.39	1.13	1.36	1.23	1.28
Fe/Mg	1.55	1.13	1.13	1.14	1.20	1.21	1.20	1.15	1.18	1.25	1.34	1.20	1.26	1.26	1.33	1.20	1.24	1.31	1.30	1.29	1.31
K/Rb	>747	830	415	664	1287	609	830	1287	623	1328	623	>913	802	996	477	581	719	664	540	560	955
Ba/Sr	0.25	0.45	0.40	0.30	0.20	0.24	0.26	0.33	0.21	1.30	0.26	0.31	0.41	0.19	0.22	0.21	0.21	0.22	0.21	0.20	0.22
CIPW Norms																					
Q	0.0	0.0	0.0	0.0	0.0	0.0	0.0	0.0	0.0	0.0	0.0	0.0	0.0	0.0	0.0	0.0	0.0	0.0	0.0	0.0	0.0
Or	0.5	1.2	1.2	1.4	1.8	1.3	1.2	1.8	1.8	1.0	0.9	0.7	1.7	1.4	1.4	0.8	1.6	1.4	1.6	1.6	1.3
Ab	24.9	19.3	21.9	21.0	25.9	24.3	24.2	25.5	23.3	24.3	24.6	22.4	26.5	26.4	25.9	25.6	22.9	26.2	26.0	27.0	26.4
An	28.1	32.3	32.1	31.4	31.7	32.5	31.8	30.1	31.4	30.6	29.9	31.2	29.5	30.5	31.1	31.3	30.3	32.3	31.9	31.7	31.4
Ne	0.0	0.0	0.0	0.0	0.0	0.0	0.0	0.0	0.0	0.0	0.0	0.0	0.0	0.0	0.0	0.0	0.0	0.0	0.0	0.0	0.0
Di	22.8	17.0	17.3	14.6	18.4	18.4	16.9	16.1	15.3	18.9	19.3	18.2	17.1	18.9	18.6	17.8	18.2	18.8	18.5	19.0	18.1
Hy	8.9	21.0	12.9	19.9	2.1	6.0	10.4	1.6	11.5	8.1	8.2	11.1	4.7	3.2	1.1	5.8	14.0	0.2	0.8	0.5	0.1
Ol	7.8	3.9	9.4	5.3	15.4	12.5	10.3	16.8	11.5	11.3	10.8	9.8	14.7	14.1	15.1	13.5	7.3	15.9	16.0	15.3	15.0
Mt	1.8	1.6	1.6	1.6	1.6	1.6	1.6	1.5	1.7	1.7	1.7	1.6	1.7	1.6	1.6	1.6	1.6	1.6	1.6	1.6	1.5
Il	3.3	2.3	2.4	2.3	2.1	2.2	1.9	1.5	2.4	2.9	3.2	2.8	2.8	2.6	2.5	2.4	2.8	2.3	2.5	2.2	2.1
Ap	0.4	0.5	0.4	0.4	0.3	0.4	1.0	0.4	0.4	0.5	0.5	0.5	0.5	0.5	0.4	0.4	0.5	0.4	0.4	0.3	0.4

Note: See Table 1, note.

Table 16. (Continued).

46	49	49	50	50	51	51	51	52	52	52	53	53	53	53	54	54	54	54	54	54	54
4	1	3	1	5	3	3	6	1	3	6	1	2	3	4	1	1	2	2	3	4	4
71	63	7	92	59	49	112	114	61	39	94	69	48	51	28	77	137	26	146	129	2	56
4	4	4	4	4	4	4	4	4	4	4	4	4	4	4	5	5	5	6	6	6	6
48.7	47.5	48.9	48.3	48.7	52.0	48.1	48.8	47.9	48.3	48.6	48.1	49.1	48.8	48.5	49.2	49.7	48.0	49.0	49.7	49.3	49.6
1.14	0.94	1.04	1.06	0.98	2.13	1.08	1.06	1.16	1.10	1.12	1.16	1.13	1.22	1.26	1.25	1.26	1.27	1.37	1.47	1.90	1.50
17.1	17.1	17.3	17.5	17.2	16.6	16.9	16.6	17.4	17.5	17.1	17.0	16.1	16.1	16.3	15.5	16.2	16.3	15.6	14.2	13.1	15.2
9.07	8.60	8.52	8.62	8.77	7.92	9.01	9.15	9.15	8.94	8.96	9.14	9.04	9.05	9.41	9.22	9.03	9.42	9.48	10.20	10.70	9.97
0.16	0.13	0.14	0.14	0.14	0.13	0.15	0.15	0.14	0.15	0.15	0.16	0.17	0.23	0.16	0.14	0.13	0.14	0.14	0.16	0.25	0.15
8.04	8.90	7.90	7.90	8.50	4.13	8.20	8.90	8.65	7.90	8.15	7.95	9.55	9.30	9.15	9.30	9.00	9.25	9.30	9.35	9.00	9.25
11.30	11.17	11.92	11.82	11.65	11.20	11.46	10.37	11.18	11.10	11.05	10.95	10.92	10.93	10.74	11.26	11.58	11.03	10.83	10.46	11.25	10.74
3.06	2.65	2.76	2.77	2.74	3.29	2.76	2.83	2.77	3.25	3.16	3.06	2.29	2.26	2.27	2.47	2.62	2.69	2.80	2.48	2.62	2.68
0.24	0.18	0.19	0.19	0.17	0.89	0.18	0.28	0.19	0.36	0.35	0.38	0.22	0.65	0.74	0.15	0.19	0.60	0.15	0.09	0.11	0.08
0.15	0.15	0.14	0.14	0.15	0.52	0.13	0.14	0.17	0.14	0.14	0.16	0.11	0.15	0.16	0.19	0.16	0.16	0.19	0.19	0.25	0.19
—	2.31	—	—	—	1.54	—	—	1.50	—	—	—	1.10	—	—	1.04	—	1.39	1.32	—	1.72	—
99.01	99.73	98.80	98.43	98.96	100.28	98.00	98.28	100.14	98.78	98.87	98.03	99.67	99.77	98.71	99.77	99.85	100.26	100.22	98.31	100.16	99.29
108	136	125	123	121	21	115	123	113	114	112	107	112	116	99	111	118	115	91	82	55	85
245	299	289	261	226	31	264	136	240	229	240	225	246	240	234	225	239	242	279	262	154	231
58	46	54	50	45	51	50	51	49	59	54	85	48	57	53	31	27	34	29	53	115	58
19	19	18	18	17	28	17	16	22	21	15	19	20	18	19	16	19	18	21	18	18	19
3	<1	2	2	2	8	1	3	3	4	4	4	2	12	13	<1	<1	7	1	<1	<1	<1
197	204	204	199	208	199	197	181	200	189	199	210	200	192	191	194	192	189	187	187	194	190
24	23	23	23	22	78	22	23	24	23	23	24	22	22	25	27	25	24	27	27	36	26
94	100	80	91	84	324	80	95	81	86	92	91	80	86	93	94	94	94	99	98	120	97
3	4	3	3	4	10	3	3	4	3	3	3	4	4	4	3	3	4	4	4	4	4
41	42	36	39	45	102	47	66	48	44	71	52	74	70	108	48	42	52	64	45	60	42
5	6	3	7	6	17	6	7	6	5	5	6	4	6	6	6	6	6	7	7	10	7
13	12	10	9	12	47	10	10	10	8	11	13	9	9	12	14	13	11	15	11	21	14
11	10	8	9	10	32	9	12	9	10	9	11	9	9	10	11	11	10	12	11	17	11
2	<1	5	7	3	2	2	<1	7	3	2	4	<1	7	2	3	4	4	2	4	7	3
3	<1	<1	3	2	3	<1	1	2	1	<1	<1	<1	<1	<1	<1	<1	<1	<1	<1	<1	<1
31	25	27	30	21	32	27	32	20	29	31	30	20	22	23	31	31	24	25	25	30	24
73	56	78	70	70	39	81	67	86	77	73	76	85	85	81	80	80	81	83	90	95	93
0.26	0.23	0.29	0.25	0.26	0.24	0.28	0.24	0.30	0.27	0.25	0.26	0.28	0.26	0.27	0.29	0.27	0.26	0.27	0.28	0.30	0.27
0.14	0.12	0.13	0.10	0.14	0.15	0.13	0.11	0.12	0.09	0.12	0.14	0.11	0.10	0.13	0.15	0.14	0.12	0.15	0.11	0.17	0.14
0.44	0.42	0.45	0.43	0.54	0.31	0.59	0.69	0.59	0.51	0.77	0.57	0.93	0.81	1.16	0.51	0.45	0.55	0.65	0.46	0.50	0.43
1.33	1.28	1.07	0.96	1.34	1.48	1.12	1.07	1.02	0.85	1.17	1.33	1.00	1.00	1.18	1.27	1.28	1.13	1.36	1.00	1.43	1.32
1.31	1.12	1.25	1.27	1.20	2.22	1.27	1.19	1.23	1.31	1.27	1.33	1.10	1.13	1.19	1.15	1.16	1.18	1.18	1.27	1.38	1.25
664	>1494	789	789	706	923	1494	775	526	747	726	789	913	450	473	>1245	>1577	712	1245	>747	>913	>664
0.21	0.21	0.18	0.20	0.22	0.51	0.24	0.36	0.24	0.23	0.36	0.25	0.37	0.36	0.57	0.25	0.22	0.28	0.34	0.24	0.31	0.22
0.0	0.0	0.0	0.0	0.0	2.5	0.0	0.0	0.0	0.0	0.0	0.0	0.0	0.0	0.0	0.0	0.0	0.0	0.0	0.0	0.0	0.0
1.4	1.1	1.1	1.1	1.0	5.2	1.1	1.7	1.1	2.2	2.1	2.3	1.3	3.9	4.4	0.9	1.1	3.5	0.9	0.5	0.6	0.5
26.1	22.5	23.6	23.8	23.4	27.8	23.8	24.4	23.4	25.0	26.0	25.9	19.4	19.4	19.5	20.9	22.2	22.7	23.6	21.3	22.1	22.8
32.5	34.5	34.8	35.2	34.5	27.8	34.0	32.4	34.3	32.5	31.9	32.1	33.0	32.4	32.6	30.9	31.8	30.4	29.5	27.9	23.6	29.3
0.0	0.0	0.0	0.0	0.0	0.0	0.0	0.0	0.0	1.5	0.5	0.3	0.0	0.0	0.0	0.0	0.0	0.0	0.0	0.0	0.0	0.0
18.8	16.3	19.6	19.0	18.6	19.9	18.8	15.4	16.2	18.2	18.4	18.1	16.7	17.4	16.5	19.3	20.0	18.7	18.6	19.2	24.8	18.7
1.0	4.0	4.8	3.0	4.5	7.9	3.9	8.4	2.9	0.0	0.0	0.0	16.2	11.4	10.0	14.0	10.7	0.1	9.3	21.7	14.9	15.3
15.2	15.0	11.4	13.1	13.4	0.0	13.6	12.9	15.6	15.8	16.2	16.2	7.5	10.4	11.7	7.7	9.0	17.9	11.3	3.3	5.3	7.4
1.6	1.5	1.5	1.5	1.5	1.4	1.6	1.6	1.6	1.6	1.6	1.6	1.6	1.6	1.7	1.6	1.6	1.6	1.6	1.8	1.9	1.7
2.2	1.8	2.0	2.0	1.9	4.0	2.1	2.0	2.2	2.1	2.2	2.2	2.2	2.3	2.4	2.4	2.4	2.4	2.6	2.8	3.6	2.9
0.4	0.4	0.3	0.3	0.4	1.2	0.3	0.3	0.4	0.3	0.3	0.4	0.3	0.4	0.4	0.5	0.4	0.4	0.4	0.5	0.6	0.5

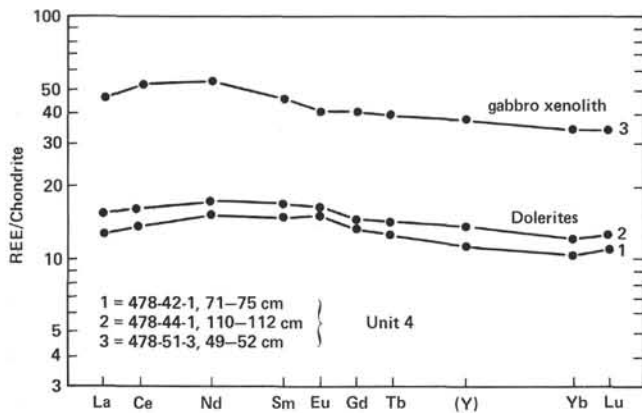


Figure 34. Chondrite-normalized REE data for basic rocks recovered at Site 478. (Analyses determined by INAA at Bedford College.)

tively 'enriched' geochemical features consistent with low degrees of melting of an undepleted mantle source. The later, second-stage melts, however, erupted as a consequence of continued diapirism, had correspondingly 'depleted' trace-element compositions; indeed, some of the later dykes cutting the complex are highly magnesian (Elthon, 1979), similar to the magnesian dolerites at Site 474. Saunders et al. (1979) and Tarney et al. (in press) felt, however, that it was not possible to exclude mantle heterogeneity in interpreting these differences. For instance, the behavior of HFS elements such as Ta and Nb in the two basalt types was not entirely consistent with dynamic melting. An alternative explanation considered was that the upper mantle source

Table 17. INAA results (Saclay) for selected samples, Hole 478.

Core Section Interval (cm) Unit	26	41	50	51	51	52	54	54
	1	4	5	3	3	3	2	4
	44-46	81-83	59-62	49-52	112-115	39-41	26-28	56-59
	1	4	4	4	4	4	5	6
Ni	59	122	132	30	132	129	120	88
Cr	222	241	243	71	234	224	239	238
Co	42.6	39.8	39.7	23.5	40.6	40.7	40.0	37.3
Se	40.0	30.5	27.8	30.7	30.9	30.4	32.5	33.7
Ba	17	25	37	92	32	23	34	39
Sr	186	240	259	215	195	243	239	234
Cs	0.18	0.23	0.14	0.19	0.23	0.32	1.64	0.11
Rb	1.4	2.9	2.5	6.9	4.0	3.3	7.7	—
U	0.09	0.07	—	0.40	0.07	0.09	0.16	0.17
Th	0.24	0.27	0.27	1.08	0.28	0.26	0.32	0.40
Zr	100	78	95	328	84	88	119	110
Hf	2.70	2.17	2.00	7.9	2.11	2.04	2.46	2.40
Ta	0.19	0.21	0.20	0.79	0.20	0.20	0.23	0.24
Sb	0.04	0.02	0.01	0.01	—	0.02	0.08	0.10
La	4.24	3.74	3.67	15.2	3.67	3.49	4.13	3.84
Ce	9.3	9.6	9.5	35.0	8.5	9.2	10.3	10.3
Eu	1.41	1.06	1.17	2.77	0.82	1.02	1.12	1.18
Tb	0.74	0.53	0.52	1.74	0.52	0.52	0.56	0.61

Note: All values in ppm.

regions beneath southern Chile had been contaminated and enriched in LIL elements during the earlier phase of calc-alkaline magmatism. Thus subcontinental mantle with LIL element-enriched characteristics would be able to contribute to basaltic volcanism during the early stages of back-arc rifting but not during the later stages as the subcontinental lithosphere was pulled apart and separated.

In the case of Bransfield Strait, a small marginal basin in the initial stages of formation between the South Shetland Island Arc and the Antarctic Peninsula mainland, Weaver et al. (1979) described the variable geochemical characteristics of basalts erupted from vol-

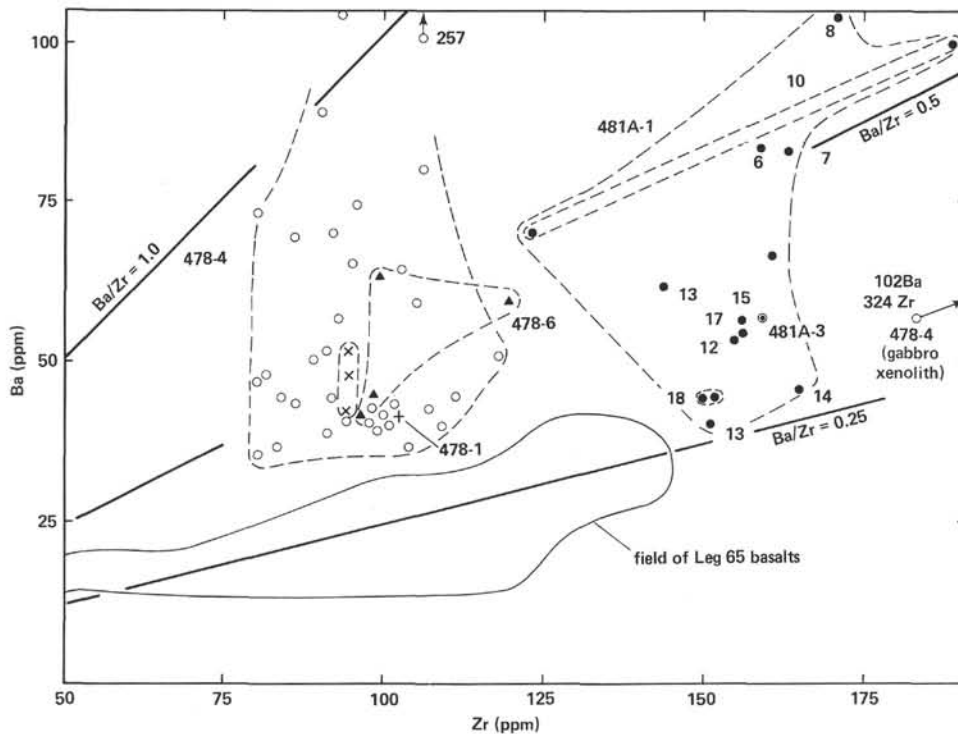


Figure 35. Ba versus Zr for basic rocks recovered at Sites 478 and 481. (Analyses determined by XRF at Birmingham. Numbers 6-18 refer to subunits of Unit 481A-1.)

Table 18. INAA results (Bedford) for selected samples, Hole 478.

Core Section	42	44	51
Interval (cm)	1	1	3
Unit	4	4	4
La	4.24	4.49	15.18
Ce	12.0	13.9	45.2
Nd	9.6	11.0	34.1
Sm	2.99	3.49	9.2
Eu	1.17	1.30	3.09
Gd	3.69	3.98	11.22
Tb	0.66	0.75	2.06
Yb	2.27	2.67	7.51
Lu	0.38	0.43	1.15
Th	0.38	0.47	1.48
Hf	2.20	2.55	7.99
Ta	0.22	0.27	0.79
La _N /Yb _N	1.25	1.24	1.36
La/Ta	19	18	19
Th/Hf	0.17	0.18	0.19

Note: Trace-element values in ppm.

canic islands located on or close to the back-arc spreading axis. They considered that mantle sources with different geochemical characteristics were involved and that some of the geochemical features had developed as a consequence of earlier calc-alkaline magmatism in the area. Of particular interest is that the lavas of Deception and Penguin Islands had significantly higher concentrations of Ba and Sr relative to the other HYG elements, and yet had low levels of K and Rb. Additionally, HFS elements, such as Nb, were also present in low concentrations. Weaver et al. (1979) stressed, in fact, that HYG elements that normally exhibited coherent behavior during magmatic fractionation at mid-ocean ridges and oceanic islands, instead appeared to be decoupled in their behavior during the early stages of back-arc rifting in a continental environment. Some of these features are clearly exhibited by the Gulf of California basalts. The simplest interpretation would appear to be that mantle sources contributing to basaltic magmatism during the early stages of opening of the Gulf are not uniform but retain some vestiges of the earlier calc-alkaline activity in the area. Such sources are dissipated fairly rapidly, however, so that basalts erupted later (like those sampled during Leg 65) are derived from rather more uniform sources more characteristic of Pacific Ocean mantle.

ACKNOWLEDGMENTS

We would like to thank all shipboard personnel for discussion, advice, and support during Leg 64. Shorebased analytical facilities at Birmingham and Bedford were made available by Drs. G. L. Hendry and G. F. Marriner, respectively; their assistance is gratefully acknowledged. We also thank Sheila Bishop who typed the manuscript, N. Sinclair-Jones who drafted the diagrams, and N. G. Marsh and M. J. Norry who reviewed and suggested improvements to the manuscript. Saunders acknowledges receipt of an NERC (U.K.) Research Fellowship while at the University of Birmingham.

REFERENCES

- Batiza, R., Futa, K., and Hedge, C. E., 1979. Trace element and strontium isotope characteristics of volcanic rocks from Isla Tortuga: A young seamount in the Gulf of California. *Earth Planet. Sci. Lett.*, 43:269-278.
- Bennett, H., and Oliver, G. J., 1976. Development of fluxes for the analysis of ceramic materials by X-ray fluorescence spectrometry. *Analyst*, 101:803-807.
- Bougault, H., Joron, J.-L., and Treuil, M., 1980. The primordial chondritic nature and large-scale heterogeneities in the mantle: Evidence from high and low partition coefficient elements in ocean basalts. *Phil. Trans. Roy. Soc. London Ser. A*, 297:203-213.
- Bougault, H., and Treuil, M., 1980. Mid-Atlantic Ridge: Zero-age geochemical variations between Azores and 22°N. *Nature*, 209:209-212.
- Bougault, Treuil, M., and Joron, J.-L., 1978. Trace elements in basalts from 22°N and 36°N in the Atlantic Ocean: Fractional crystallization, partial melting and heterogeneity of the upper mantle. In Melson, W. G., Rabinowitz, P. D., et al., *Init. Repts. DSDP*, 45: Washington (U.S. Govt. Printing Office), 493-506.
- Chayes, F., 1966. Alkaline and subalkaline basalts. *Am. J. Sci.*, 264:128-145.
- Chayla, B., Jafreziec, H., and Joron, J.-L., 1973. Analyse par activation dans les mentions épithermiques. Application à la détermination d'éléments en trace dans les roches. *Comp. Rend. Acad. Sci. Paris*, 277:273-275.
- Dalziel, I. W. D., in press. Back-arc spreading in the southern Andes: A review and critical reappraisal. *Phil. Trans. Roy. Soc. London*.
- Dalziel, I. W. D., de Wit, M. J., and Palmer, K. F., 1974. Fossil marginal basin in the southern Andes. *Nature*, 250:291-294.
- De Paulo, D. J., and Wasserburg, G. J., 1976. Nd isotopic variations and petrogenetic models. *Geophys. Res. Lett.*, 3:249-252.
- Dickinson, W. R., and Snyder, W. S., 1979. Geometry of subducted slabs related to San Andreas transform. *J. Geol.*, 87:609-627.
- Dixon, T. H., and Batiza, R., 1979. Petrology and chemistry of Recent lavas in the northern Marianas: Implications for the origin of island arc basalts. *Contrib. Mineral. Petrol.*, 70:167-181.
- Dupré, B., and Allègre, C. J., 1980. Pb-Sr-Nd isotopic correlation and the chemistry of the North Atlantic mantle. *Nature*, 286:17-22.
- Einsele, G., Gieskes, J. M., Curray, J. R., et al., 1980. Intrusion of basaltic sills into highly porous sediments, and resulting hydrothermal activity. *Nature*, 283:441-445.
- Elthon, D., 1979. High magnesia liquids as the parental magma for ocean floor basalts. *Nature*, 278:514-518.
- Frey, F. A., Bryan, W. B., and Thompson, G., 1974. Atlantic Ocean floor: Geochemistry and petrology of basalts from Legs 2 and 3 of the Deep Sea Drilling Project. *J. Geophys. Res.*, 79:5507-5527.
- Frey, F. A., Green, D. H., and Roy, S. D., 1978. Integrated models of basalt petrogenesis. *J. Petrol.*, 19:463-513.
- Gastil, G., Krummenacher, D., and Minch, J., 1979. The record of Cenozoic volcanism around the Gulf of California. *Geol. Soc. Am. Bull.*, 90:839-857.
- Gastil, G., Phillips, R. P., and Allison, E. C., 1975. Reconnaissance geology of the State of Baja California. *Mem. Geol. Soc. Am.*, 140.
- Gibson, I. L., Marriner, G. F., Matthey, D. P., et al., 1976. Is the extrusive portion of the Oceanic crust vertically compositionally zoned? *Bull. Soc. Geol. Fran.*, 18:897-902.
- Gill, J. B., 1976. Composition and age of Lau Basin and Ridge volcanic rocks: Implications for evolution of an inter arc basin and remnant arc. *Geol. Soc. Am. Bull.*, 87:1384-1395.
- Hanson, G. N., 1977. Geochemical evolution of the suboceanic mantle. *J. Geol. Soc. London.*, 134:235-253.
- Hart, S. R., 1971. K, Rb, Cs, Sr, and Ba contents and Sr isotope ratios of ocean floor basalts. *Phil. Trans. Roy. Soc. London Ser. A*, 268:573-587.
- _____, 1976. LIL-element geochemistry, Leg 34 basalts. In Hart, S. R., Yeats, R. S., et al., *Init. Repts. DSDP*, 34: Washington (U.S. Govt. Printing Office), 215-226.
- Hart, S. R., Erlank, A. J., and Kable, E. J. D., 1974. Seafloor basalt alteration: Some chemical and strontium isotopic effects. *Contrib. Mineral. Petrol.*, 44:219-230.
- Hart, S. R., Schilling, J.-G., and Powell, J. L., 1973. Basalts from Iceland and along the Reykjanes Ridge: Sr-isotope geochemistry. *Nature*, 246:104-107.
- Harvey, P. K., Taylor, D. M., Hendry, G. L., et al., 1973. An accurate fusion method for the analysis of rocks and chemically related materials by X-ray fluorescence spectrometry. *X-Ray Spectrom.*, 2:33-44.

- Hawkesworth, C. J., Norry, M. J., Roddick, J. C., et al., 1979. $^{143}\text{Nd}/^{144}\text{Nd}$, $^{87}\text{Sr}/^{86}\text{Sr}$, and incompatible element variations in calc-alkaline andesites and plateau lavas from South America. *Earth Planet. Sci. Lett.*, 42:45-77.
- Hawkesworth, C. J., O'Nions, R. K., Pankhurst, R. J., et al., 1977. A geochemical study of island-arc and back-arc tholeiites from the Scotia Sea. *Earth Planet. Sci. Lett.*, 36:253-262.
- Hendry, G. L., 1975. X-ray fluorescence. In Nicol, A. W. (Ed.), *Physicochemical Methods of Mineral Analysis*: New York (Plenum), pp. 87-152.
- Jakeš, P., and White, A. J. R., 1972. Major and trace element abundances in volcanic rocks of orogenic areas. *Geol. Soc. Am. Bull.*, 83:29-40.
- Joron, J.-L., Bollinger, C., Quisefit, J. P., et al., 1980. Trace elements in basalts at 25°N, old crust, in the Atlantic Ocean: Alteration, mantle, and magmatic processes. In Donnelly, T. W., Francheteau, J., Bryan, W., et al., *Init. Repts. DSDP*, 51, 52, 53, Pt. 1: Washington (U.S. Govt. Printing Office), 1087-1098.
- Joron, J.-L., and Treuil, M., 1977. Utilisation des propriétés des éléments fortement hygromagmatophiles pour l'étude de la composition chimique et de l'hétérogénéité du manteau. *Bull. Soc. Geol. France*, 19:1197-1205.
- Karig, D. E., 1974. Evolution of arc systems in the western Pacific. *Ann. Rev. Earth Plan. Sci.*, 2:51-75.
- Karig, D. E., and Jency, W., 1972. The proto-Gulf of California. *Earth Planet. Sci. Lett.*, 17:169-174.
- Kay, R. W., Hubbard, N. J., and Gast, P. W., 1970. Chemical characteristics and origin of oceanic ridge volcanic rocks. *J. Geophys. Res.*, 75:1585-1613.
- Langmuir, C. H., Bender, J. F., Bence, A. E., et al., 1977. Petrogenesis of basalts from the FAMOUS area: Mid-Atlantic Ridge. *Earth Planet. Sci. Lett.*, 36:133-156.
- Larson, R. L., 1972. Bathymetry, magnetic anomalies, and plate-tectonic history at the mouth of the Gulf of California. *Geol. Soc. Am. Bull.*, 83:3345-3360.
- Larson, P. A., Mudie, J., and Larson, R. L., 1972. Magnetic anomalies and fracture zone trends in the Gulf of California. *Geol. Soc. Am. Bull.*, 83:3361-3368.
- Larson, R. L., Menard, H. W., and Smith, S. M., 1968. Gulf of California: A result of ocean-floor spreading and transform faulting. *Science*, 161:781-784.
- Lawver, L. A., and Hawkins, J. W., 1978. Diffuse magnetic anomalies in marginal basins: Their possible tectonic and petrologic significance. *Tectonophysics*, 45:323-339.
- Lawver, L. A., Williams, D. L., and Von Herzen, R. P., 1975. A major geothermal anomaly in the Gulf of California. *Nature*, 257:23-29.
- Leake, B. E., Hendry, G. L., Kemp, A., et al., 1969. The chemical analysis of rock powders by automatic X-ray fluorescence. *Chem. Geol.*, 5:7-86.
- Lewis, B. T. R., McClain, J., Snyderman, W. E., et al., 1975. Gulf of California IPOD site survey, final report (unpublished).
- Lloyd, F. E., and Bailey, P. K., 1975. Light element metasomatism of the continental mantle: The evidence and consequences. In Ahrens, L. H., Press, F., Runcorn, S. K., and Urey, H. C. (Eds.) *Physics and Chemistry of the Earth*: Oxford (Pergamon), pp. 389-416.
- Ludden, J. A., and Thompson, G., 1979. An evaluation of the behavior of the rare earth elements during the weathering of sea floor basalt. *Earth Planet. Sci. Lett.*, 43:85-92.
- Marsh, N. G., Saunders, A. D., Tarney, J., et al., 1980. Geochemistry of basalts from the Shikoku and Daito Basins, Deep Sea Drilling Project Leg 58. In Klein, G. deV., Kobayashi, K., et al., *Init. Repts. DSDP*, 58: Washington (U.S. Govt. Printing Office), 805-842.
- Mitchell, W. S., and Aumento, F., 1977. Uranium in oceanic rocks: Deep Sea Drilling Project Leg 37. *Can. J. Earth Sci.*, 14:794-808.
- Moore, D. G., and Buffington, E. C., 1968. Transform faulting and growth of the Gulf of California since the late Pliocene. *Science*, 161:1238-1241.
- Moore, G. F., Becker, K., Bibee, L. D., et al., 1978. Gulf of California IPOD site summary, final report (unpublished).
- O'Hara, M. J., 1977. Geochemical evolution during fractional crystallisation of a periodically refilled magma chamber. *Nature*, 266:503-507.
- O'Nions, R. K., Hamilton, P. J., and Evensen, N. M., 1977. Variations in $^{143}\text{Nd}/^{144}\text{Nd}$ and $^{87}\text{Sr}/^{86}\text{Sr}$ ratios in oceanic basalts. *Earth Planet. Sci. Lett.*, 34:13-22.
- Pearce, J. A., and Norry, M. J., 1979. Petrogenetic implications of Ti, Zr, Y and Nb variations in volcanic rocks. *Contrib. Mineral. Petrol.*, 69:33-47.
- Phillips, R. P., 1964. Seismic refraction studies in Gulf of California. In van Andel, Tj. H., and Shor, G. G., Jr. (Eds.), *Marine Geology of the Gulf of California—A Symposium*: Tulsa (American Association of Petroleum Geologists), pp. 90-210.
- Ringwood, A. E., 1974. Petrological evolution of island arc systems. *J. Geol. Soc. London*, 130:183-204.
- Saunders, A. D., in press. The Gulf of California: Geochemistry of basalts recovered during Leg 65 of the Deep Sea Drilling Project. In Robinson, P., Lewis, B. T. R., et al., *Init. Repts. DSDP*, 65: Washington (U.S. Govt. Printing Office).
- Saunders, A. D., and Tarney, J., 1979. The geochemistry of basalts from a back-arc spreading centre in the East Scotia Sea. *Geochim. Cosmochim. Acta*, 43:555-572.
- Saunders, A. D., Tarney, J., Marsh, N. G., et al., 1980. Ophiolites as ocean crust or marginal basin crust: A geochemical approach. *Proc. Int. Ophiolite Conf.*, Nicosia, Cyprus, pp. 193-204.
- Saunders, A. G., Tarney, J., Stern, C. R., et al., 1979. Geochemistry of Mesozoic marginal basin floor igneous rocks from southern Chile. *Geol. Soc. Am. Bull.*, 90:237-258.
- Saunders, A. D., Tarney, J., and Weaver, S. D., 1980. Transverse geochemical variations across the Antarctica Peninsula: Implications for the genesis of calc-alkaline magmas. *Earth Planet. Sci. Lett.*, 46:344-360.
- Schilling, J.-G., 1971. Sea-floor evolution: Rare-earth evidence. *Phil. Trans. Roy. Soc. London Ser. A*, 268:663-706.
- Shaw, D., 1970. Trace element fractionation during anatexis. *Geochim. Cosmochim. Acta*, 34:237-243.
- Shepard, F. P., 1964. Sea-floor valleys of Gulf of California. In van Andel, Tj. H., and Shor, G. G. (Eds.), *Marine Geology of the Gulf of California—A Symposium*: Tulsa (American Association of Petroleum Geologists), pp. 157-192.
- Smewing, J. D., and Potts, P. J., 1976. Rare earth abundances in basalts and metabasalts from the Troodos Massif, Cyprus. *Contrib. Mineral. Petrol.*, 57:245-258.
- Smewing, J. D., Simonian, K. O., and Gass, I. G., 1975. Metabasalts from the Troodos Massif, Cyprus: Genetic implications deduced from petrography and trace element geochemistry. *Contrib. Mineral. Petrol.*, 51:49-64.
- Stern, C. R., 1979. Open and closed system igneous fractionation within two Chilean ophiolites and the tectonic implication. *Contrib. Mineral. Petrol.*, 68:243-258.
- , 1980. Geochemistry of Chilean Ophiolites: Evidence for the compositional evolution of the mantle source of back-arc basin basalts. *J. Geophys. Res.*, 85:955-966.
- Sun, S.-S., Nesbitt, R. W., and Sharaskin, A. Ya., 1979. Geochemical characteristics of mid-ocean ridge basalts. *Earth Planet. Sci. Lett.*, 44:119-138.
- Tarney, J., Saunders, A. D., Matthey, D. P., et al., in press. Geochemical aspects of back-arc spreading in the Scotia Sea and west Pacific. *Phil. Trans. Roy. Soc. London*, A.
- Tarney, J., Saunders, A. D., Weaver, S. D., et al., 1979. Minor-element geochemistry of basalts from Leg 49, North Atlantic Ocean. In Luyendyk, B. P., Cann, J. R., et al., *Init. Repts. DSDP*, 49: Washington (U.S. Govt. Printing Office), 657-691.
- Tarney, J., Wood, D. A., Saunders, A. D., et al., 1980. Nature of mantle heterogeneity in the North Atlantic: Evidence from Deep Sea Drilling. *Phil. Trans. Roy. Soc. London*, A, 297:179-202.
- Tarney, J., Wood, D. A., Varet, J., et al., 1979. Nature of mantle heterogeneity in the North Atlantic: Evidence from Leg 49 basalts. In Talwani, M. (Ed.), *Results of Deep Sea Drilling in the Atlantic: Maurice Ewing Series 2*: Washington (American Geophysical Union), 285-301.
- Terrell, D., J., Pal, S., Lopez, M., et al., 1979. Rare-earth elements in basalt samples Gulf of California. *Chem. Geol.*, 26:267-275.
- Thompson, G., Bryan, W. B., Frey, F. A., et al., 1976. Petrology and geochemistry of basalts from DSDP Leg 34, Nazca Plate. In Yeats, R. S., Hart, S. R., et al., *Init. Repts. DSDP*, 34: Washington (U.S. Govt. Printing Office), 215-226.

Thompson, R. N., Gibson, I. L., Marriner, G. F., et al., 1980. Trace-element evidence of multistage mantle fusion and polybaric fractional crystallization in the Palaeocene Lavas of Skye, NW Scotland. *J. Petrol.*, 21:265-293.

Treuil, M., Jafrezic, H., Deschamps, N., et al., 1973. L'analyse des lanthanides, du hafnium, du scandium, du chrome, du manganèse, du cobalt, du cuivre et du zinc dans les minéraux et les roches par activation non tronique. *Radiat. Chem. Cong. Int. Anal. Activ. Sp. Iss.*, Paris, 1972.

Weaver, S. D., Saunders, A. D., Pankhurst, R. J., et al., 1979. A geochemical study of magmatism associated with the initial stages of back-arc spreading: The Quaternary volcanics of Bransfield Strait, from South Shetland Islands. *Contrib. Mineral. Petrol.*, 68: 151-169.

White, W. M., Schilling, J.-G., and Hart, S. R., 1976. Evidence for the Azores mantle plume from strontium isotope geochemistry of the central North Atlantic. *Nature*, 263:659-663.

Wood, D. A., 1979. Dynamic partial melting: Its application to the petrogenesis of basalts erupted in Iceland, the Faeroe Islands, the Isle of Skye (Scotland) and the Troodos Massif (Cyprus). *Geochim. Cosmochim. Acta*, 43:1031-1046.

Wood, D. A., Joron, J.-L., Treuil, M., et al., 1979a. Elemental and Sr-isotope variations in basic lavas from Iceland and the surrounding ocean floor. *Contrib. Mineral. Petrol.*, 70:319-339.

_____, 1979b. A re-appraisal of the use of trace elements to classify and discriminate between magma series erupted in different tectonic settings. *Earth Planet. Sci. Lett.*, 45:326-336.

Wood, D. A., Tarney, J., Varet, J., et al., 1979. Geochemistry of basalts drilled in the North Atlantic by IPOD Leg 49: Implications for mantle heterogeneity. *Earth Planet. Sci. Lett.*, 42:77-97.

Table 19. X-ray fluorescence analyses, Hole 481A.

Core Section Level (cm) Unit	15 1 11 1-3	15 2 62 1-6	15 2 121 1-7	15 3 27 1-8	15 3 69 1-10	15 3 115 1-10	16 1 121 1-12	16 2 111 1-13	16 3 15 1-13	16 3 31 1-14	17 1 36 1-15	17 1 100 1-17	17 1 112 1-18	17 2 6 1-18	33 1 91 3
SiO ₂	49.7	49.6	49.8	50.1	50.1	50.0	49.1	49.8	49.7	50.0	49.9	49.3	49.8	49.4	50.0
TiO ₂	2.14	2.07	2.16	2.25	1.97	2.14	2.10	1.95	2.00	2.24	2.10	2.09	2.07	1.98	2.41
Al ₂ O ₃	15.2	15.0	15.1	15.4	15.2	15.6	14.8	15.3	14.9	14.7	15.0	15.1	14.9	15.2	14.7
tFe ₂ O ₃	10.60	10.44	10.75	10.94	10.89	10.96	10.93	10.00	11.08	11.05	10.95	10.95	10.55	10.39	11.57
MnO	0.16	0.17	0.17	0.17	0.17	0.18	0.17	0.15	0.15	0.15	0.15	0.15	0.14	0.15	0.18
MgO	7.25	7.55	7.30	6.82	7.05	6.25	7.65	7.65	7.30	7.25	7.50	7.35	7.50	8.05	5.86
CaO	10.16	10.23	10.02	9.90	10.38	9.81	10.94	10.73	10.01	10.20	10.28	11.05	10.67	10.56	10.96
Na ₂ O	3.11	2.98	3.09	3.22	3.20	3.14	2.69	2.87	2.66	2.87	2.96	2.68	2.70	2.68	3.11
K ₂ O	0.35	0.49	0.41	0.51	0.37	0.59	0.44	0.14	0.83	0.48	0.38	0.50	0.40	0.16	0.33
P ₂ O ₅	0.32	0.33	0.31	0.34	0.25	0.45	0.27	0.32	0.32	0.32	0.32	0.24	0.30	0.29	0.27
LOI	—	—	—	—	0.46	—	—	0.95	—	0.70	—	—	—	1.00	0.82
Total	98.94	98.94	99.12	99.67	100.04	99.11	99.08	99.86	98.99	99.96	99.48	99.46	99.12	99.85	100.21
Trace Elements (ppm)															
Ni	88	95	99	87	80	82	121	121	101	90	106	114	108	142	40
Cr	190	186	188	174	180	226	210	171	183	171	179	196	193	206	118
Zn	79	79	87	100	68	82	73	60	61	55	55	47	42	53	83
Ga	22	22	22	22	20	24	23	24	17	17	20	17	26	29	30
Rb	4	8	3	5	4	7	11	3	14	6	5	12	9	1	2
Sr	201	199	206	208	203	212	196	208	190	196	193	205	198	198	192
Y	41	39	42	44	35	50	39	36	37	43	39	39	39	37	46
Zr	161	159	163	171	123	189	155	151	144	165	156	156	152	151	159
Nb	6	5	7	6	5	7	6	7	6	6	6	6	7	6	7
Ba	67	84	83	105	71	99	54	41	62	46	57	55	45	45	57
La	10	9	10	11	8	11	10	9	9	9	9	5	8	6	9
Ce	22	21	23	24	16	29	22	23	20	23	22	21	21	21	21
Nd	18	17	19	18	14	22	16	18	15	18	16	16	17	17	18
Pb	6	3	4	8	5	3	2	<1	7	6	3	2	6	4	4
Th	<1	3	<1	<1	1	<1	<1	2	4	1	<1	<1	3	1	3
Selected Ratios															
Zr/Nb	27	32	23	29	25	27	25	22	24	28	26	26	22	25	23
Ti/Zr	80	78	79	79	96	68	81	77	83	81	81	80	82	79	91
Y/Zr	0.25	0.25	0.26	0.26	0.28	0.26	0.25	0.24	0.26	0.26	0.25	0.25	0.26	0.25	0.29
Ce/Zr	0.14	0.13	0.14	0.14	0.13	0.15	0.14	0.15	0.14	0.14	0.14	0.13	0.14	0.14	0.13
Ba/Zr	0.42	0.53	0.51	0.61	0.58	0.52	0.35	0.27	0.43	0.28	0.37	0.35	0.30	0.30	0.36
(Ce/Y) _N	1.32	1.32	1.35	1.34	1.12	1.42	1.39	1.57	1.33	1.31	1.39	1.32	1.32	1.39	1.12
Fe/Mg	1.70	1.60	1.71	1.86	1.79	2.03	1.66	1.52	1.76	1.77	1.69	1.73	1.63	1.50	2.29
K/Rb	726	508	1134	847	768	700	332	387	492	664	631	346	369	1328	1370
Ba/Sr	0.33	0.42	0.40	0.50	0.35	0.47	0.28	0.20	0.33	0.23	0.30	0.27	0.23	0.23	0.30
CIPW Norms															
Q	0.0	0.0	0.0	0.0	0.0	0.0	0.0	0.0	0.0	0.0	0.0	0.0	0.0	0.0	0.0
Or	2.1	2.9	2.4	3.0	2.2	3.5	2.6	0.8	5.0	2.8	2.3	3.0	2.4	0.9	1.9
Ab	26.6	25.5	26.4	27.3	27.1	26.8	23.0	24.3	22.7	24.3	25.2	22.8	23.0	22.7	26.3
An	26.6	26.5	26.3	26.3	25.9	26.9	27.3	28.6	26.6	25.7	26.6	27.9	27.7	28.9	25.1
Ne	0.0	0.0	0.0	0.0	0.0	0.0	0.0	0.0	0.0	0.0	0.0	0.0	0.0	0.0	0.0
Di	18.1	18.5	17.8	17.0	19.6	15.8	21.0	18.4	17.6	18.6	18.5	20.9	19.3	17.7	22.6
Hy	14.2	13.7	14.7	13.5	11.8	16.7	12.8	17.3	17.3	18.2	15.7	12.6	18.4	19.1	14.1
Ol	4.7	5.5	4.6	4.8	5.8	2.2	5.8	2.5	3.4	1.7	4.2	5.3	1.6	2.6	1.0
Mt	1.9	1.8	1.9	1.9	1.9	1.9	1.9	1.7	1.9	1.9	1.9	1.9	1.9	1.8	2.0
Il	4.1	4.0	4.1	4.3	3.7	4.1	4.0	3.7	3.8	4.3	4.0	4.0	4.0	3.8	4.6
Ap	0.8	0.8	0.7	0.8	0.6	1.1	0.6	0.8	0.8	0.8	0.8	0.6	0.7	0.7	0.6

Note: See Table 1, note.

Table 20. INAA results (Saclay) for selected samples, Hole 481A.

Core Section	15	15	15	16	16	17	17	33
Interval (cm)	11-13	121-123	69-71	111-113	15-17	112-114	6-8	91-95
Unit	1-3	1-7	1-10	1-13	1-13	1-18	1-18	3
Ni	95	95	88	133	110	109	142	50
Cr	210	202	198	169	158	202	223	159
Co	37.2	36.8	38.9	39.1	41.5	38.1	40.8	39.0
Sc	34.5	34.2	37.7	40.2	35.9	33.6	31.6	37.4
Ba	46	48	33	33	45	33	21	42
Sr	223	239	218	256	234	242	241	222
Cs	0.77	0.87	0.45	0.53	2.64	1.06	0.88	0.06
Rb	4.4	4.0	3.2	2.5	15.1	8.9	1.9	2.7
U	0.10	0.18	0.16	0.14	0.14	0.15	0.16	0.24
Th	0.55	0.63	0.46	0.49	0.48	0.49	0.45	0.60
Zr	181	176	151	157	169	153	148	199
Hf	4.12	4.13	3.57	3.69	3.94	3.85	3.61	4.24
Ta	0.45	0.45	0.36	0.52	0.42	0.42	0.41	0.42
Sb	0.25	0.28	0.01	0.19	0.39	0.86	0.58	0.02
La	7.20	7.24	6.12	6.60	6.71	6.67	5.39	6.97
Ce	16.8	17.6	14.7	16.7	16.8	16.8	15.0	16.2
Eu	1.88	1.77	1.56	1.68	1.34	1.63	1.68	2.01
Tb	0.97	0.97	0.97	0.87	1.00	0.91	0.85	1.07

Note: All values in ppm.

Table 21. INAA results (Bedford) for selected samples, Hole 481A.

Core Section	15	15
Interval (cm)	27-29	69-71
Unit	1-8	1-10
La	8.36	6.1
Ce	24.2	18.0
Nd	18.3	15.8
Sm	5.52	—
Eu	1.94	1.65
Gd	6.29	5.41
Tb	1.20	1.07
Yb	4.24	3.48
Lu	0.65	0.56
Th	0.75	0.61
Hf	4.24	3.40
Ta	0.44	0.41
La _N /Yb _N	1.32	1.17
La/Ta	19	15
Th/Hf	0.18	0.18

Note: Trace-element values in ppm.

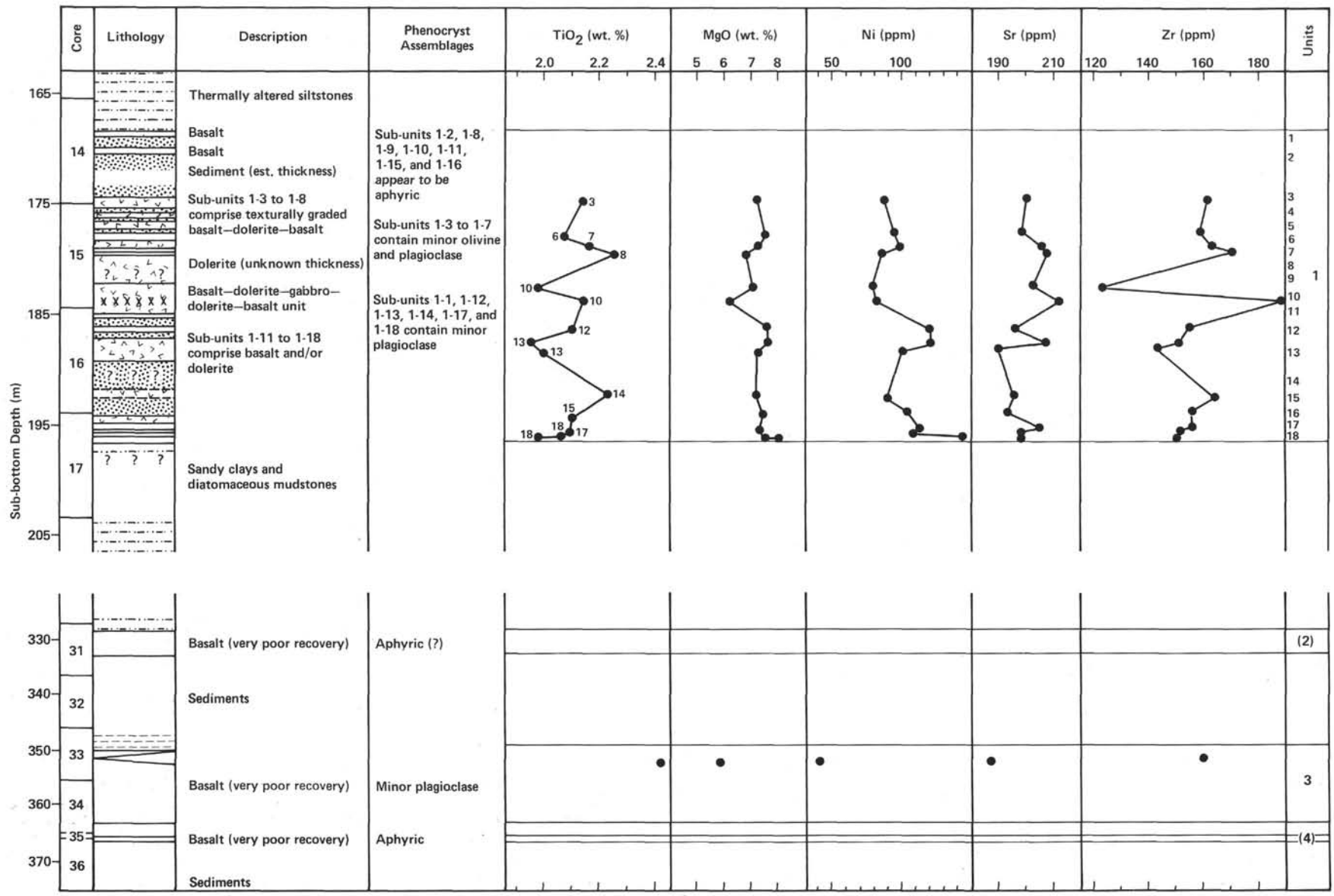


Figure 36. Downhole variations in lithology and selected geochemical parameters, Hole 481A.

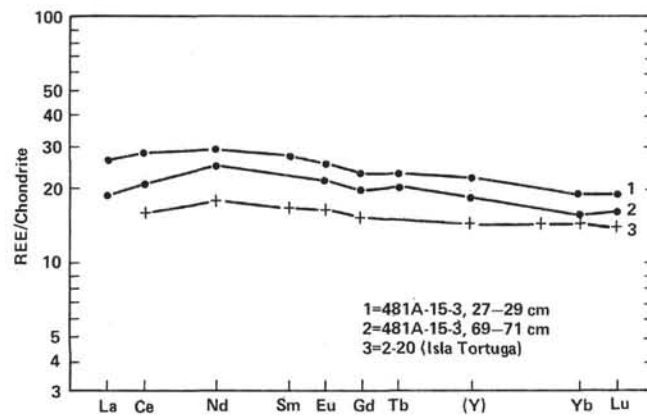


Figure 37. Chondrite-normalized REE data for basic rocks recovered at Site 481. (Sample 2-20 is a primitive basalt from Tortuga Island [Batiza et al., 1979]. Site 481 analyses determined at Bedford College.)

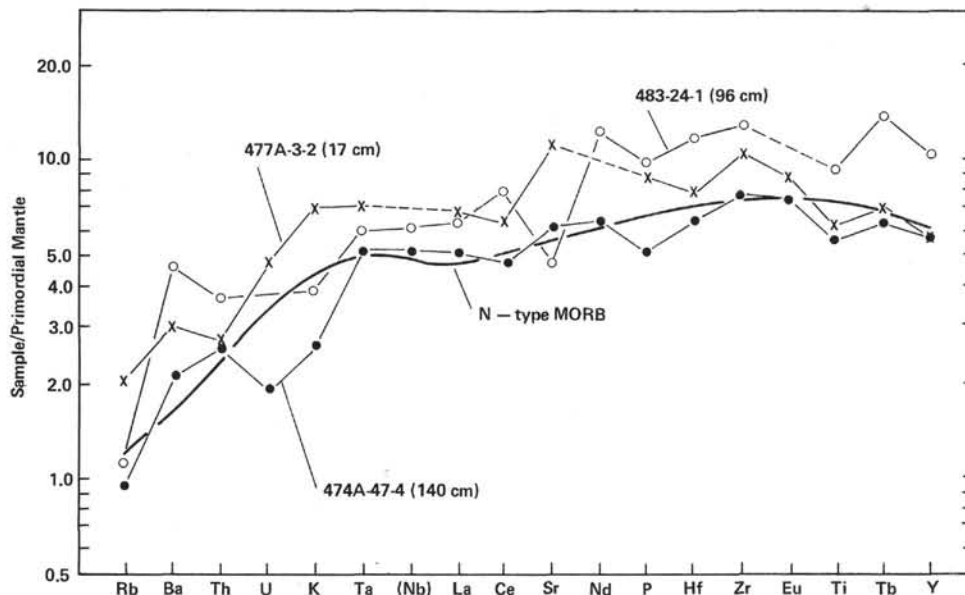


Figure 38. Data for basaltic samples from the Guaymas Basin (Site 477) and from the mouth of the Gulf (Sites 474 and 483 [Leg 65]) plotted on a mantle-normalized diagram. (N-type MORB and normalizing values from Wood et al., [1979b].)